Development of an innovative and eco-compatible composite material for the reversible trapping of pollutants : application to the depollution of industrial effluents

Almaza Abi Khalil

UNIVERSITÉ D'ORLÉANS

ÉCOLE DOCTORALE Énergie Matériaux Sciences de la Terre et de l'Univers (EMSTU)

ICMN Interfaces, Confinement, Matériaux et Nanostructures

DMP : Déchets et Matières Premières

THÈSE présentée par :

Almaza ABI KHALIL

Soutenue le :16 Janvier 2023

Pour obtenir le grade de : **Docteur de l'Université d'Orléans**

Discipline/ Spécialité : Chimie des matériaux

Development of an innovative and eco-compatible composite material for the reversible trapping of pollutants: application to the depollution of industrial effluents

THÈSE dirigée par :

M. MULLER Fabrice	Maître de conférence, HDR, Université d'Orléans

RAPPORTEURS :

Mme BRENDLE Jocelyne	Professeure, IS2M- Université haute-Alsace
M. DUCLAUX Laurent	Professeur, EDYTEM-Université de Savoie Mont Blanc

JURY :

Mme DELPEUX Sandrine	Ingénieure de recherche, ICMN/CNRS
M LAHCINI Mohammed	Professeur, Université Cadi Ayyad
Mme PEULON Sophie	Chargée de recherche CEA/CNRS
M SERON Alain	Expert scientifique en matériaux, BRGM
M. SINTUREL Christophe	Professeur, ICMN/CNRS **(Président du jury)**
Mme BETELU Stéphanie	Expert scientifique en chimie analytique, BRGM (Invitée)

To my family

My biggest motivation and my support system to whom I will always be grateful

To my friends

Who were there for me whenever I needed support and advices

Acknowledgment

I reserve these few lines, with great pleasure, to express my sincere gratitude and appreciation to everyone who has helped this work be completed, whether directly or indirectly.

My grateful appreciations go to my supervisors, Alain Seron, Fabrice Muller, Stéphanie Betelu, and Sandrine Delpeux, who welcomed me warmly at BRGM and ICMN. Thank you for providing me with the opportunity to fully benefit from your knowledge in various domains and for providing me with numerous helpful advices. There are no words to express my gratitude to my supervisors, not only for their involvement in the direction of my work, but also in the direction of my future. I am overjoyed that they have now become part of those who have left their mark on my life.

I would like to thank Mme. Jocelyne Brendle, M. Laurent Duclaux, M. Mohammed Lahcini, Mme Sophie Peulon and M. Christophe Sinturel for agreeing to evaluate my work, provide constructive feedback, and be part of the jury members.

Mme Virginie Bazin, M. Cedric Duee, Mme Marjorie Roulet, M. Stéphane Touzelet, and Mme Fabienne Warmont will also be acknowledged for their contributions to the success of this thesis through experimental and technical work. I would also like to thank my friends Adeline Po, Charles, Chahinez, Samir, Clément, Romain, Ali, Ramona, Céline, Florian, Thibault with the excellent vin chaud, Taleb, Oumayma, Sahar, Dalia and Safayooo. I will never forget the pleasant moments, the coffee breaks, the laughs and jokes we lovingly shared.

Special thanks will be directed to Fadoua, fedo ma chérie, for her presence and support during her internship at ICMN. Radia, thank you for giving me the chance to meet you and work together. Pauline, paupau, it was great meeting you, you helped me with my experiments and you missed your coffee breaks because of me :D. Thank you all for contributing in the success of this work.

I want to express my heartfelt gratitude to those who have been the most supportive of me, Rana, Yves, Ariane, Syrine and Anita.

Rana, my best friend, the one who makes me laugh so hard that I could barely breathe. RANA HELLO, the one with a golden heart, thank you for being here, for giving me the chance to be a close friend of yours. Thank you for your support and for pampering me with your delicious chicken stroganoff.

F. Yves, YVEE, le petit pain, I couldn't sit on for 2 days. Thank you for the crab dance, for the beautiful moments we share during our parties. I still remember the weekend spent at Pénestin, where you made sure I worked the whole weekend by preparing my coffee every time. Thank you for cooking a lot of French cuisine, you are one of the best encounter made in this lab.

My Ariane Ariane, I have been waiting for you for 2 years, and now I am leaving (Hello leaving). My best friend, my drinking partner, my top chef et pizza buddy, my tac, my little turtle, my Gryffindor. All of these nicknames describe how much you mean to me. 5 days after we met, I invited you to the HOP POP HOP festival and we clicked in an amazing way. That is when I knew you are going to be a special friend of mine. Thank you for being there for me when I needed someone, thank you for opening your apartment to party and drink, thank you for being the amazing beautiful person you are.

Syrine, habibet albe, I could never thank you enough for what you did! You were the best person I met in 2022 and I do not regret this encounter. We met by luck but we decided to be close friends willingly and that is the best choice I did, even though we ran into many hard moments the past year, we managed to pass all of them and become more and more close. Thank you is not enough, you gave me a lot of motivation when I was about to give up, if it was not for you I would not manage to make it in a better way. Thank you for always being by my side, nhebek.

My batata, my ohana "*ohana means family, family means no one got forgotten or left behind*", I love you so much, you borne me for 15 years and still counting… Thank you for being my psychologist, my best friend, my family albaaaa. You always stood by my side and helped me become a better version of myself. Thank you for supporting me, for helping me, for giving me the best advices all the time. You are my best person, my soulmate, my ohana no matter where… I could never thank you enough, you know your worth, I love you my batata.

Finally, my warmest acknowledgment goes to my family, my support system and my power. Mama and Papi, thank you for your sacrifices, thank you for your patience and for having faith in my achievement. Thank you for your unconditional love and for cheering me up when I needed support the most. Thank you for believing in me and for having faith in me. Finally, I am a doctor as if I always said I would be. I did what I promised I'll do and I hope that you will always be proud of me. Fakher, my love, my power and strength, my motivation, I did it I am not an egha anymore, I know that you are proud of me as I am of you. I love you. The best is for the last, Renooo, my world, my doctor, my big sister, my motivation and strength, my everything. Without your sacrifices, I could never travel and achieve all the things I did. You

were always there for me, supporting me and believing in me. You are my whole world and I am extremely lucky to have you as a loving sister. I love you my reno and I am extremely proud of you. Boubou Habibi, thank you for supporting me even when you do not understand what is happening you are my baby.

Résumé

Les industries spécialisées dans le domaine du traitement de surfaces métalliques, de l'agroalimentaire et bien d'autres génèrent des effluents contaminés par des métaux comme le Cr, Zn, Ni, Cu … et des polluants organiques et inorganiques comme les encres, les pesticides, les produits médicamenteux, les phosphates, nitrates, nitrites et sulfates… La non biodégradabilité et la toxicité des métaux, en particulier le Zn, rejeté dans l'environnement par différentes industries, de même que la capacité d'eutrophisation portée par les anions minéraux, sont des causes majeures actuelles de pollution environnementale, ce qui rend la recherche de procédés de traitement de ces types de polluants particulièrement pertinente.

Afin de répondre aux normes environnementales européennes de plus en plus contraignantes, différents procédés de dépollution sont utilisés par certains industriels pour le traitement de leurs effluents. Dans ce contexte, les travaux de recherche effectués durant cette thèse concernent le développement de composites innovants constitués d'hydroxydes doubles lamellaires (HDLs) et d'oxyde graphitique (OG). Les premiers sont utilisés pour la capture par intercalation interfoliaire des anions majeurs en raison de la charge structurelle portée par de tels matériaux du fait de substitutions isomorphiques. Quant à l'oxyde graphitique, chargé négativement pour des valeurs de pH supérieures de pKa des groupements oxygénés, il est utilisé pour la capture par adsorption de surface des différents métaux cités précédemment. Le matériau composite est réalisé sous forme de billes hybrides par dispersion des adsorbants dans une matrice de chitosane (CS), un bio polymère naturel extrait des coquilles de crustacées. La mise en forme en billes a été choisie pour la facilité de mise en œuvre de ces objets notamment dans les applications industrielles.

Les HDLs carbonatés (CO_3^{2-} en interfoliaire) avec des rapports cationiques Co/Fe compris entre 2/2 et 10/2, ont été synthétisés en utilisant la méthode de co-précipitation à pH variable. Les valeurs de pH, 8,0 et 11,5, ont été choisies sur la base des courbes de titration des solutions des cations Co et Fe. Après co-précipitation, une maturation à 60°C pendant 24h est mise en œuvre dans le but d'augmenter la cristallinité et la taille des particules. A l'issue de cette période, la suspension de HDL est dialysée en utilisant une solution de carbonate de sodium afin d'échanger tous les anions initialement présents dans l'espace interfoliaire, en carbonates. Des HDLs chlorurés (Co/Fe-Cl^-) ont également été synthétisés en boîte à gants afin d'obtenir des HDLs facilement échangeables pour favoriser la capture des polluants anioniques.

Des oxydes graphitiques (OG) ont été synthétisés par voie chimique suivant la méthode de Hummers modifiée. Après exfoliation du graphite dans un mélange d'acide sulfurique et phosphorique, le $KMnO_4$ utilisé comme agent oxydant a été ajouté afin de permettre la création de groupements oxygénés types carboxylique, époxy, hydroxyle, etc… en surface. Un lavage à l'eau milli-Q et un séchage suivi d'un broyage a permis l'obtention de la poudre d'OG.

En vue d'étudier l'activité de chacun des composants ainsi que leurs interactions potentielles, des billes de différentes compositions : chitosane pure (CS), chitosane et HDL (CS/ HDL), chitosane et OG (CS/OG), ainsi que chitosane, HDL et OG (CS/HDL/OG) ont été élaborées en formulant une solution visqueuse adaptée. Divers protocoles d'élaboration des billes ont été envisagés. Pour l'élaboration des billes CS/HDL/OG, le protocole retenu est le suivant : la poudre de chitosane est dissoute dans de l'acide acétique dilué pour former un gel de chitosane. Puis l'OG dispersé par traitement ultra-sonique est ajouté. Après homogénéisation, les précurseurs de HDL (sel de métaux) sont ajoutés. La solution visqueuse est ensuite transférée dans une solution de soude afin de former les billes avec le diamètre désiré (2-3 mm). Une étape finale de lavage est nécessaire pour faire baisser le pH dans les billes jusqu'à une valeur favorisant la formation des HDLs au sein des billes.

La caractérisation physico-chimique des matériaux obtenus a été réalisée en utilisant différentes techniques comme la diffraction de rayons X, la spectroscopie infra-rouge, la microscopie électronique à transmission, la microscopie électronique à balayage, l'analyse thermogravimétrie, l'analyse élémentaire par pyrolyse couplée à une chromatographie en phase gazeuse, et la mesure de surface BET. Les HDLs Co/Fe-CO_3^{2-} obtenus avec les rapports cationiques Co/Fe compris entre 2/2 et 8/2 sont bien cristallisés. Pour le rapport 10/2 une faible quantité d'impureté de type Co_3O_4 a été détectée par DRX (***Figure.1***). La spectroscopie FTIR et la spectroscopie d'absorption atomique (SAA) ont permis de préciser la composition chimique des produits de synthèse en termes à la fois d'anions interfoliaires et de rapport Co/Fe. Cependant, les analyses EDX réalisées sur des particules individualisées ont montré que le rapport Co/Fe pouvait varier localement, spécifiquement pour les compositions 2/2 et 10/2. L'étude des solides par MET et MEB ont confirmé la morphologie hexagonale des particules.

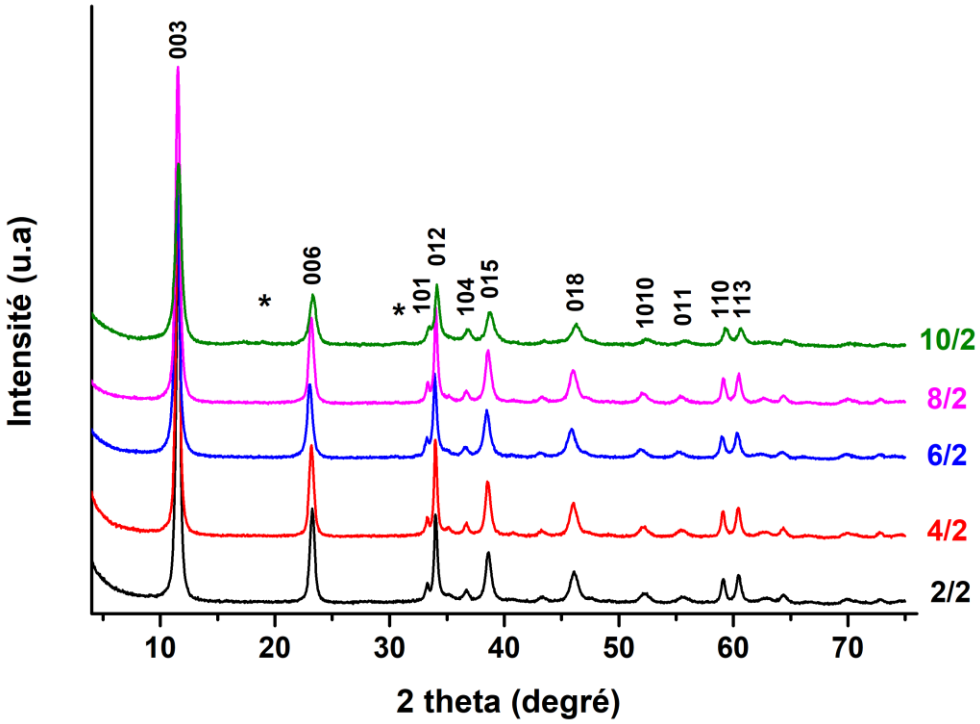

Figure 1.Diagramme de DRX du 2/2,4/2,6/2,8/2 et 10/2 synthétisés à pH= 8.0,

(*) Co_3O_4

Concernant les HDLs Co/Fe-Cl^- synthétisés à une valeur de pH 8,0, les différentes techniques de caractérisation ont montré la présence des phases HDLs cristallisées, présentant les rapports cationiques recherchés et une absence d'anions carbonates dans l'espace interfoliaire.

Les caractérisations par analyse élémentaire et par XPS ont montré la présence de groupements oxygénés en surface de type C-O et C=O dans l'OG synthétisé. La titration acido-basique a permis de quantifier les groupements de surfaces susceptibles de participer à l'adsorption du Zn^{2+} : à pH = 5,0, 1 $mmol.g^{-1}$ de groupements COOH participent à la capture du Zn^{2+}.

La capacité des matériaux à piéger des cations a été testée en ciblant le zinc qui est un polluant fréquent dans les eaux industrielles issues du traitement de surface des métaux. Pour cerner les éventuelles interactions entre les différents composants ainsi que leur contribution propre au piégeage des polluants ciblés, les études d'adsorption ont été réalisées par SAA sur a poudre d'OG, les billes de CS, les billes de CS/OG et CS/HDL/OG.

Afin de réaliser les expériences d'adsorption dans des conditions optimales, le choix de la valeur du pH égale à 5 a pris en compte les phénomènes suivants :

- La dissociation au-delà d'un pH de 3 d'une partie des groupements carboxyliques présents sur la surface du OG qui induit à la formation d'une charge négative à la surface de ce matériau ;
- Le risque de précipitation du zinc à partir d'un pH de 6-6,5 ;
- La dissociation des groupements aminés du chitosane au-dessous de leur valeur de pKa située à 6,5 qui conduit à l'apparition d'une charge positive globale sur ce composé potentiellement néfaste à la capture du zinc.

Pour l'élaboration des billes de CS/OG, un rapport de 3/1,5 a été choisi afin de permettre l'ajout de la quantité de HDLs requise pour former le composé final tout en maintenant une bonne cohésion au sein des billes.

Les essais d'adsorption du Zn^{2+} par les billes de CS ont permis de montrer que la capacité de capture du chitosane vis-à-vis de ces cations est proche de zéro à cause de la présence des groupement NH_3^+ sur les chaines de CS à des pH inférieurs à 6,5 (pKa des groupement amino). Les billes CS/OG ont montré une capacité d'adsorption du Zn^{2+} de 42,0 mg par g de OG. Cette valeur est inférieure à la capacité de sorption du zinc sur l'oxyde graphitique seul qui s'élève à 65,1 mg/g. Cet abaissement de la capacité de capture est très probablement dû à l'interaction entre le CS chargé positivement et l'OG chargé négativement. La densité de charge du chitosane étant de 6,5 meq/g alors que celle de l'OG est de 1,55 meq/g, cette interaction conduit à la neutralisation d'une partie des sites d'adsorption de l'OG et donc à la diminution de la capacité de capture du zinc.

Concernant la capture du zinc par les billes de CS/HDL/OG, la capacité de capture observée est de l'ordre de 64.4 mg de zinc par g d'OG présent dans la bille. La différence (22,4 mg /g) entre la quantité de zinc adsorbée par les billes de CS/OG et celle par les billes de CS/HDL/OG peut être reliée à l'effet tampon du HDL à un pH $\geq$ 8.0. Cette augmentation de la valeur du pH à l'intérieure de la bille conduit à la déprotonation des groupements NH_3^+ et inhibe l'interaction entre le CS et l'OG qui reprend sa capacité de sorption initiale (65.1 mg/g). De plus l'effet tampon du HDL peut conduire à une précipitation d'une partie du Zn^{2+}. Par ailleurs, le point de charge nulle des HDLs est voisin d'une valeur de 8.0. De ce fait, à des pH supérieurs à 8.0, la surface des HDLs est chargée négativement ce qui peut résulter en une adsorption de Zn^{2+} et par là même expliquer l'augmentation de la capacité de capture du zinc en présence de HDLs.

Une évaluation de la capacité d'échange anionique des HDLs a été menée en étudiant la capacité de capture des sulfates, nitrates et nitrites par les HDLs carbonatés et chlorurés par chromatographie ionique. L'absence d'échange vis-à-vis des carbonates a été confirmée, en accord avec la grande affinité des HDLs vis-à-vis de ces anions. Dans le cas des HDLs chlorurés, il apparait que l'affinité de ces matériaux pour les sulfates est supérieure à celle pour les nitrates et nitrites. Par exemple, pour le composé obtenu avec le rapport Co/Fe 6/2, 50% des sulfates en solution sont échangés, alors que respectivement 26% et 24% des nitrates et nitrites sont intercalés (***Figure.2***).

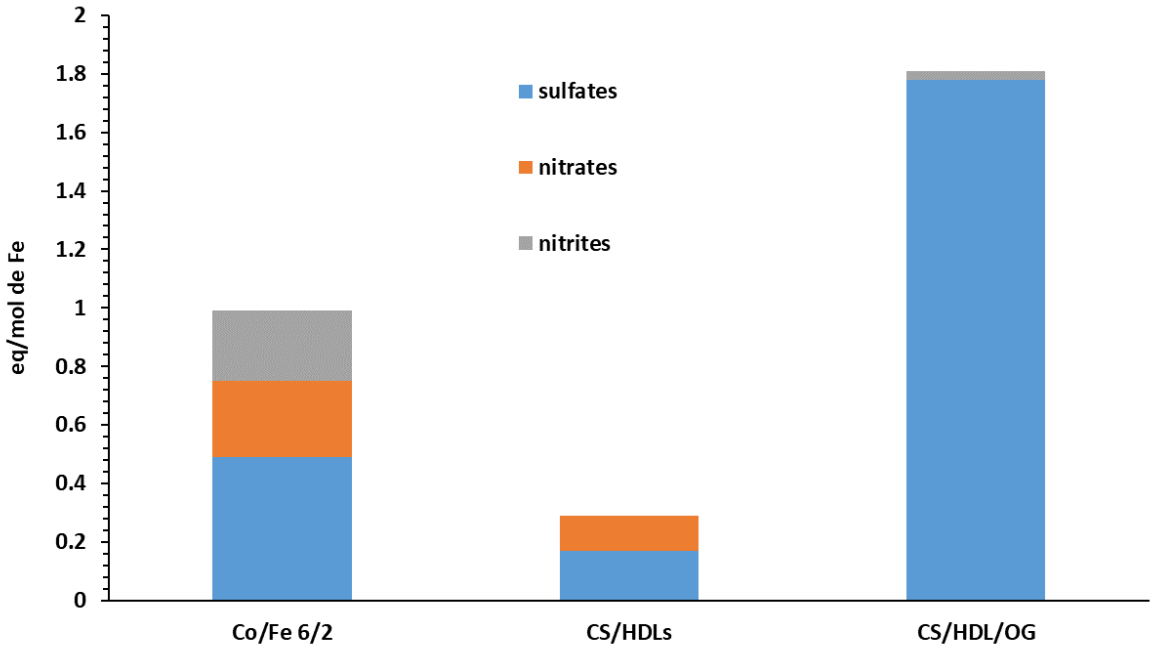

Figure.2. Echange des anions SO_4^{2-}, NO_3^- et NO_2^- sur le HDL Co/Fe 6/2, billes de CS/HDL et billes de CS/HDL/OG

L'étude de l'échange sur les billes de CS/HDLs a montré un taux de capture des anions (0,3 eq/mol de Fe) inférieur à la capacité d'échange du HDLs Co/Fe 6/2 présent dans les billes (1 eq/mol de Fe). Cela peut être expliqué par une contamination par des anions carbonates pendant l'élaboration des billes, difficilement échangeables. L'échange anionique pour les billes CS/HDL/OG a montré une capacité d'échange supérieure (1,8 eq/mol de Fe) à l'excès de charges positive apportées par le Fe (1 eq/mol de Fe), ainsi qu'une forte affinité pour les sulfates. Ceci peut être due à la présence des groupements NH_3^+ provenant des chaines de chitosane, qui a des pH inférieurs à 8,5, présentent toujours une partie des groupement amino protonnés.

Table of content

List of abbreviations

LDHs	Layered double hydroxides
3R	Three-layer rhombohedral polytype
2H	Two-layer hexagonal polytype
1H	One-layer hexagonal polytype
AEC	Anionic Exchange Capacity
MOs	Metal oxides
EES	Electrical Energy Storage
GO	Graphene oxide
MGO	Multilayered Graphene Oxide
C/O	Carbon/Oxygen ratio
CS	Chitosan
DD	Deacetylation Degree
MW	Molecular Weight
PAAS	Polyacrylic Acid Sodium
Co/Fe-CO_3 LDH	Carbonated Cobalt II /Iron III Layered Double Hydroxide
Co/Fe-Cl LDH	Chlorided Cobalt II/Iron III Layered Double Hydroxide
CS/LDH	Chitosan 3%/Layered Double Hydroxide beads
CS/MGO	Chitosan 3% /Multilayered Graphene Oxide 1.5% beads
CS/LDH/MGO	Chitosan 3% / Layered Double Hydroxide/Multilayered Graphene Oxide 1.5% beads
XRD	X-Ray Diffraction
FTIR	Fourier Transformer Infrared
AAS	Atomic Absorption Spectroscopy

TEM	Transmission Electron Microscope
SEM	Scanning Electron Microscope
EDX	Energy-dispersive X-Ray Spectroscopy
XPS	X-ray Photoelectron Spectroscopy
TGA	ThermoGravimetric Analysis
S_{BET}	Specific Surface Brunauer, Emmett, and Teller (BET)
CHONS	Elemental analysis
IC	Ion Chromatography

List of figures

List of tables

General introduction

"If there is magic on this planet, it is contained in water"-Loren Eiseley

Water is the most essential element for the survival of all living organisms on Earth. The seeking of drinkable water ruled population movements and has been a central concern from the beginning of humankind. However, it is under actual threat today due to the growing population, increased agricultural and industrial demands, and the worsening effects of climate change. If the industrial age allowed true technological development in the last century, it resulted in an unavoidable global anthropization of water resources, resulting in significant changes in groundwater and surface water quality. Different industries such as food industries, metal treatment industries and much more generates effluents rich in heavy metals such as Cu, Zn, Ni, Pb.. and anions like sulfates, nitrates, nitrites ... Since heavy metals are, toxic and non-biodegradable, their accumulation in soils and sediments is a major concern. For the anionic pollutants such as nitrates and phosphates, they cause eutrophication of the water surface leading to the decrease of the amount of oxygen dissolved, causing blooms of algae and microalgae, sometimes toxic, which generate major disturbances for aquatic ecosystems. The importance to preserve water resources are high and necessary, leading to find new methods to treat polluted water before releasing it in nature. Different water treatment methods are available for water depollution such as chemical precipitation, electrochemical processes, ion exchange and adsorption processes. It was demonstrated that the ion exchange and adsorption methods were suitable to depollute water from metallic and anionic contaminants as well as to recover the important pollutants that can be valorized for other applications. Ionic exchange process can be performed using different type of materials, such as layered double hydroxides, and adsorption process is mostly performed using carbon-based materials such as multilayered graphene oxide. WHO legislations specified the maximum amount of the following pollutants in drinkable water for Zn^{2+} 4 mg/L, nitrates 50 mg/L and nitrites 3mg/L.

The main issue in water treatment processes is the mixing of pollutants having different physico-chemical properties. Therefore, one of the challenges currently preoccupying the scientific community, is to develop hybrid materials or processes able to treat all kind of pollutant, whatever their nature hydrophobic or hydrophilic and regardless of their charge: neutral positive or negative.

The presented work was performed between the two laboratories of the Bureau de Recherche Géologique et Minière (BRGM) having a great experience in LDHs synthesis and the laboratory

Interfaces, Confinement, Matériaux et Nanostructure (ICMN, CNRS) working on functional carbons for fifty years.

The main objective of the thesis focuses on developing a new, hybrid material possessing a wide range of adsorption properties for the trapping of cationic and anionic pollutants such as Zn^{2+}, sulfates, nitrates and nitrites as well as the multiscale characterization and optimization of the synthesized composites properties. In order to achieve this objective, the elaboration and optimization of a hybrid composite containing two types of adsorbents were studied. The two adsorbents used were layered double hydroxides (LDHs) for the anionic exchange which acts like anionic resins to exchange toxic anions present in wastewater, and multilayered graphene oxide (MGO), a carbon-based non porous and functional material with graphene sheets possessing a high amount of functionalities able to be dissociated at neutral pH to give negatively charges sites for the adsorption of metallic cations. Different paths can be used for the elaboration of MGO from graphite, in this work the modified Hummer's method was used because of its simplicity and efficiency.

For the LDH synthesis, the cations chosen were cobalt and iron. The cobalt was chosen in order to have an electroactive metal present on LDH sheets for regeneration purposes. However, the iron helps with the conduction of electrons for electrochemical uses. LDHs were synthesized using the coprecipitation method. As far as powders are difficult to manage in an industrial process, both adsorbents were grouped in a biopolymer matrix made of chitosan (CS) under the form of colloidal beads. The elaboration of the desired composite adsorbent under the form of beads of millimeter size range was chosen for the facility of the manipulation for further industrial applications.

The benefit of this work lies on the obtainment of well-crystallized Co/Fe LDHs with a wide range of cationic ratios between 2/2 and 10/2 as well as their multiscale characterization. In addition, the second challenge includes the achievement of chitosan beads containing LDH phases and MGO at the same times without altering the unique properties of each functional material i.e. the capacity to adsorb cationic metals (Zn^{2+}) for MGO and to exchange anions (sulfate, nitrates and nitrites) for LDHs.

This manuscript is divided into three main chapters. The first one constitutes the bibliographical review. It starts with a context about the importance of water, the main sources of water pollution and the different methods used for water depollution regarding heavy metals and anionic pollutants. Following that, a literature review concerning layered double hydroxides, multilayered graphene oxides, relating to their synthesis, characterization and physico-chemical

properties was detailed. The different pathways to get chitosan gels and for beads elaboration were also displayed.

The second chapter describes the materials and methods applied for the obtainment and the characterization of the different adsorbents and composite materials used.

The third chapter, including the results and discussion obtained, was divided into three parts:

1- The first part includes the synthesis and full characterization of carbonated and chlorided Co/Fe LDHs with different cationic ratios between 2/2 and 10/2. This section presents the results of XRD analysis for phase identification, AAS and FTIR analysis for the determination of the cationic ratio and the interlayer anions, along with TGA and S_{BET} analysis for the thermal degradation and surface area determination. Additionally, the study of the anionic exchange capacity of chlorided Co/Fe LDHs towards major anions, i.e. sulfates, nitrates and nitrites anions is developed.

2- The second part of this chapter describes the synthesis of multilayered graphene oxide. The characterization of the obtained powder was performed using elemental analysis, XPS and FTIR techniques for the determination and quantification of the functional groups created on the surface of the graphene. The study of the adsorption of Zinc (Zn^{2+}) using MGO will also be detailed in this part.

3- The final part includes the elaboration and the characterization of the chitosan beads with different compositions: pure chitosan, chitosan/layered double hydroxides, chitosan/multilayered graphene oxide and chitosan/layered double hydroxide/multilayered graphene oxide. The elaboration of these materials was performed through the formation of chitosan gel while adding to it dispersed MGOs and precursors of LDH. After this step, dropping the gel in alkaline solution was required in order to form chitosan-based beads. The study of the adsorption capacity of Zn^{2+} by these beads as well as the anionic exchange capacity against sulfates, nitrates and nitrites are discussed.

A general conclusion followed by some perspectives are presented at the end of the manuscript.

Chapter 1: Literature review

Water is one of the most valuable resources of nature because it is required for all forms of life on earth. This equates to approximately 1,360 million km^3 of water on the surface of the earth. As a result, each human being would have 250,000 million liters, not to mention the water needs of animal farms and agriculture. Water seems to be an infinite resource from various views... However, only 3% of Earth water is sweet, 2% is found in glaciers, and 1% is found in waterways, lakes, subterranean nappes, and the atmosphere. To put it another way, only 1% of the water on Earth is suitable for human use.

When numerous compounds that may be considered as pollutants are introduced directly or indirectly into groundwater or waterways (rivers, oceans, lakes, etc.), the water is considered as polluted. If these contaminants are present in modest concentrations, ecosystems have the natural ability to eliminate them and rebalance naturally. However, as soon as they exceed the absorption capacity of the system, water contamination becomes a concern. Pollution of rivers, aquifers, and lakes is mainly caused by human activities, leading to the extinction of natural flora and a reduction in the amount of oxygen available to fish and other aquatic species. While freshwater pollution has a negative influence on the ecosystem, it also has a negative impact on humans. Worse, water contaminants are as diverse as they are numerous. The WHO legislation establishes some standards to specify the maximum amount of each pollutant present in water without endangering the environment, including a maximum of 4 mg/L for Zinc in drinkable water, 500 mg/L for sulfates, 50 mg/L for nitrates and 3 mg/L for nitrites.

There are several sources of water pollution:

- First, agriculture, which consumes more than 70% of the freshwater of the earth and releases pollutants (nitrates, perchlorates, pesticides, herbicides…) into surface and ground-water;
- Second, industrial activities, which release toxic compounds (zinc, lead, mercury, etc…) into the water;
- Finally, domestic activities, particularly the use of detergents, solvents, nitrogen organics, and other household chemicals.

Different strategies are employed to solve water pollution, such as lowering the use of fertilizers and pesticides, stopping the degradation of wetlands owing to overpopulation and urbanization, and minimizing deforestation because trees avoid rainwater vaporization and consequently aid in groundwater restoration. In addition to such solutions, one must consider the "zero wastewater" principle, which entails collecting rainwater in a permeable vessel and controlling

it. Because water is a renewable but finite resource, it is critical to conserve and regulate its usage. As a result, water management and economics should be implemented to protect this vital resource. The most water-intensive industries (food, beverage and tobacco, metals and mining, oil and gas) must implement strategies to limit their need. Every individual could make some economic adjustments to lower the amount of water consumed in daily activities. Limiting shower time, repairing water leaks, not leaving the water sink running needlessly, utilizing rainwater, and many other measures should be taken to reduce water consumption.

Water pollution is a major concern, and rules are becoming increasingly rigorous because of the need to find new ways to treat water pollutants. The main sources of water contaminants, as well as various depollution procedures, will be described in the next section.

I.1. Main source of pollutants in water

Water is considered polluted when various substances referred to as contaminants are present in excessive amounts. These compounds come from a variety of sources, including industrial reagents and co-products, agricultural fertilizers, mining effluents, coal combustion, sewage water, and many others. Human activities, as noted previously, are the primary sources of such pollutions. Because water pollutants are diverse and numerous, this paragraph will place a special emphasis on heavy metals and mineral anionic pollutants.

When metals like Cd, Pb, Zn, Cr, Cu, Ni, As, and Hg are discharged into the aquatic environment, they pose a serious risk. Because these contaminants are non-biodegradable and hazardous, they will build up in natural water and sediments, becoming more concentrated after each step of the food chains. For example, numerous invertebrates consume sediment and absorb dangerous heavy metals, which are then passed on to fish and humans leading to devastating impacts on the ecosystem [1], [2]. A number of factors influences heavy metal toxicity, including water pH, temperature, presence of biological species, and environment, among others. Copper, for example, tends to form complexes with organic ligands found in wastewater, making filtration easier while nickel tends to remain in the ionic form [3]–[5]. Aside from heavy metals, other anions, like phosphates, sulfates, nitrates and nitrites, resulting from the overuse of fertilizers and pesticides cause serious damage to the aquatic environment. Pollutants produced by the agriculture industry primarily cause eutrophication. Because these contaminants contain phosphates and nitrogen compounds, the amount of oxygen dissolved in rivers, lakes, and coastal zones is reduced causing negative consequences for oceanic species [6], [7].

I.2.Water treatments

Wastewater must be treated before being discarded in the environment, especially if it includes harmful compounds. To limit and avoid the presence of various contaminants in water, numerous procedures such as chemical precipitation followed by coagulation-flocculation, electrodeposition, ion exchange, adsorption, and others have been applied. A brief summary will be given of the different mentioned treatment methods.

Chemical precipitation: This technique requires four stages. First, the addition of reagents, second, coagulation-flocculation, third sedimentation and finally solid-liquid separation [8]. Such water treatment was commonly employed to remove heavy metals [9]. The first and second stages, involve converting the free form of metals to insoluble compounds by altering the pH of the medium and using different precipitant agents such as lime, calcium hydroxide and ferrous or aluminum sulfates depending on the metal to be removed [10], [11]. Some oxidizing agents such as potassium permanganate or dichromate can be used for the removal of organic impurities as well as for the multi-valence metals to change the oxidation degree before its precipitation. Suspended colloids were present in water throughout the coagulation process. Such particles have a surface charge depending on the pH value. To remove them, a flocculant with an opposite charge was added to the water, modifying the surface charges of these colloids, and inducing aggregates settling down as a result. The structure and charge features, ionic properties, molecular weight, and functional groups of the chosen coagulant/flocculant agent are all factors that influence the coagulation/flocculation procedure. This is why different coagulant/flocculant agents can be used depending on the coagulation/flocculation mechanism. Traditional coagulants such as aluminum sulfates, ferric chloride, poly-aluminum chloride, and others are employed because of the predominant insoluble suspension in water has negative charges. Synthetic and natural organic polymers, such as polyacrylamide (PAM), are frequently used as flocculants. Because the flocculation process relies on colloidal particles bridging after coagulation, polymeric materials with flexible and long chains were required.[12]–[14]. Chemical precipitation method generates sludge and needs to always be followed by physical methods in order to separate the sludge and the liquid phase. Sedimentation and decantation were frequently used for the removal of big flocs. This stage involves the holding of the waste in a tank and the separation of the solid particles and the supernatant liquid occurs under gravity. After that, filtration or centrifugation was performed in order to obtain pure filtrate, ready to be discharged in the environment.

Concerning the sludge generated due to the precipitation method, it was dried before being stored in landfills [15]. Even though this method can remove a variety of contaminants from water, it is restricted by the high consumption of chemical reagents, which leads to high operating expenses, as well as the regeneration of a large amount of hazardous sludge.

Electrochemical processes are environmental friendly methods used for the degradation of pollutants using the anodic reactions or the removal and recovery of heavy metals from wastewater. Direct oxidation, in which contaminants were eliminated on the surface of the anode, is part of the anodic process. This approach requires forming physically or chemically adsorbed oxygen sites directly on the surface of the anode, resulting to pollutant degradation by combustion of organic compounds (physically active oxygen sites) or by the participation in the formation of oxidation products (chemically active oxygen sites) [16]. Glassy carbon [17] , granular graphite [18], and MnO_2 [19] are among the materials that can be utilized to make the anode for this method.

Cathodic deposition and cathodic reduction are the two primary phases in the cathodic process [20]. Heavy metals such as Cd, Pb, Cu, and Cr were removed from wastewater using electrodeposition, and metals such as Pt and Au were recovered using electrodeposition. The cathodic reduction concept was based on the following reaction for metal recovery:

$$M^{n+} + ne^{-} \rightarrow M_{(s)}$$

Where M is the metal, n is the oxidation number of the metal and M(s) is the metal deposited on the surface of the cathode [21].

Electrodeposition is a technique that uses an electrolyte solution containing various metals. The electrolyte used varies based on the metals to be electrodeposited as well as the redox potential range. Copper, for example, is difficult to be electrodeposited using water as an electrolyte due to its low reduction potential, which causes water to decompose into hydrogen and oxygen. Copper electrodeposition, as a result, necessitates basic pH effluents [22]. Despite the benefits of electrodeposition techniques, most studies focused on synthetic effluents with a basic pH, whereas research on synthetic acid effluents used a combination of processes such as electrolysis and electro dialysis [23], [24]. As a result, extracting metals from real wastewater is more difficult to achieve only by electrodeposition.

I.3.Focusing on ion exchange and adsorption treatments

As previously stated, the various processes used for water treatment have significant limitations when compared to their ability to depollute water; for example, the cost of chemical precipitation and coagulation/flocculation processes, as well as the toxic waste produced, are more disadvantageous than their depolluting capacities. For real wastewaters, electrochemical processes are still under study, and their applications were confined to metallic contaminants and some organic compounds. Ion exchange and adsorption techniques allow wastewater depollution, as well as the regeneration of adsorbent/exchanger materials and the recovery of important pollutants. As a result, the following paragraph will go through ion exchange and adsorption procedures in greater depth.

I.3.1.Ion exchange

For the ions exchange process, many materials with surface charges were used. Resins, cationic and anionic materials with an exchange capacity are the most frequent ions exchangers. Ion exchange water processes rely on the ability of a solid phase and a gas or liquid phase to trap ions through charges interactions. This process has been used in a variety of treatments, including water softening, removal of toxic metals from water in the environment, wastewater treatment, and many others [25].

Let's take the example of resins to detail the principle of ion exchange: The first phase is the ion exchange resin, which is an insoluble phase in which an ion is electrostatically bonded to the cross-linked polymer matrix; when it comes into contact with the second phase, which is the liquid containing similarly charged ions, an ion exchange can occur. This exchange is affected not only by the charge of the ions, but also by its concentration and affinity for the insoluble phase (resin). Cation and anion resins were made based on the ion to be exchanged; the difference between the two resins is the polymers and ligands bound to the polymers used [25].

The reactions mentioned below describe the exchange process between the resins and the ions in the solution:

Anion exchange resin: $[Polymer] = X^{+A-} + B^{-} \rightarrow [Polymer] = X^{+B-} + A^{-}$

Cation exchange resin: $[Polymer] = Y^{-C+} + D^{+} \rightarrow [Polymer] = Y^{-D+} + C^{+}$

Where $[Polymer] = X^+/Y^-$ are the anion/cation exchange resins, A^-/ C^+ are the counter anion/cation respectively and B^-/D^+ are the exchanged anion/cation respectively.

Because ion exchange resins are insoluble in liquid, their separation after exchange is simple, using filtration or columns and chromatographic separations. Their insolubility makes them environmentally friendly because the cycle of exchange/regeneration/re-exchange allows them to be used for many years.

The ion-exchange principle was applied in a variety of materials, including zeolites, certain coals, clays, and a wide range of mineral species [26]. Many synthetic inorganic compounds, including layered double hydroxides, an anionic clay, composed of positively charged sheets with anions in the interlayer region, exhibit ion exchange behavior. As a result, LDHs can be used for anionic exchange applications. The interlayer anion will migrate to the substrate, allowing other anions in the solution to access the interlayer space [27].

I.3.2. Adsorption

This process is based on mass transfer, which results in the accumulation of substances at the interface of liquid-solid or gas-solid phases on the surface or in the pore network of the material. The adsorbate is the substance being adsorbed, and the adsorbent is the adsorbing material [11], [28]. Adsorption will occur due to the difference in attraction forces between the two phases. Depending on its chemical properties and its affinities within the two media, the adsorbate is shared between the solvent and the adsorbent.

Two types of adsorption can be distinguished based on the nature of the bond between the adsorbent and the adsorbate: physisorption, which is caused by physical forces, and chemisorption, which is caused by chemical forces.

The physisorption mechanism is based on Van der Waals, hydrogen and electrostatic bonds. Van der Waals forces are characterized by dipolar interactions between the adsorbate and the adsorbent. For the hydrogen bonding, the hydrogen atoms of the adsorbate and the oxygen atoms of the adsorbent are bonded with an energy of 10-15 kJ/mole. However, electrostatic forces are based on the attraction of opposite signs and can occur when the adsorbent and the

adsorbate are oppositely charged. Because the bonds are weak, the physisorption process is highly reversible.

In contrast to physisorption, chemisorption is based on a chemical reaction between the adsorbate and the adsorbent. The formed complex (adsorbent-adsorbate) remains on the surface. Because of the strong bond between the phases, the adsorbate is difficult to remove, resulting in an irreversible adsorption process [28], [29].

Table 1.Difference between physisorption and chemisorption [30]

Physical adsorption	Chemical adsorption
1- The forces are weak Van der wall's forces 2- The heat of adsorption is low about 20-40 Kj.mol^{-1} 3- The process is reversible either by increasing the temperature or decreasing the pressure 4- No activation energy is required 5- Not specific in terms of adsorbate nature 6- Multimolecular layers are formed	1- The forces operating are ionic or covalent bonds 2- The heat of adsorption is high about 40-400 Kj.mol^{-1} 3- The process is irreversible 4- Activation energy is required 5- Highly specific in nature, only occurs when the formation of chemical bonds is possible 6- Unimolecular layers are formed

This process is influenced by a variety of factors, most notably the surface area of the adsorbent, the solution pH, temperature, and adsorbate concentration.

Because adsorption is a surface phenomenon, the extent of adsorption is proportional to the specific surface area, which is the portion of the total surface area available for adsorption [31], [32]. As a result, the more the solid is finely divided and porous, the more the amount of adsorption accomplished per unit weight of the solid adsorbent increases [33]. The specific surface area and the adsorption capacity are proportional, which means that as the surface area increases, so does the adsorption capacity. Aside from the specific surface area of the adsorbent, the pH of the solution plays an important role in the adsorption process. The pH has an effect on the distribution of the surface charge of the adsorbent [28–31]. The adsorption of methylene blue (cationic pollutant with pKa = 3.8) on sawdust and crushed brick, for example, increases as the pH value increases. Adsorption decreases at lower pH (pH 5) [34] because both

adsorbents are positively charged at these pH values. For the adsorption of cadmium on goethite, an increase in the quantity of cadmium adsorbed at a pH range of 6-8, which is the pH value of many natural water and soils was observed [35], [36]. Another important factor to consider during the adsorption process is the temperature. Adsorption reactions are mostly exothermic; as referred to Le Chatelier's principle in order to increase the adsorption area, temperature should decrease [37]–[39]. This effect was also related to the water solubility of the adsorbent, because as temperature rises, so does water solubility, making adsorption on the adsorbent surface less favored.

Finally, the concentration of the pollutants present can influence the adsorption process. As long as the adsorption sites were not saturated, an increase in the initial concentration of adsorbate (heavy metals and most pollutants) leads to an increase in the adsorption capacity of the adsorbent. The higher initial concentration provides an essential driving force to withstand the mass transfer resistance between heavy metals and the solid phase [40]. Bhattacharya *et al.* [41], for example, investigated the adsorption of Zn (II) on various adsorbents. The initial concentrations of zinc studied were 10, 25, 40, 50, 80 and 100 mg/L using 10 g/L of adsorbent. The Langmuir model illustrates the chemical mechanism involved. It was demonstrated that increasing the initial concentration of Zn (II) leads to higher adsorption capacities. Malkoc *et al*. [42] found that increasing the Ni (II) concentration from 50 to 300 mg/L increased the adsorption capacity from 4.413 to 14.04 mg/g of bio sorbent extracted from tea plants waste .

In what follows, the exchange and the adsorption processes using LDHs and GOs respectively will be discussed deeply in this manuscript.

II. Layered double hydroxides (LDHs)

One of the most efficient water treatment processes is ion exchange, which is a property of many inorganic materials particularly cationic clays (*e.g.* montmorillonite) and anionic clays (*e.g.* layered double hydroxides). The structure and polytypes of LDHs, as well as the numerous synthesis methods and conditions for these materials, will be discussed in depth in this section. This paragraph will also cover the main properties and applications of those materials.

II.1. Generalities about layered double hydroxides

Layered double hydroxides (LDHs) also known as hydrotalcite-like compounds, are members of a large family of anionic clay materials with the general formula $\left[M^{2+}_{(1-x)}M^{3+}_{x}(OH)_2\ \right](A^{n-}_{x/n})\,.mH_2O$: where M^{2+} are the divalent cations, M^{3+} are the trivalent cations, A^{n-} are the interlayer anions which contribute to charge neutrality, x is the charge density proportional to the molar ratio $M^{3+}/(M^{2+}+M^{3+})$ with a value in the range of 0.2 - 0.33, m is the number of water molecules part of which are linked to the anions.

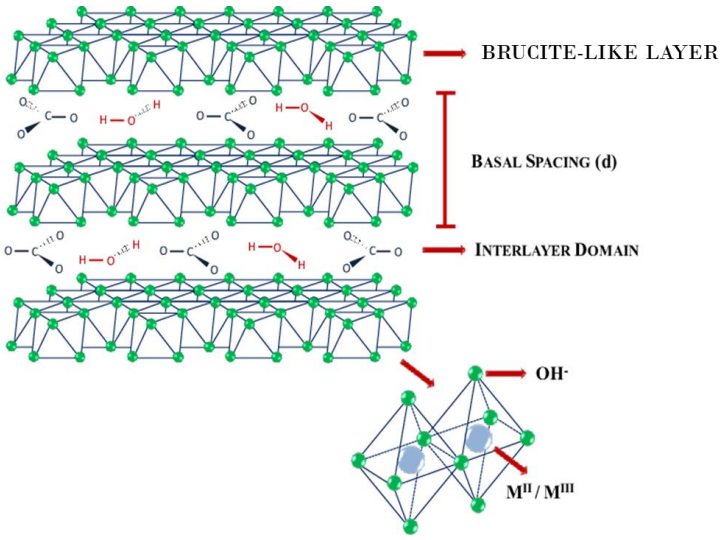

Figure.3. Layered double hydroxide representation [43]

LDHs are composed of brucite-like layers in which a fraction of divalent cations (Fe^{2+}, Co^{2+}, Mg^{2+}, Zn^{2+}, Cu^{2+}, Ni^{2+}) were replaced by trivalent cations (Al^{3+}, Cr^{3+}, Mn^{3+}, Ga^{3+}, Fe^{3+}), resulting in positively charged sheets [44], [45]. Divalent and trivalent cations are linked to hydroxyl groups in an octahedral coordination. The hydroxyl groups are oriented toward the interlayer region, which allows hydrogen bonds to form between the LDH layers and the interlayer anions and water molecules. LDHs can be synthesized using a wide variety of divalent/trivalent metals. The nature and the molar ratio of these cations along with the nature of the interlayer anions have an impact on the obtained LDHs. LDHs are synthesized using various methods of which the most used are co-precipitation, anionic exchange, and reconstruction. These synthesis pathways are simple to carry out [46]. LDHs can be found in

deposits as various mineral forms such as hydrotalcite $Mg_6Al_2(OH)_{16}(CO_3),4H_2O$ and pyroaurite $Mg_6Fe_2(OH)_{16}(CO_3)$, zH_2O [47].

II.2. Layered double hydroxides structure and polytypes

Since LDHs are formed of positively charged sheets, columbic attraction between the positive charge of the layers and the negative charge of the interlayer anions were responsible for the cohesive bond between metal hydroxide layers inside the LDH structure. The strength of such bonds is mainly proportional to the layer charges: when the substitution degree “x”, which is the fraction of trivalent cations replacing divalent ones, increases, the cohesive bonds will increase. Thus, the charge and the coordination symmetry of the interlayer anions affects the LDHs lattice. For example, the carbonate ions are intercalated with a plane symmetry parallel to the LDH sheets leading to a maximum hydrogen bonding between them [48], [49]. In this case, the basal spacing, which is the space between the brucite-like layers, decreases because of the coordination symmetry and electrostatic forces. In a hexagonal state, the distance between two metals is given by the parameter “a”; the distance between metal and oxygen is given by the "b" parameter, and finally the “c” parameter is related to the basal spacing ‘d’ of the material, correlated to the specific charge and geometry of the interlayer anion that affects the cohesion forces between the layers.

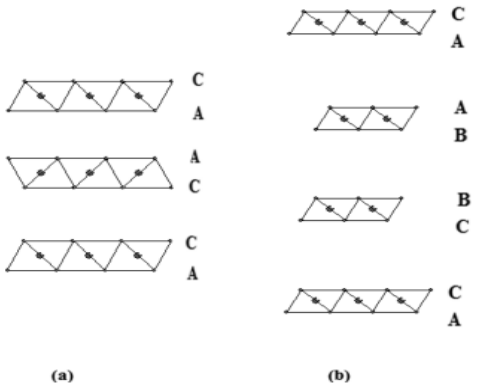

Figure 4. Schematic presentation of (a) $2H_1$ polytype and (b) $3R_1$ polytype [50]

The stacking of the layers presents three types: three-layer rhombohedral polytype (3R) devided into $3R_1$ and $3R_2$ polytypes, two-layer hexagonal polytype (2H) and one-layer hexagonal polytype (1H) also devided into $2H_1/1H_1$ and $2H_2/1H_2$. The most common and stable polytype for LDH stacking is 3R. These polytypes differ from each other by the nature of the interlayer sites generated. For example, the $3R_1$ and $3H_1$ polytypes generate trigonal-prismatic interlayer

sites, whiles, $3R_2$ and $2H_2$ polytypes generate octahedral sites. For instance, carbonated LDHs crystallize in $3R_1$ or $2H_1$ polytypes with prismatic interlayer sites (***Figure 4***). These kind of sites provide crystallographically well-defined sites for C and O atoms of the carbonate anion and facilitates the hydrogen bonds between the oxygen atoms of the carbonates and the hydroxyl of the layer. For other anions, different symmetries were expected for other polytypes [51], [52].

II.3. Synthesis methods of layered double hydroxides

Different synthesis routes were applied in order to obtain the desired LDHs with the required molar cationic ratios and interlayer anions. The most commonly used is the co-precipitation method because it is an easy way to obtain large quantities of LDHs. Anionic exchange and reconstruction, which also represents LDH properties (described in section **II.5. LDHs properties**), were used as well to synthesize LDHs. This paragraph will go in depth through the co-precipitation process, as well as briefly discusses the other methods for synthesizing LDHs.

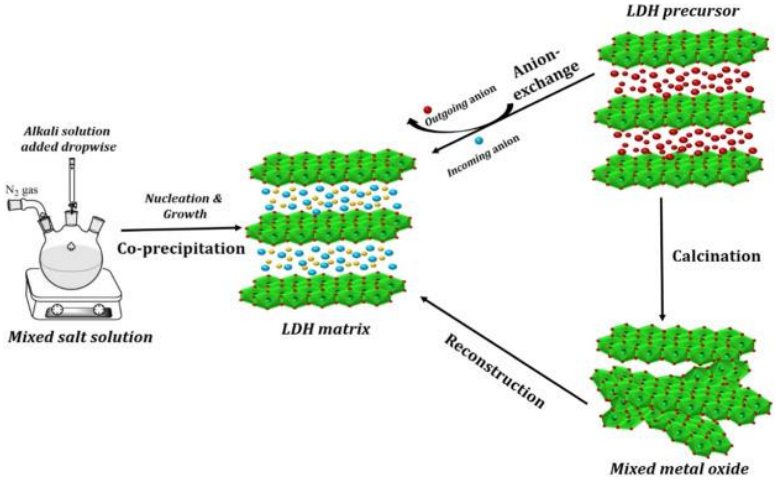

Figure 5. Illustration of the different synthesis routes of LDHs detailed in the following paragraph [53].

II.3.1.Co-precipitation method

This method is the most popular and simple way of making layered double hydroxides since it yields a large number of LDHs with a variety of interlayer anions and divalent and trivalent cations. This procedure involves adjusting the pH value to achieve the supersaturation of an aqueous solution while co-precipitation of the two or more cations (M^{2+} and M^{3+}) with the intercalating anion(s) (***Figure 5***) [54]. The co-precipitation method is based on the

condensation of complexes in solution to form brucite-like layers with a uniform distribution of metallic cations and interlayer anions. Particularly, the use of a pH that is either greater or equivalent to the pH, at which the most soluble cation hydroxide precipitates, is required. Usually, the co-precipitation method is followed by an ageing step during which the reactor containing the LDH suspension is heated at a temperature in the range of 273 K - 373 K over various durations (hours or days). This process is performed to increase the crystallinity of materials mainly those which are amorphous or badly crystallized [55].

Four distinct co-precipitation methods can be used for the synthesis of LDHs:

- Precipitation at constant pH at low supersaturation.
- Precipitation at constant pH value at high supersaturation.
- Precipitation at variable pH value.
- Urea hydrolysis method

Precipitation at low supersaturation

During this procedure, a reactor was filled with the solution containing the required interlayer anion(s) at the predetermined pH value. Metals precipitate in the form of LDHs by gradually adding the metal salt solution with the selected cationic M^{2+}/M^{3+} ratio in the anionic solution. Since the pH of the solution is supposed to vary because of the co-precipitation of the metallic cations, a second alkali solution (*e.g.* NaOH or, $NaOH/Na_2CO_3$) was also introduced to the anionic solution at a chosen rate in order to maintain a constant pH value. The addition of different solutions have to be controlled [47], [55] by using a manual or automatic titration device. The desired interlayer anion must have a high affinity for the LDHs and/or be present in the solution at high concentrations in order to be intercalated. Special attention must be paid to the counter-anion of the used metal salts. Since nitrates or chlorides have a low affinity for intercalating the LDH layers, they are often used as counter-anion of the introduced metal salts. Since CO_2 from the atmosphere can be rapidly dissolved into the solution and then intercalated in the LDH structure due to the strong affinity of LDHs for carbonate anions, synthesizing LDHs with anions having lower affinity compared to CO_3^{2-} (i.e, NO^-_3, Cl^-) may need an inert atmosphere [47], [55]. The co-precipitation at low supersaturation technique was used to synthesize LDHs with several intercalated anions and different metallic cations. For instance, carbonate-intercalated LDHs [56], [57], nitrate-intercalated LDHs [27], tetraphenylporphyrins-intercalated LDHs [58] , as well as pharmaceuticals or biomolecules-intercalated LDHs, such as vitamins (A, C, and E) [59], nucleoside monophosphates and DNA [60], nifedipine [61], and

many more can be synthesized. Using this approach, LDHs with diverse metal compositions, among which Mg/Al, Mn/Al, Zn/Cr, Ni/Al, and Co/Al [62], were also developed for a variety of applications.

Precipitation at high supersaturation

This method involves mixing an alkaline solution containing the chosen intercalating anion with a solution containing M^{2+}/M^{3+} cations. Due to the large amount of crystallization nuclei produced by high supersaturation, LDHs, obtained after co-precipitation are typically less crystalline under these conditions. After co-precipitation, ageing process was necessary as a solution for less crystalline or amorphous particles. This method was used to synthesize LDHs with different cationic metals. For example, Constantino *et al.* [63] made a series of Mg/Al LDHs with various interlayer anions, such as OH-, Cl-, and SO_4^{2-}, using the precipitation at high supersaturation method.

Precipitation at variable pH value

This method involves the co-precipitation of LDHs by adding alkaline solution (NaOH, Na_2CO_3, KOH...) to a metal salts (M^{2+}/M^{3+}) solution to reach the desired pH value. Using this method, the small particle sizes with good crystallinity and purity were obtained. First, trivalent cations precipitates under the form of metal hydroxides at low pH values (Fe^{3+} at pH=3.5 and Al^{3+} at pH=2.5). These compounds will act as reaction intermediate allowing the formation of LDHs at higher pH values. The synthesis of Mg/Al LDHs, for example, was performed using chlorided metal salts solution where NaOH solution was added to reach the pH value of 10. After the copecipitation of LDHs, a dialysis of the solid in water was performed for a month. Chloride ions were exchanged with carbonates coming from the dissolution of atmospheric CO_2 leading to crystallized LDH particles [64]–[66].

Urea hydrolysis method

The characteristics of urea make it an excellent precipitation agent. Urea is a weak Brønsted base (pKb = 13.8) and extremely soluble in water. Adjusting the temperature can easily affect the rate of urea hydrolysis, which is temperature dependent. The first step of the urea hydrolysis results in the formation of ammonium cyanate (NH_4CNO) [55]. The second

step is the fast hydrolysis of cyanate to ammonium carbonate, as demonstrated in the following reactions:

$$CO(NH_2)_2 \rightarrow NH_4CNO$$

$$NH_4CNO + 2H_2O \rightarrow 2NH_4^+ + CO_3^{2-}$$

The ultimate pH value of 9, which is ideal for the precipitation of a significant number of metal hydroxides, is produced by the hydrolysis of cyanate, resulting in the production of carbonates and ammonium ions. For instance, Costantino *et al.* [67] used the urea hydrolysis method to prepare M^{2+}/Al LDHs (M^{2+} = Mg, Zn, and Ni). It is observed that dissolving the solid urea in a solution of 0.5 M metal salts with a cationic molar ratio of $Al/(Al + M^{2+}) = 0.33$ and urea/metal ratio = 3.3 produces LDHs with high crystallinity. For 36 hours, the solution was kept at 100 °C. As the rate of urea hydrolysis is temperature dependent, the reaction temperature affects the particle size distribution. Due to the poor nucleation rate, bigger particles were produced at lower temperatures [68].

II.3.2. Ion-exchange method

Ion exchange is mostly dependent on the electrostatic interactions between the positive LDH sheets and the exchanging anions [55], [69]. This method works by exchanging the interlayer anions with the guest ones introduced in the solution.

The following equation is used to carry out the ion exchange process:

$$LDH.\ A^{m-} + X^{n-} \rightarrow LDH\ (X^{n-})_{m/n} + A^{m-}$$

Anions present in the solution, such as X^{n-}, were easily exchanged with LDHs initially containing anions such as chloride, nitrate, perchlorate, etc. that have weak electrostatic interactions with the layers. The affinity for incoming anions is one of several characteristics that affects the exchange process. Anions can be exchanged with other anions depending on their charge and ionic radius. The exchange ability will increase as the anions charge increases and their ionic radius decreases. For example, Bontchev *et al* [70]. studied the anionic affinity of different anions using Mg/Al-LDHs. During their study, the use of Mg/Al-Cl, Mg/Al-Br, Mg/Al-I and Mg/Al-NO_3 LDHs was applied. The experiment was carried out as follow, 0.5 g of Mg/Al-Cl LDH is dispersed in aqueous solution containing 1M of NO_3^-, Br^- and I^- for 12h at room temperature. After the exchange process, the solid was dissolved in sulfuric acid and then

analyzed using ion chromatography. The results showed that the monovalent anions affinity towards Mg/Al LDHs is as follow: $Br^- > Cl^- > NO_3^- > I^-$.This study also showed that 100% of anionic exchange could not occur since all the anionic exchange experiments showed the presence of a minimum of two anions in the interlayer region.

The anionic exchange process also depends on the pH value of the solution. For example, Li *et al.*[71] studied the effect of the synthesis pH on the nature of the interlayer anions of Ni/Al LDHs. It was shown that up to a pH value of 8, 97% of NO_3^- were present in the interlayer region leaving only 3% for carbonate anions. On the other hand, when the pH increased to reach the value of 9, 80% of carbonates were observed in the interlayer region.

II.3.3. Reconstruction of calcined LDHs

The reconstruction method is based on the memory effect of LDHs. It demonstrates the ability of the corresponding mixed MII-(MIII)O metal oxide to recover into their original layered structure. The mixed MII-(MIII)O oxide were obtained using a calcination process of LDHs. When a LDH loses progressively physisorbed water, then interlamellar water molecules, and finally the dehydroxylation of the layers, along with the interlayer anions, the collapse of the layered structure occurs leading to the formation of calcined LDH. The temperature at which this phenomenon occur depends on the chemical composition of the LDH; but generally, above 400 °C a mixed oxide is formed.

The reconstitution of calcined LDHs, is caused either by mixing metal oxides with aqueous solution containing anions, for example for 24 hours or by leaving the metal oxide in contact with the atmosphere. However, if the calcined LDH was only exposed to water or water vapor, LDHs with OH^- as charge compensating anions were obtained [72].

The calcination/reconstitution process is not very reversible. A study using Mg/Al LDHs showed that 20% of Al changed to a tetrahedral coordination instead of an octahedral position resulting in the formation of a small amount of amorphous Al_2O_4 spinel. Although, to form a spinel from a pure Mg/Al LDH phases a temperature of 800 °C is required. Hibino et al [73] noticed during their study that the quantity of carbonates, compensating anions, decreased after each calcination/rehydration cycle. This indicates that small amount of Al does not return in the LDH structure after calcination.

II.4. Influence of synthesis conditions using co-precipitation method

Co-precipitation is the most widely used method for precipitating a large variety of LDHs with different metals and interlayer anions. Consequently, a wide range of variables can have an impact on the precipitation of LDHs, as well as their form, nature, and purity. The following variables will receive special attention: molar cationic ratio, synthesis pH value, nature of the alkaline solution and ageing temperature and time.

Molar cationic ratio (M^{2+}/ M^{3+})

The obtainment of pure LDH phases is impacted by the molar cationic ratio used for the synthesis. For pure LDH phases, the M^{2+}/M^{3+} molar cationic ratio should be between 4/2 and 6/2. At higher ratios, impurities are formed along with LDH phases. The structural stability of LDHs is based on the combination of electrostatic forces and hydrogen bonds; the intensity of these interactions is related to the layers charge, the nature of the cations of the brucite layer and the interlayer anions. The increase of the layer charge (x) lead to the increase of the electrostatic interactions between the cationic layer and the intercalated anions resulting in significant contraction of the interlayer space. Grégoire *et al.*[74] studied the effect of the molar cationic ratio on the synthesis of M^{2+}/M^{3+} LDHs (M^{2+}: Co^{2+}, Ni^{2+}, Mg^{2+}, Fe^{2+} and M^{3+}: Fe^{3+}, Al^{3+}). These LDHs were prepared using the coprecipitation at constant and variable pH value method. The results obtained from the coprecipitation at variable pH value were discussed in this section. Chloride salts were dissolved in distillate water with a total concentration of 0.4M. To the metal salt solution, alkaline solution (Na_2CO_3 1M) was added at quick or low rate to reach the pH value of 9. They found that for x values higher than 0.33, some of the trivalent cations become first neighbors leading to a sensitive increase of the electrostatic repulsion in the cationic layer [74]. Except for Ni/M^{3+} LDHs, which can be formed at x of 0.09 and 0.33. Grégoire *et al.*[74] also proved that the increase in the x value leads to a decrease in the c parameter related to the interlayer distance. This is caused by the increase of the electrostatic attraction of the positively charged layers and the interlayer anions. For example, the decrease in the c parameter from 23.05 to 22.77Å and from 23.10 to 23.06 Å for Co/Al and Co/Fe LDHs respectively was observed.

Another study was performed using Zn/Al-LDHs [75]. The synthesis of this LDH was performed using the coprecipitation method where alkaline solution Na_2CO_3 was added to a mix of $Zn(NO_3)_2$ and $Al(NO_3)_3$ solution to reach a final pH value of 10. The Zn^{2+}/Al^{3+} cationic molar ratio ranges from 2/2 to 10/2. Whatever the molar cationic ratio, the precipitation of LDHs was achieved as demonstrated by XRD analysis. All samples displayed distinct and symmetric LDH phase reflections. An addition phase of ZnO was observed, appearing when the cationic molar ratio increases [75]. TEM analysis also showed the presence of nanorodes particles on the surface of the Zn/Al LDHs at higher cationic ratios (higher than 2) and were attributed to the ZnO phase. Another study performed by Ahmed *et al.* [76] who investigated the purity of the synthesized Zn/Al LDHs with the increasing cationic ratio. Similarly, to the previous study, Zn/Al LDHs synthesized using the coprecipitation method showed at higher cationic ratios the production of ZnO.

Synthesis pH

Another important parameter to consider while using the co-precipitation method is the synthesis pH value. This parameter highly influences the crystallinity, the morphology, the crystallite size and the nature of the interlayer anions. The study of the Mg/Al LDH with a cationic ratio of 4/2 by Seron et al. [77] showed that the synthesis pH value affects the crystallinity of the obtained LDH. At a pH value of 8.5, Mg/Al LDH were obtained with low crystallinity. Higher than pH value of 10, this study showed a total coprecipitation of LDH materials i.e. Mg^{2+} and Al^{3+} totally precipitate. Above pH value of 10 and until the pH value of 13 was reached, these authors showed that the crystallinity increases with the increase of the pH. This phenomenon is explained the amphoteric characteristic of Al, which causes the dissolution – reprecipitation of Al into the LDH structure leading to an increase in crystallinity and particle size of the LDHs.

The influence of pH on intercalated anions in the interlayer space was studied by Li *et al.*[71] on Ni/Al 4/2 LDHs. The obtainment of LDH phases has been observed from a pH value of 7. The measurements carried out by FTIR analysis on the solids synthesized at this pH value, showed the presence of nitrate and carbonate anions in the interlayer space with a strong preponderance of nitrate anions. Higher than the pH value of 7, and up to pH value of 13, the intensity of the absorbance band at 1384 cm^{-1} attributed to nitrates in the interlayer space decreases as the absorbance bands at 1375 and 1365 cm^{-1} attributed to carbonates increase. Additionally, this result was confirmed using DRX analysis. Indeed, the interlayer distance of

LDHs synthesized at a pH value of 7, d = 8.8 Å, which is in good agreement with the presence of nitrates in the interlayer space. At pH value of 10, the interlayer distance was equal to 7.8 Å, which is in agreement with the preponderant presence of carbonate anions in the interlayer space.

Nature of the alkaline solution

The precipitation of cationic metals to form LDH phases can be obtained using different precipitating agents such as alkaline solution like NaOH, Na_2CO_3, ammonia or urea. The alkaline solution affects the nature of the interlayer anion. For example, the synthesis of MgAl-LDH with the molar cationic ratio of 2 was performed using the coprecipitation method. The mixed metal nitrate salts solution was added dropwise to an appropriate amount of alkaline solution until a pH value of 10 was reached. For comparison, the LDH was synthesized using NaOH or ammonia as alkaline solution. The XRD pattern indicated the presence of LDH phases in both samples. The basal d-spacing obtained from the (003) and (006) planes depends on nature of the interlayer anion. For the sample prepared using the coprecipitation method with ammonia as alkaline solution showed d-spacing values corresponding to the presence of nitrates in the interlayer space generated from the nitrate salts used for the synthesis, while the use of sodium hydroxide as alkaline solution produced carbonated LDHs [55]. The presence of nitrates in the interlayer region was also confirmed using FTIR analysis as it shows a band at 1384 cm^{-1}. Note that ammonia inhibits the intercalation of carbonates since its dissociation in water produces OH^- and NH_4^+ ions. The ammonium ions obtained react with carbonate ions in the solution preventing their incorporation in the interlayer region [78].

Aging time and temperature

Aging is a stage, which consists on maintaining the synthesized LDH suspension, under mechanical agitation, at a temperature higher than the temperature chosen for the synthesis. This results in phenomena of nucleation reactivation and crystal growth [148] through the Ostwald ripening, which is the growth of particles by dissolution-reprecipitation phenomenon. Additionally, the high temperature increases Brownian motion of LDH particles. Under optimal conditions, this limits the aggregation of the coprecipitated nanoparticles. All these phenomena depend on a minimal temperature, chemical composition, physico-chemical characteristics of the precipitated species, the nature and concentration of the species dissolved in the medium and the viscosity of the suspension [79].

For instance, Xu et al.[80] demonstrated, for an Mg/Al-Cl 4/2 LDH, an increase in temperature from 80 to 125°C for 8 hours leads to particle growth from 90 to 125 nm. For a maturation period of 16 hours, the agglomerates were made up of particles having sizes greater than 4 µm at 125 or 150°C. Another study on Mg/Al-LDHs was made using the coprecipitation method (pH value not stated). The suspension was aged at 100°C for 2, 6 or 13 hours. As shown by XRD, the crystallite size increased with aging time as confirmed by the peaks, which grew narrower [81].

II.5. LDHs properties

II.5.1. Anion exchange

The anion-exchange features of LDHs are connected to its bidimensional structure and the type of weak interactions between the positively charged layers and the charge-compensating anions. The iono-covalent structure of the bonds is preserved during the anionic exchange process. The amount of anion per unit depends on the rate at which the divalent metals were substituted by trivalent metals, x. The ability to exchange anions is dependent on the molar ratio R= M^{2+}/M^{3+} and on the nature of the anions. The R ratio of the LDH sheets (M^{2+}/M^{3+}) has a great influence on the anionic exchange capacity (AEC) of the material. The more the mole fraction of trivalent cations increases, the more the anionic exchange capacity increases. Commonly, AEC is between 200-400 meq per 100g of LDH solid.

Delorme *et al.* [82] clearly demonstrated the influence of the cationic composition of Mg_4/Al_{2-x}-Fe_x LDHs on the anionic affinity. The Mg_4Al_2 LDH has an affinity for carbonate and sulfate anions, up to 90% and 10% respectively of the AEC. The gradual incorporation of the trivalent cation Fe into the LDH sheet modifies the percentage of carbonates and sulfates intercalated in the interlayer region. A solution containing carbonate, sulfate and nitrate anions with equivalent charges was used. When the substitution rate of Al with Fe reaches 75% and plus, these authors noted the intercalation of traces of nitrate anions. When Al were fully substituted with Fe, the quantity of nitrates in the interlayer was close to 4% and the quantity of carbonates and sulfates were 90 and 7% respectively.

II.5.2. Delamination

Only lamellar crystalline materials can experience delamination. It involves the unending expansion of interlayer space between LDH sheets, which yields stable colloidal solutions. One way to create positively charged thin sheets for usage as inorganic-inorganic nanomaterials [83], [84] or nano-composites for polymers [85], [86] is through the delamination of LDHs. The delamination of LDH sheets can occurs using various solvents such as butanol [87] and a low-density polyethylene solution in xylene [88]. These solvents are inserted between the LDH sheets leading to their exfoliation Wu et al.[89] showed that Mg/Al-NO_3 LDH were easily exfoliated in water under ultrasonic treatment using low LDH concentrations. The interlayer anion affects the delamination process, for example, the carbonated Mg/Al-LDHs did not exfoliated in formamide compared to the nitrated LDH, and that was due to the strong bonds between carbonate anions and LDH sheets compared to nitrate anions.

II.5.3.Thermal treatment

Metal oxides (MOs) are derived from the thermal treatment of LDHs in an intermediate temperature range, between 200 and 500°C [90], [91]. They are formed by the dehydroxylation of the LDH layer and the departure of interlayer anions. Two mechanisms are proposed for the formation of MOs from the calcination of LDHs. The first mechanism consists in the partial substitution of M^{2+} (i.e.Mg^{2+}) by M^{3+} (i.e.Al^{3+}) in the M^{2+}-O (MgO) network, which leads to a positive charge in the structure. Thus, the ions O^{2-} become unsaturated. For each insertion or substitution of a trivalent cation by a divalent one, two active M^{2+}-O (Mg-O) were formed. The second mechanism consists of a partial migration of the trivalent cation from the octahedral sites of LDH to tetrahedral sites in the structure of MOs during heat treatment. This departure of trivalent cations leads to octahedral vacancies and the formation of three active M^{2+}-O species around the trivalent cation [92], [93] occurs.

II.6. Different applications of LDHs

Since a wide variety of divalent/trivalent metals and interlayer anions can be used to generate LDHs, these materials can be used for a variety of aaplications, including wastewater treatment, ion exchangers, antacids, stabilizers for polymers, pharmaceutical and agricultural uses, catalyst precursors, electro-photoactivity, and more.

Environmental uses: Wastewater usually discharged in nature contains several pollutants such as phosphorus, nitrogen and much more. These cited pollutants are the main reason of eutrophication, which leads to the destruction of the aquatic species, causing harmful effects on the environment. Layered double hydroxides are promising materials for depollution processes since they showed i) tunable composition of the layers where the divalent/trivalent metals are present, ii) high anion exchange capacity due to the presence of exchangeable anions in their interlayer region and iii) controllable interlayer distance and dimension depending on the interlayer anions used. All these properties allows the use of LDHs for water depollution, especially for nitrate and phosphorus components. For example, Santos *et al* [94], studied the adsorption of nitrates using Mg/Al LDHs. For this, they prepared Mg/Al-Cl LDHs using the coprecipitation at constant pH value method until a pH value of 10 was reached. The initial concentration of nitrates used was 50 mg/L and the adsorbent dosage was 10 g/L. The contact time was 6 hours. They concluded that 18.17 $mg.g^{-1}$ of nitrates were adsorbed at 30°C and the equilibrium was reached within 10 min of contact time indicating the feasibility of Mg/Al LDHs towards nitrates adsorption. On the other hand, Zhang *et al* [95], synthesized Mg/Al-Cl LDHs using the coprecipitation method for the removal of phosphorus compounds. 76.1 $mg.g^{-1}$ of phosphates were removed using Mg/AL-Cl LDHs under 25°C using adsorption, ion exchange and electrostatic attraction processes. The anion exchange process was the main one among the others.

Drug delivery applications: LDHs are the center of attention of numerous studies due to the potential of their biomedical applications in the future. Some LDH materials were used for drug delivery because they are biocompatible and have minimal toxicity [96]. It can be used as drug delivery systems since the accessibility and stability of the drugs inside the carrier were both increased by intercalating it in LDHs [97].The ability of the LDHs layer to protect and release the desired drug on the targeted spots as well as to lessen drug degradation improves the bioavailability of the drugs [98].

Electrochemical uses for energy storage: The development of highly efficient electrical energy storage (EES) and delivery systems has been the main focus of researchers since fuel depletion began, driving the need to discover new cutting-edge methods of generating energy and electricity [99] was required. For this, specialized materials as LDHs can be used for the creation of supercapacitors (ECS). Supercapacitors have proven to be able to give higher

power density than batteries and can store more energy than conventional capacitors. The use of LDHs containing transition metals enhances the supercapacitors capability for charge-discharge cycles [100]–[102]. For example, Ni/Co LDHs were used as supracapacitor materials [103].

III. Graphene oxide (GO)

Adsorption is a highly effective method for the treatment of a variety of effluents, including wastewater, hazardous gases and the removal of heavy metals and pesticides from soil. Adsorbents, which can be diverse carbon-based materials such as graphene oxide (GO), activated alumina (Al_2O_3), silica gel (SiO_2), zeolites, and polymeric adsorbent were used for the removal of pollutants during the adsorption mechanism. Since carbon-based materials have good adsorption/regeneration properties, they are frequently used in the adsorption process. They can be classified into two categories. The first type is a porous carbon-based substance like activated carbons, where the adsorption is accomplished by π-π interactions. The second type of adsorbents includes the multilayered graphene oxide (MGO), which is a functionalized carbon material given with oxygenated groups, primarily weak acid groups capable of dissociating into $-COO^-$ ideal for the capture of metallic cations. MGO is an interesting carbon-based substance with cationic exchanger resin-like applications. A special focus on MGO will be given in the following paragraph where the discussion of its different synthesis methods, properties, cation adsorption, and various applications.

III.1. Generalities and structure

A graphene derivative having a two-dimensional network is called graphene oxide (GO). MGO was created when a C-O covalent bond was formed at the surface of the graphene structure [104]. Because of its capacity to form films, to remain exfoliated in water in the form of single atomic sheets, and to be converted back to graphene, GO is of a great interest. The use of GO in various applications, particularly in electronics, electrode materials, and conductive films, was made possible because of these properties [104]–[106]. Since there was no precise model that exemplifies the true structure of a GO, the GO structure is still a subject of discussion and each synthesis method can lead to different types of GO presenting slight differences in

their structure. GO may be produced through different oxidation mechanisms of graphite depending on the synthesis method used. Different techniques such as infrared spectroscopy, X-ray diffraction, NMR-C, XPS, elemental analysis and much more can be used to characterize GO but these techniques were not sufficient enough to define its structure. The amorphous, non-stoichiometric atomic composition are the primary causes of the unclear GO structure. Despite the fact that several barriers were encountered, the GO structure was determined using various structural models. For instance, the structure presented by Hofmann and Holst was made up of epoxy groups that were present on the basal surface of the graphite [107]. On the other hand, Ruess suggested that there might be hydroxyl groups in the basal spacing because the GO indicated the existence of hydrogen atoms. He also changed the Hofmann and Holst's sp^2 model to an sp^3 hybridization model of the basal plane [108]. Then, Scholz and Boehm proposed a model in which quinoidal groups in a folded backbone fully replace the epoxide and other groups [109]. The most current model was developed by Lerf and Klinowski, who focused on the nonstoichiometric and amorphous phases rather than lattice-based models. They mostly employed nuclear magnetic resonance (NMR) spectroscopy to prove that alcohols, epoxides, and carboxylic functional groups were present (***Figure.6***).

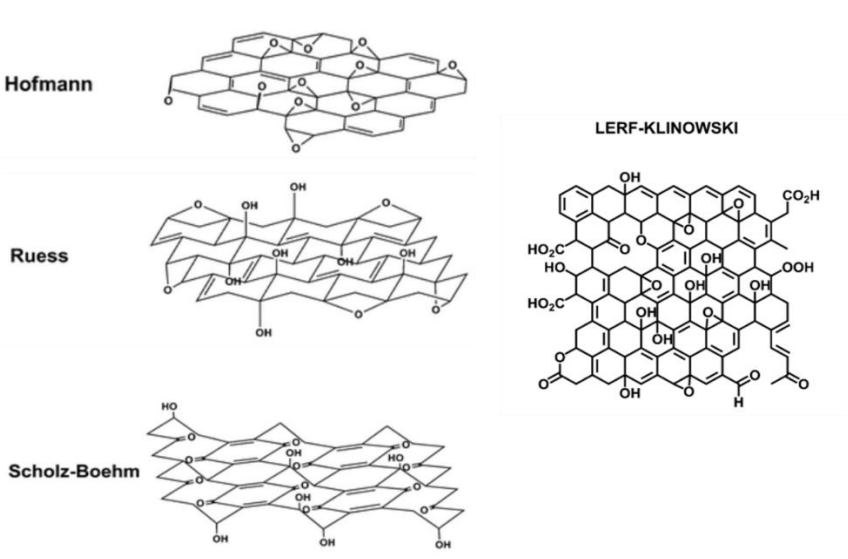

Figure.6. Summary of structural models of GO that have been proposed [104], [110]

There were significant distinctions between graphene and graphene oxide. The carbon atoms in graphene are in sp^2 hybridization while those in graphene oxide are in sp^2 and sp^3 hybridization mostly because of the creation of oxygen functional groups. This will have an impact on the chemical and physical reactivity and properties of the material; for instance, graphene has a higher conductivity than graphene oxide [111].

III.2. Synthesis methods

Due to the vast range of unique properties and potential uses in areas such as adsorption, catalysis, metal removal, and more, this material was used in a multitude of fields. Numerous synthesis strategies, such as chemical, electrochemical, and microbiological ones, were used to produce GO. These processes primarily involve exfoliation of graphite sheets followed by an oxidation step. The description of the different GO synthesis will be summarized in the following paragraph.

Oxidative exfoliation of graphite

Chemical methods:

Brodie method. In order to analyze the graphite structure, Benjamin Brodie developed this technique in 1859 by treating graphite with powerful oxidizers, a mixture of potassium chlorate and fuming nitric acid. The graphite was heated at 60 °C for three to four days in the presence of $KClO_3$ and HNO_3 mixture. Using the resulting product, this oxidative procedure was repeated several times (four to seven). The obtained product was primarily made of carbon, hydrogen, and oxygen. Brodie also made some further observations, where he noticed that the substance was soluble in pure water but floated in an acidic solution [112].

Staudenmaier, Hofmann methods. By altering the amount of sodium chlorate and including sulfuric acid in the mixture, L. Staudenmaier modified the Brodie's procedure. The primary function of sulfuric acid was to acidify the mixture, which will speed up the chemical process. Nitric acid fuming was harmful; hence lowering pH reduces the release of harmful gases like NO_2, N_2O_4 and ClO_2. The risk of an explosive by-product beneath the heat can be reduced by introducing potassium perchlorate in decreasing amounts over time as opposed to all at once. The substance that was produced using this technique exhibited similar qualities to the one obtained using Brodie's method [113]. Hofmann, on the other hand, created a safer technique employing non-fuming nitric acid and potassium perchlorate. However, in comparison to the other procedures, the produced GO had reduced levels of oxidation.

Hummer's method. This procedure was acknowledged as being the most significant in the field of chemical oxidative exfoliation of graphite. It was created by Hummers and Offman [114] and is the quickest and safest way to generate GO. Their technique involved overdosing

graphite with potassium permanganate, sulfuric acid, and sodium nitrate. The safe aspect of this approach was that no explosive ClO_2 was released during synthesis because no chlorate-based oxidant was used. By employing an H_2O_2 solution to neutralize the excess $KMnO_4$, non-toxic manganese and easily removed components were obtained, such as manganese sulfate salts and oxygen. However, hazardous gases like NO_2 and N_2O_4 were produced when nitrate sodium was present in an acidic media.

The previously mentioned approaches, developed by Brodie, Staudenmaier, and Hummers, demonstrated defective GO in terms of atypical forms, holes and the presence of impurities. These were mainly caused by the presence of covalent bonds formed between sulfur/nitrates and GO. However, the Hummer's technique was a simple process that can be used to obtain significant amounts of GOs.

Tour's method. This method is a modified Hummer's method, where the sodium nitrate was replaced by the phosphoric acid (H_3PO_4) [115]. This was an improved procedure for the preparation of GO with high oxidation degree. The phosphoric acid was a dispersive and an impregnate agent used to assist the oxidative chemical exfoliation of graphite in order to obtain GO. The GO obtained using Tour's method had higher oxidation degree, less impurities and more regular structure compared to those obtained through Hummer's, Brodie's and Staudenmaier's methods.

Electrochemical methods:

Large-scale synthesis of graphene oxide can be carried out using electrochemistry. It enables graphite to be oxidized and exfoliated into electrochemical graphene oxide (EGO). Compared to the chemical approaches previously mentioned, electrochemistry was a more environmentally friendly method of GO production since multiple electrolyte reuses and a reduced washing procedure result in less waste being produced [116], [117]. Comparing electrochemical to chemical approaches for GO generation enables the production of GO with less remaining contaminants, since using an aqueous electrolyte results in higher-quality GO [117]. Graphite sheets must be exfoliated as part of this procedure. When electrons were propelled into the graphite electrode under cathodic or anodic conditions, the electrolyte was forced to be intercalate between the graphite layers, which causes the exfoliation [116]–[118]. The application of an oxidation potential, which was necessary, will enable the formation of oxygen groups on the surface of the exfoliated graphite sheets.

Microbial methods:

Because microbial approaches typically entail inexpensive and environmentally acceptable processes, graphitic materials that have been oxidized by biological systems are now extremely important for practical applications. The graphite was not uniformly oxidized after being grown with bacteria and the exfoliated GO sheets from the bulk were suspended in the medium. As of now, research on the bio-oxidation of graphite has demonstrated that coming into contact with bacteria and graphitic materials encourages electron transfer and, consequently, oxidation. For instance, after three days at 30 °C in a $FeSO_4$, $7H_2O$ buffer solution, Acidithiobacillus ferroxidase can oxidize graphite [119]. Additionally, after 5 days in a nitration buffer medium with nitrifying bacteria, graphite can provide GO [120]. Despite being slow processes, biotransformation can produce multilayered GO materials with low oxidation degree containing carboxyl, epoxy and phenol groups. The size of bacterial cells is probably going to put a restriction on the effective oxidation range. Within a circle with a diameter of approximately 1 µm, one bacterial cell comes into touch with graphite. Same surface area may be exposed to oxidation several times, and the most extensively oxidized regions will be at the intersections of these circles, whose diameters are smaller than 1µm. Because of this, oxidation of graphite with an average particle size of 122 µm cannot occur uniformly, and some severely oxidized regions peel from the sheets to produce GO. The creation of holes, which were likewise less than 1 µm in size, was likely caused by the same factor that causes the bacterial destruction of GO [121].

III.3. Chemical and physical properties of graphene oxide

Based on the synthesis methods described above, GO exhibits various physical and chemical properties such as the production of various oxygen groups and the modulation of the stacking of GO layers. Additional characteristics were also investigated, such as the ability to create partly reduced GO and, the interactions between the functional groups of the GO and the solution (pH and pKa). The presence of impurities and metallic contaminants resulting from the synthesis procedure and chemicals affects the properties of GO. Such elements will be discussed later on.

III.3.1. Carbon/Oxygen ratio

GO is a carbon-based compound with a two-dimensional structure that contains oxygen and hydrogen atoms having a non-stoichiometric general formula of "$C_xH_yO_z$". When synthesizing GO, oxygen containing functional groups are created on the surface of the graphete

resulting in C/O atomic ratio. This ratio a crucial factor to take into account, it is typically between 1.5 and 2.5 [122]. The C/O ratio influences the hydrophobicity, chemical reactivity, electrochemical resistance, layer stability, and colloidal interactions of the GO [104], [111], [123]–[125]. Different characterization methods, including elemental analysis through flash-pyrolysis, high resolution X-ray photoelectron spectroscopy (XPS), thermogravimetric analysis (TGA), and others, were used to ascertain the atomic composition of GO. For example, TGA analysis performed at a heating rate of 10°C/min under Argon atmosphere showed three degradation stages for the GO. The first stage corresponds to a mass loss of 20% occurring below 100 °C corresponds for the evaporation of adsorbed water molecules. The second stage, which is roughly 30% of mass loss, occurs at a temperature of approximately 200°C attributed to the decomposition of unstable oxygenated groups such as hydroxyl, carboxylic and carbonyl groups. The final stage is seen around 620 °C with a mass loss of 40% mainly caused by the destruction of the carbon skeleton under argon atmosphere [126], [127].

Calculating the C/O ratio to compare various synthesis methods and environmental conditions was made possible by the deconvolution of the XPS peaks or by the determination of the carbon and oxygen percentage using elemental analysis.

Independently on the oxidation method used to obtain GO, carbon, hydrogen and oxygen were always present with different percentage as elemental analysis showed. The following table, shows the variation of the main elements of GO based on the synthesis method chosen.

Table 2. Elemental analysis of GO synthesized using Staudenmaier (GO-ST), Hofmann (GO-HO), modified Hummers (GO-HU) and Tour (GO-TO) methods.

Materials	C (%)	H (%)	O (%)	C/O
GO-ST	52.68	2.42	44.89	1.17
GO-HO	52.09	2.39	45.50	1.15
GO-HU	44.18	2.92	52.89	0.84
GO-TO	41.22	2.92	55.86	0.74

By comparing the different percentage of oxygen and carbon obtained as well as the C/O ratio, the synthesis methods using chlorate (GO-ST and GO-HO) showed lower oxygen content and higher C/O ratio than the synthesis methods using permanganate (GO-HU and GO-TO). This clearly shows the effect of the synthesis method on the obtainment of oxygen-rich GO.

XPS C_{1s} and O_{1s} spectra were also used for the identification of oxygenated groups and for the determination of C/O ratio. The deconvolution of the C_{1s} spectrum allows the determination of the different C bonds. The C-C, C-O, C=O, O-C=O and π-π* were assigned to the following binding energies of 284.80, 286.82, 288.30, 289.70 and 292.5 eV respectively. The deconvolution of the O_{1s} spectrum showed the presence of peaks with binding energies of 530.97, 531.77, 532.60 and 533,33 eV that can be attributed to the O-C=O, C=O, C-OH and C-O-C respectively. The determination of the atomic ratio C/O was also performed using the XPS analysis and was found to be 1.81. In comparison to the chlorate oxidation method, GO obtained through the synthesis methods using permanganate as the oxidizing agent had higher oxygen content [128], [129] .

III.3.2. Stacking

Carbon, oxygen, and hydrogen atoms were rearranged into monolayers with a thickness of 1 nm to create the GO solids [130].The thickness of the layers of GO fluctuates depending on the hydration level. GO particles can be produced in a variety of shapes, including spheres, flakes, sheets, and platelets [104], [111], [124]. A material with several layers made of variously stacked GO layers was called graphite oxide or multilayered graphene oxide MGO. The interlayer gap varies depending on the oxidation synthesis method used. As an illustration, the GO produced using the Tour's method revealed the biggest interlayer spacing of 0.95 nm [131], followed by Hummer's method (0.81 nm), Hofmann method (0.72 nm), and finally the Staudenmaier method, which yielded the shortest interlayer value of 0.71 nm [132]. Aside from the synthesis method employed, the interlayer can be affected by water, reagents, metals, and solvent molecules by attaching to the GO structure and thickening the interlayer space [133]–[135]. Depending on how many layers were present, the GO was given several classes. The stacking process was known as bi-layer when it involves two layers and tri-layer when it involves three levels. The GO was known as multilayered system above seven sheets stacked.

III.3.3. Interactions: pH and pKa

A single layer of graphite with diverse hydrophilic oxygenated functional groups is what is known as a GO sheet. Ionizable groups were predominantly near the edges of GO sheets, while hydroxyl and epoxide groups were mostly found on the basal planes. Due to their easily ionized carboxyl groups, the electrostatic repulsion between GO sheets prevented them from aggregating in an aqueous solution. When the pH of the solution containing GO sheets

decreases, the dispersion of GO sheets decreases in water because the hydroxyl and epoxy groups were not protonated at acidic pH values, therefore there were fewer repulsive forces, resulting in a decrease in the dispersion of the GO sheets [134]. Baskoro *et al.* [136] showed that the increase of the pH value leads to a more negatively charged surface (-24 mV at pH = 3 to – 38 mV at pH = 10). This phenomenon is caused by the deprotonation of the carboxylic groups. The zeta potential was between – 31 mV and – 33 mV in neutral pH value. Since the dissociation of carboxylic and hydroxyl groups occurs at pH values greater than 4, GO sheets were typically negatively charged and have three different pKa values, 4.3, 6.6 for acidic groups and 9.0 for phenolic groups [137], [138]. The usage of GO and long-term stability were both increased by the presence of high hydrophilic COOH groups. Moreover, the carboxylic groups increase the sorption ability for heavy metals of GO for environmental applications [139].

III.3.4. Impurities

There were two different types of impurities that were detected: the first type was caused by the synthesis process, and the second one was due to the metallic contamination coming from the chemicals utilized for the synthesis. The N, Mn, and S residues in the resulting graphene play a significant and active part in the electrocatalysis of oxygen. Since this process relies on using a great amount of permanganate, the GO synthesized using the Hummer's oxidation method for example, demonstrated the highest presence of these types of contaminants compared to the other synthesis methods[140].

It has been discovered that both natural and synthesized graphene contain certain metallic elements that were stacked or intercalated between the graphene layers. Even after oxidation and reduction processes, these contaminants persist in the samples [141]. Thermal or chemical processes were used to partially reduce such contaminants. It was demonstrated that Fe and Ni impurities present after the synthesis of GO can change the electrochemical characteristics, absorptivity, and redox potential of the GO. These metals also demonstrated significant catalytic effects used in toxicology [142].

III.4. Cations adsorption using GO

Different functional groups, including carboxyl, epoxy and hydroxyl, are present in the GO structure making it suitable for the adsorption of cationic metals (***Figure 7***). Zhao et al. [143] prepared graphene oxide (GO) using Hummer’s method. The obtained GO was used for

Pb^{2+}adsorption tests. The adsorption capacity was equal to 842 $mg.g^{-1}$ of Pb^{2+}. The adsorption capacity of GO regarding various water pollutants, particularly cationic metals, is generally influenced by various parameters such as the pH, contact time and ionic strength. The various elements influencing the adsorption of heavy metals using GO will be covered in the following paragraph.

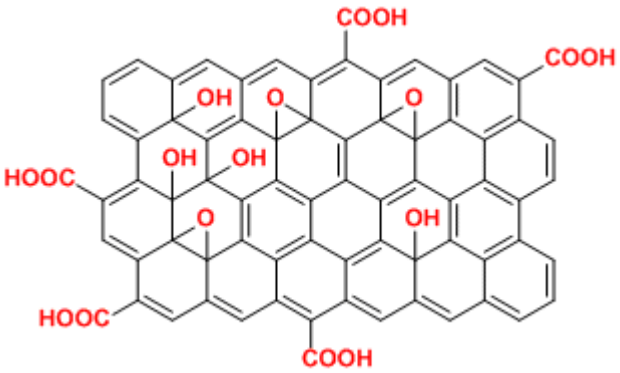

Figure 7. Illustration of graphene oxide [144]

Effect of the pH value. The choice of the pH value significantly influences the speciation of heavy metals present under either cationic/neutral or anionic form along with the protonation/deprotonation of the surface functional groups. When the pH value of the solution was higher than the pH_{pzc} of the GO (pH_{pzc} = 3.9), the surface was predominately negatively charged, this is why at these pH values, GO has the ability to adsorb cationic species and repulse anionic ones. Increasing the pH value of the solution will increase the adsorption capacity of GO facing the metallic cations present, for example, the removal percentage of copper increased from 20 % to 97.4 % when the pH value increased from 1.5 to 7 [145]. However, the forms of the metals in aqueous solution are $M(OH)_{n+2}^{2-}$, $M(OH)_{n+1}^{-}$, $M(OH)_n$, $M(OH)_{n-1}^{+}$, $M_xO_y^n$, and M^{n+}. The adsorption capacity decreased at higher pH values where the metals were present as $M(OH)_{n+2}^{2-}$ and $M(OH)_{n+1}^{-}$,due to electrostatic repulsion between negatively charged metals and negatively charged surfaces [146]. On the other hand, when the pH of the solution was lower than the pH_{PZC} of the GO, the surface of the material was positively charged leading to a very small sorption of anionic species and a repulsion of the cationic ones.

Effect of contact time. The mass transfer rate of contaminants during the adsorption process was significantly influenced by the contact time. The removal efficiency for the majority of metal ions initially rises sharply and then gradually until the contact duration was prolonged to approach equilibrium. The explanation for this phenomenon was that GO is first slightly porous, the carboxylate anions on the edges of the graphene sheets were easily accessible, and there

were initially sufficient adsorption sites on GO surfaces (***Figure 7***). As the contact time increases, fewer sites were available on GO surfaces, and the driving force for metal ions to the binding sites decreases, causing a slowdown adsorption behavior until the saturated adsorption capacity was reached [147]. For instance, White et al [145] investigated the impact of the contact time of copper using GO with a range of 0 to 120 minutes.

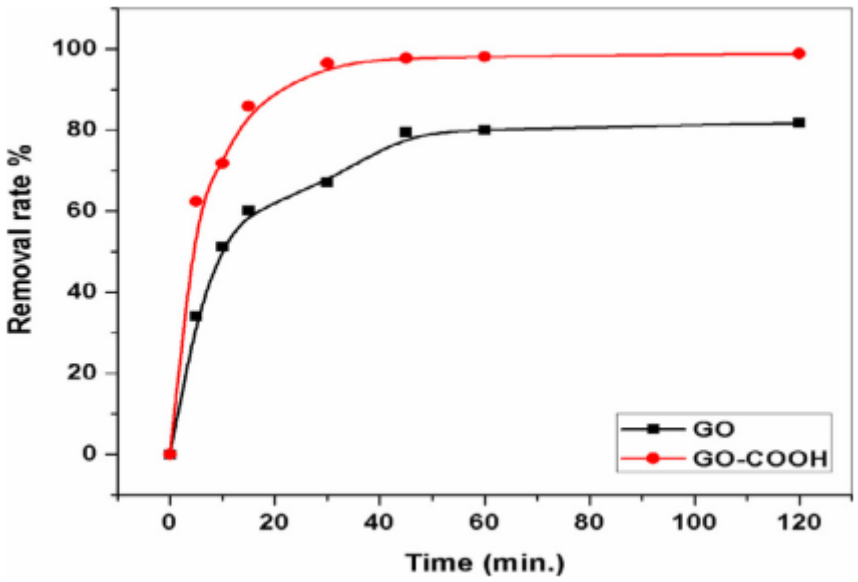

Figure 8. Effect of the contact time on Cu(II) adsorption using GO (black curve) [145].

At pH = 6 and at room temperature, the initial concentration of copper was 170 mg/L combined with 20 mg of GO. It was demonstrated that as contact duration increases from zero to 60 minutes—the time required achieving equilibrium—the adsorption capacity increases as well. Nothing has changed in terms of adsorption after 60 minutes. Copper absorption quickly increased until 15 minutes with a 60% removal rate. The number of vacant adsorption sites dropped after 15 minutes, which reduced the amount of copper adsorbed until equilibrium was established after 60 minutes with an 80% removal rate. Due to its low porosity, adsorption on GO was almost instantaneous (within few minutes) as compared to adsorption on porous activated carbons which needs higher contact times, several days, to reach equilibrium.

Effect of ionic strength. The presence of other ions in the solution affects the sorption capacity of the metals. Three main reasons explain the effect of the ionic strength on the sorption capacity:

1. The binding of metal ions to solid particles depends on their affinity; foreign ions will compete with contaminants for a limited number of reaction sites on solid particle surfaces, which lowers the adsorption capacity of the adsorbed material.
2. The electrostatic interactions between particles could be significantly impacted by the concentration of foreign ions, which would subsequently have an impact on particle aggregation and consequently on the specific surface of the adsorption.
3. Pollutant activity coefficients were impacted by the concentration of other metal ions, which limits the amount of pollutants that may migrate from aqueous solutions to adsorbent surfaces [143].

In general, before using GO based materials in practical applications, it is better to take into account the total concentration of various distinct metal ions in wastewater because the adsorption is impacted by ionic strength.

III.5. Different applications of GO

Graphene oxide as described previously is a highly functionalized material with lesser conductivity than graphene but conductor enough to be used in different electrochemical applications. These characteristics, together with others, made it possible to use GO in a variety of applications, including energy storage and conversion, absorbers, medical detections, electrochemical sensors and more importantly cations removal from wastewater. The ability of GO to have negatively charged surface; can lead to the removal of cationic metals by adsorption mechanism. For example, Zhao et *al*. [183] studied the removal of Cd (II) and Co (II) using GO as adsorbent. The GO was synthesized using the modified Hummers method, and characterized using different characterization techniques such as acid-base titration, XPS, FT-IR, TGA and many more. It was shown that increasing the pH value of the solution until 9, lead to an increase in the adsorption of Cd(II). About 98% of Cd(II) were adsorbed on the surface of the GO at pH values higher than 9. In the case of Co (II), the sorption of this cation slowly increases at pH values lower than 6, between pH 6-9, the sorption of Co(II) increases quickly. As the acid-base titration showed pH_{pzc} of the synthesized GO is equal to 3.9, at pH lower than pH_{pzc} the surface of the GO was positively charged since the protonation reaction between the oxygen containing functional groups (-OH) and H^+ cations ($=SOH+H^+ \rightarrow =SOH_2^+$) occurred. This will lead to an electrostatic repulsion between the cationic metals and the positive charge of the GO. At pH higher than pH_{pzc}, the surface of the GO was negatively charged because of the deprotonation process ($=SOH \rightarrow =SO^- + H^+$). With the increasing of the pH, the surface of the GO was more

negatively charged leading to stronger electrostatic interaction between the metals and the GO resulting in higher sorption. At pH lower than 8, the Cd(II) was predominantly present under the form of Cd^{2+} and its removal was mainly done using sorption. However, the precipitation of Cd(II) begins at a pH=9.1, where 90% of the Cd(II) were adsorbed on the GO surface. This is why; it was difficult to precipitate the remaining Cd (II) since it was present at low concentration in the solution. Speaking of Co (II), at pH lower than 8, Co(II) was present under the form of Co^{2+} and its removal was mainly accomplished using adsorption reaction. The precipitation curves of Co (II) showed that the precipitation of this metal begins at pH=8.2, therefore, at pH higher than 8.2, the sorption of Co (II) was partly done by precipitation. The maximum adsorbed quantity of Cd(II) and Co(II) on GO was 68.2 mg/g and 106.3 mg/g respectively.

IV.Chitosan

Chitosan is one of the most abundant biopolymer obtained from the deacetylation of chitin. It contains different functional groups such as amino and hydroxyl, which makes it usable in a variety of industries including food, biomedicine, and environmental remediation. This polymer can be used to create various films, beads, membranes, and other materials by dissolving it in organic acids (acetic acid). This paragraph will cover how chitosan was prepared, and then go through its chemical properties and various applications.

IV.1. Characteristics of chitosan

Chitin, the second-most prevalent polymer and nearly the only polysaccharide found in nature , is deacetylated to produce chitosan [148]. The source of chitin was mainly the skeletal remains of arthropods, crab, shrimp shells and certain fungus [149]. Crustaceans shell was made of 20-30% of Chitin, 30-40% of proteins, 30-50% of calcium carbonate and lipid colors such as carotenoids (astaxanthin, astathin, canthaxanthin, lutein and -carotene). These proportions change depending on the species and the season. Chitin and chitosan are linear polysaccharides with different amounts of acetyl (NH-Ac) and amino (NH_2) groups (***Figure 9***).

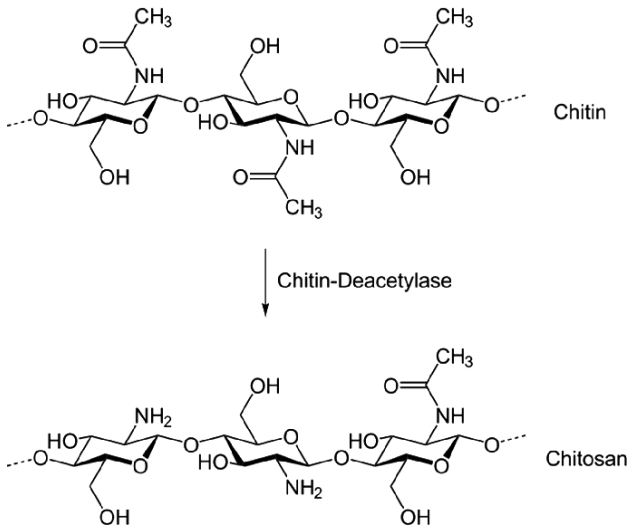

Figure 9. Chemical structure of chitin and chitosan [150]

Chitin is insoluble in acidic solution because it contains a small amount of 2-amino-2-deoxy-D-glucose. Contrarily, chitosan can dissolve in acidic conditions because of the large concentration of 2-amino-2-deoxy-D-glucose it contains and the free amino group present on its chains. According to certain studies, chitosan contains 60% 2-amino-2-deoxy-D-glucose residues [151].

In water-based or basic solvents, chitosan is not soluble. On the other hand, it has only a low solubility in inorganic acids but dissolves readily in organic acids. Chitosan also has a high water binding capacity, a high viscosity, and the ability to be used to create gels [152]–[154].

Inherent benefits of chitosan as a natural biopolymer include its biocompatibility, biodegradability, non-toxicity, inexpensive, and effective sorption qualities. Additionally, in particular, the free aminohydroxyl groups (***Figure 9***) allow water solubility, extraordinary protein affinity, gel-forming capabilities, heavy metal ion chelation capability, antimicrobial qualities, and simplicity of processing and modification [151].

IV.2. Preparation of chitosan: deacetylation degree (DD)

As was already discussed, chitin was extracted from various natural sources. However, due to the vast amount of waste produced as a byproduct of food processing, commercial chitins (α-chitin) were typically extracted from marine crustaceans like crab shells. The chains in α-chitin are stacked or arranged in sheets, with each sheet having a unique chain direction (anti parallel chain alignment). The α-chitin was connected to a lower carbonate concentration but a larger protein content in crustacean shells (***Figure 10***).

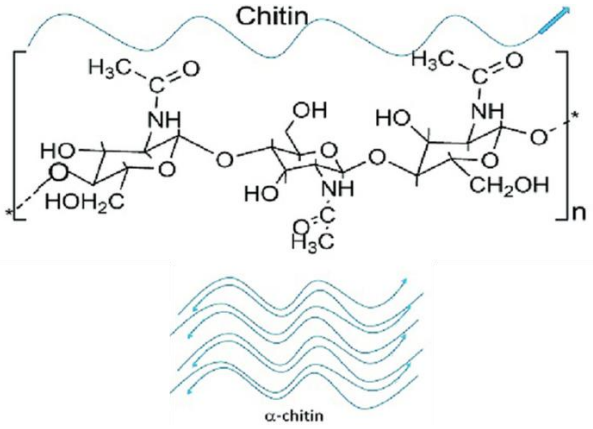

Figure 10. α-chitin structure [155]

Since crustaceans shell contains chitin, proteins, calcium carbonate and lipids, the extraction of chitin requires multiple procedures. First the dissolution of calcium carbonate in an acid solution was performed, following that the proteins were removed using alkaline solution, and finally depigmenting the result was required, primarily by removing the astaxanthin, to produce a colorless product [156]. After the removal of the unwanted molecules, chitin was obtained.

To partially deacetylate chitin in order to form chitosan, an alkaline hydrolysis treatment of the acetamide groups was required. This process was explained using the following equation:

$$R\text{-}NH\text{-}CO\text{-}CH_3 + NaOH \rightarrow R\text{-}NH_2 + NaO\text{-}CO\text{-}CH_3$$

The deacetylation process occurs when the reaction between the alkaline solution and the acetylate groups present on the polymer chains results in their removal.

The alkaline solution used was usually sodium or potassium hydroxides with a concentration of 30 - 50% w/v at a temperature of 100°C [157]. Generally, two methods were used for the formation of chitosan with different deacetylation degree. The first heterogeneous deacetylation includes a reaction with the amorphous part of solid chitin and was known as solid chitin deacetylation. This procedure calls for deacetylating chitin with NaOH 40 to 50% (w/v) at 100 °C for one to twelve hours. Deacetylated chitosan with an 85%–99% deacetylation degree results from this process. However, mixing alkali solution NaOH (40–50% w/v) with chitin under vacuum (by lowering the pressure) and allowing the reaction to proceed for 12–24 hours at room temperature will achieve homogenous deacetylation [158]. Different parameters such as the concentration of the alkali solution, particle size and density of the chitin, acid hydrolysis treatment, contact time and temperature the deacetylation degree. The particle size and density affects the penetration rate of alkaline solution into the amorphous region of chitin, which was

necessary for the hydrolysis to take place. For example, Liang *et al.*[159] studied the effect of alkaline concentration and temperature on the deacetylation degree of chitin extracted from shrimps. It was shown that the increase in temperature or alkaline concentration leads to an increase in the deacetylation degree, the optimal NaOH concentration was found to be 60% at a temperature of 107 °C, using 26 mL of NaOH for each gram of chitin. The contact time required to obtain the maximal deacetylation degree rate was two hours.

IV.3. Properties

Chitosan is considered a strong alkaline polysaccharide, with a cationic character in acidic medium. It is the only naturel cationic polyelectrolyte [160]. Because there are so many hydroxyl and amine groups at the level of the glucose units in chitosan, it is both a hydrophilic polymer and a polar molecule. It is interesting to note that each glucosamine in chitosan has three reactive groups: one NH_2 group and two OH groups (***Figure 9***). These functionalities are particularly used for grafting, alkylation, cross-linking and other chemical reactions with aldehydes and ketones [161] [162]. Moreover, the presence of free amine groups (pKa = 6.5) along the chitosan chains which are able to protonate and combine into the soluble $R\text{-}NH_3^+$ form, enhances its dissolution in diluted acidic solutions [150], [157]. These amino groups, positively charged between pH= 3 and 6.5, allow their electrostatic interaction with negatively charged chemicals. Regarding the basic pH values, these amino functions are neutral allowing them to form covalent amide or imine (R-NH-R) bonds with other components [163].

IV.3.1. Solubility

Chitosan is the only commercially available cationic biopolymer that is soluble in diluted acidic solutions at pH values below 6.5, but insoluble in neutral and alkaline aqueous solutions [164], [165]. The presence of an amine group in the carbon chain with a pKa value of 6.5 gives the chitosan an acid-base behavior [166].

As mentioned previously, at pH values lower than 6.5 (pKa of amino groups), the NH_2 of the chitosan chains are positively charged leading to a water-soluble polymer. Acidic solution, such as acetic acid [167], has been frequently used to protonate these amino groups. However, at pH

values higher than pKa, the amino groups were no longer protonated leading to an insoluble chitosan molecule.

It is well known that the solubility of chitosan in water is affected by deacetylation degree and molecular weight. When the deacetylation degree increases, the amino groups also increase, leading to the enhancement of its water solubility. Cho *et al.*[168] studied the effect of the deactylation degree on the solubility of chitosan, and it was found that, when the deacetylation degree was 49%, chitosan was water-soluble compared to 28% where acid solution was required to solubilize the biopolymer. On the other hand, the lower the molecular weight (MW) of chitosan is, the more soluble it is in water. It has been demonstrated that chitosan with MW lower than 30 kD showed water solubility without the need of acidification process. Nevertheless, when the MW is higher than 30 kD, the use of acidic solution was required to protonate the amine groups in order to obtain water soluble polymer.

IV.3.2. Chemical properties

Stability of chitosan. The characteristics and behavior of chitosan were very susceptible to several experimental conditions affecting its stability. Various factors should be considered, including the deacetylation degree, the molecular weight of the chitosan, the concentration of acid used for the hydrolysis, the concentration of polymers and others. For example, the use of diluted acid for the hydrolysis of chitosan was important, 1% in terms of mass concentration of lactic acid was enough to obtain a good hydrolysis reaction without causing a deactetylation of chitosan at a prolonged time. The molecular weight of chitosan used affects the hydrolysis rate, for example, a solution of 1% of chitosan was used due to its low viscosity. When the chitosan has a low MW, a solution containing 2% of chitosan was used. The study of the effect of temperature and of the MW of chitosan on the hydrolysis rate was performed. It is shown that increasing the temperature from 8 to 37°C increases the hydrolysis rate of 25 to 50%. The chitosan having higher MW showed higher hydrolysis rate than lower MW chitosan (5-10%). At equal MW but different deacetylation degree (15, 33 and 47%), the higher the deacetylation degree is the higher the hydrolysis rate [169].

On the other hand, the thermal stability of chitosan was also studied using TGA analysis at 10°/min between 30°C and 950 °C. It was shown that the maximal degradation rate of chitosan occurs at a temperature of 280.5°C. When the deacetylation degree increases the

thermal stability of the chitosan decreases leading to a maximal degradation temperature lower than 280.5 [170].

Chemical modification. Because of its hydroxyl functionalities and primary amine, chitosan has a wide range of chemical functionalization options. The active amine and hydroxyl groups of the biopolymer chain allow it to interact with specific chemical agents altering its structure. Due to their electronegativity, which was higher for oxygen than nitrogen, OH was more likely to engage in a nucleophilic reaction than nitrogen, giving rise to formation of covalent bonds [214], [215]. These include simple changes like N and O substitutions as well as copolymerization *via* free radical grafting. These changes have been suggested to enhance the inherent qualities of chitosan, including pore size, chemical stability, hydrophilicity, and mechanical resistance, even adding new qualities [171]. Chemical modification using cross-linking agents such as glutaraldehyde, dialdehyde etc... allows the formation of chitosan under the form of films, nanoparticles and so on. In fact, these different forms of chitosan make them useful for different applications. In this context, Jiang *et al.* [171] studied the effect of polyacrylic acid sodium (PAAS) used as co-spinning cross-linking agent on the preparation of uniform chitosan nanofiber. It was proven that the increase in the PAAS concentration causes a decrease in the viscosity of the chitosan, which will make the electrospinning process easier. The change in the form of chitosan composite was observed by increasing the PAAS concentration. In fact, changes in the chitosan shapes from beads to beaded-nanofibers to uniform nanofibers with a diameter of 389 ± 140 nm was observed when the concentration of PAAS reached 4 wt%.

IV.4. Different applications

As previously mentioned, chitosan has the ability to form positive polyelectrolyte by the protonation of the amino groups present on the surface of the chains when the pH was higher than 6.5 (100% protonation at pH=8.5). Besides using chitosan under the positive form, neutral form of chitosan can also be used to adsorb metals using the free pair electrons on the nitrogen atoms. Taking also into account the possibility of tuning its shape (beads, nanofibers etc…), the chitosan is highly used in various applications such as food [172], biomedical [173], [174] and wastewater treatments [175]. A special focus on the wastewater treatment is detailed in the following paragraph.

Wastewater treatments. Due to the possible toxicity of the latter to humans, the chemical contaminating of water by a wide range of harmful chemicals, such as metals, aromatic compounds, dyes, and so on, is a severe environmental issue. It is highly desirable to use inexpensive and bio sourced polymers like chitin and chitosan to remove water contaminants[175]. The adsorption process, mainly used for the removal of pollutants, requires an adsorbent material. Chitosan, being a functionalized biopolymer, is an efficient adsorbent material used for the removal of metals ions [176], [177].

The study of the adsorption of different heavy metals including copper, lead, cadmium etc.. and anionic pollutants such as nitrates and phosphates using chitosan or chitosan derivatives adsorbents was discussed.

Zhang *et al* [178]. studied the adsorption of copper using chitosan membranes. This experiment, conducted at room temperature at a pH value of 6, showed that the adsorption of Cu(II) rate increases the first 20 minutes and then stabilizes at 93%. 20 minutes was the required time to saturate the chitosan adsorption sites. The pH of the solution plays an important role in the adsorption process. The adsorption was performed using the electron pairs on the nitrogen atom of the amino group. At acidic pHs, the amino groups were positively charged ($NH_2 + H^+ \rightarrow NH_3^+$), this positive charge will cause an electrostatic repulsion between the amino groups and the Cu^{2+}cations limiting the adsorption of this metal. Increasing the pH value will lead to the creation of neutral amino groups (pka=6.5) for a better Cu^{2+} adsorption.

The adsorption of nitrates and phosphates has been also studied, where 100 mg of magnetic-kaolin chitosan beads were used. Different parameters affecting the adsorption process such as contact time and the solution pH value were investigated. The required time to reach the equilibrium was 40 minutes for phosphates and nitrates. The optimal working pH range was compromised between 3 - 7, because at this range, the beads were positively charged and the phosphate were under the form of HPO_4^{2-} and nitrates under the form of NO_3^- leading to an electrostatic attraction between them [179].

V. Hybrid materials based on chitosan

As previously discussed, chitosan is dissolved at low pH values to form gels, beads, films, and much more. It is most notably used for the purification of water by adsorbing anionic and cationic contaminants. Additionally, to chitosan, other materials, such as graphene oxides

and layered double hydroxides, can be included into the chitosan gel used as adsorbent. The synthesis of pure chitosan materials in the form of beads, as well as chitosan/graphene oxide and chitosan/layered double hydroxide two components beads were discussed in the paragraph that follows.

V.1. Structural properties of chitosan (beads formation)

Chitosan obtained under the form of flakes has low-porosity and low surface area. For adsorption purposes, the modification of chitosan chains by forming hydrogels or adding cross-linking agents was required to obtain more internal sorption sites. The conversion of raw chitosan flakes into beads leads to the improvement of the adsorption capacity of the material by increasing the porosity and the surface area of the chitosan. The chitosan beads were usually formed by dissolving the chitosan flakes in an acidic solution. This step will allow the protonation of amino groups that will lead to interactions with water molecules, forming water-soluble composite. The solution was then injected in an alkaline solution to obtain chitosan beads. The alkaline solution will neutralize the acetic acid present inside the beads and leading to the coagulation of the chitosan in spherical form.

A study about the adsorption of Fe (II) was conducted using chitosan beads [180]. The adsorption process, as explained before, was highly impacted by the pH of the solution, since at low pH (<6.5) values amino groups were positively charged, causing a decrease in the adsorption of Fe (II). On the other hand at pH values higher than 7, the removal of Fe(II), will be performed using precipitation process instead of adsorption process. It has been shown that the highest adsorption capacity, 45 mg/g of Fe (II), of chitosan beads was obtained at pH value of 5 using 10 mg of chitosan beads, where 40 minutes were required to reach the adsorption equilibrium. [180].

V.2.Chitosan/graphene oxide beads

Graphene oxide, which was described in ***III. Graphene oxide (GO)***, has many functional groups able to be negatively charged such as carboxylic groups, and are used for the adsorption of cations present in wastewater by primarily electrostatic attractions. A hybrid material composed of chitosan and graphene oxide could therefore combine the adsorption properties of both components for the adsorption of wastewater pollutants. For this purpose, chitosan gel (acidic solution), was used to combine chitosan and graphene oxide through electrostatic forces between the negatively charged functional groups of the GO and the

positively charged amino groups (NH_3^+) of the chitosan at acidic pH [181], [182]. ***Figure 11*** shows the possible bonds between the amino (NH_3^+) of chitosan and the carboxylic acid (COO^-) of GO involved in the interactions between the two adsorbents [181], [183], [184].

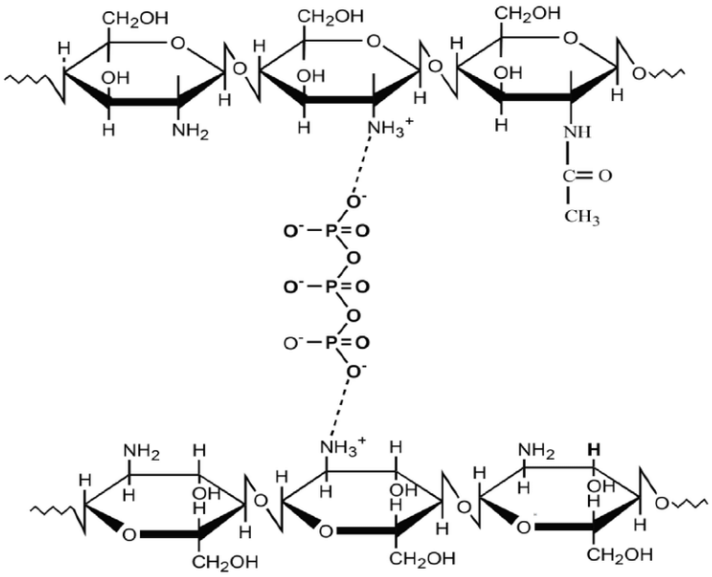

Figure 11. Possible interactions between chitosan and GO network [185].

To obtain the hybrid solution, chitosan flakes were dissolved in acetic acid, which was then thoroughly combined with GO using sonication or vigorous shaking to create a homogeneous slurry. The beads were then formed by dropping the gel in a NaOH solution. Exfoliated and non-agglomerated GO sheets were found in the chitosan matrix according to various investigations, including XDR, TEM, and FTIR characterization [186]. This obtained eco-friendly, cost-effective and recyclable hybrid network has been widely used for a variety of applications such as medical [187], [188], food and water treatment.

For instance, heavy metals present in wastewater can be removed using GO material, because it contains negatively charged oxygen groups (COOH). Although GO was quite effective at removing heavy metals from water, its separation from the water after pollution removal constitutes a serious issue. One of the most effective solution consists in embedding the GO in a eco-friendly biopolymer matrix, This allows not only an easier material recovery but also a better performance. In fact, the chitosan together with the GO particles has the ability to adsorb hydrophobic aromatic molecules and also to adsorb metallic ions on dissociated carboxylic groups. In addition, chitosan can decrease the overlaps between graphene sheets and prevents agglomeration, increasing the surface area, which increases the adsorption capacity [189].

V.3.Chitosan/LDHs beads

LDHs, known as anions exchangers, were discussed in section II.1, can be used in wastewater treatment to remove harmful anions. However, LDHs require a lot of energy to be separated from the treated water using a filtration process causing a rising of expenses in the depollution process.[190]–[192]. To solve this issue, various investigations on the inclusion of an adsorbent in various materials, such as chitosan, were conducted. These embedded sorbents demonstrated greater sorption capacity and kinetics since the production of sorbents with increased surface area are obtained. Furthermore, they can be obtained with variable porosity, and a variety of chemically reactive surfaces [193]–[195].

Li *et al.* [196] revealed two methods for the elaboration of chitosan/Mg-Al LDH beads. First, combining the Mg-Al LDH powder and chitosan gel in a syringe. Followed by adding the mixture to an alkaline solution after that (NaOH). In the second method, LDH precursors were mixed with chitosan gel before it was dipped into NaOH solution. The alkaline solution was added to enable the formation of LDHs phases inside the chitosan beads. XRD studies revealed the presence of LDHs in the formed beads. The sorption of Mg^{2+} and Al^{3+} on the functional groups of the chitosan chains provides an explanation for the integration of LDHs in the chitosan gel [196].

Lyu *et al.*[197] studied the adsorption of Pb^{2+} and Cd^{2+} using chitosan/Mg-Al layered double hydroxides beads. Chitosan powder was mixed with Mg/Al LDH in an acetic acid solution. The pH was then regulated at a value of 9 using NaOH 0.1M solution. The interlayer anion was manily carbonates. 0.05g of CS/Mg-Al beads used lead to the adsorption of 99.59% of Pb^{2+} (initial concentration = 300 mg/L) and 99.93% (initial concentration = 100 mg/L) of Cd^{2+}.At a pH value of 6, the adsorption equilibrium for Pb^{2+} was reached within 10 minutes of contact time compared to Cd^{2+} with 60 minutes of contact time. In order to understand the adsorption mechanism, XRD analysis has been carried out showed. The results showed that, after adsorption of Pb^{2+} and Cd^{2+}, new peaks were identified as $Pb_3(CO_3)_2(OH)_2$ and $CdCO_3$, which were formed when the cationic metals were incorporated in the interlayer region and interacted with carbonate anions.

VI. Positioning of this work

The objective of this first chapter was to explain the significance of water, the primary sources of pollution, the many depollution techniques, and the various materials used to depollute water. This PhD work focused mainly on the adsorption and anionic exchange processes employing multilayered graphene oxide (MGO) and Co/Fe layered double hydroxide grouped in a chitosan matrix. When it comes to cationic and anionic contaminants, the adsorption and anionic exchange processes were thought to be the most effective, environmentally acceptable, and reasonably priced methods that may be used for water depollution.

For layered double hydroxide, several techniques were used to synthesize these anionic clays, but the co-precipitation method using metal salts solution and alkaline solution ($NaOH/Na_2CO_3$) was particularly important. The characteristics of LDHs included anionic exchange, delamination and memory effect, were the major cause for their broad range of usage, especially for environmentally beneficial ones like wastewater depollution. The Co/Fe based LDHs were chosen in order to obtain electroactive materials for regeneration purposes using electrochemistry. Additionally, the usage of carbon-based compounds like graphene oxide (GO) in the adsorption process is very common. Because the functional groups produced were used in the adsorption process, particularly for the removal of cationic metals from wastewater, GO was synthesized using many ways, most prominently the modified Hummers method.

The elaboration of the composite under the form of beads was worthwhile because they are homogeneous in terms of adsorbent content and simple to handle. The creation of such beads requires the usage of chitosan, a biopolymer made from chitin. Chitin taken from crustaceans was deacetylated to produce chitosan. Since this biopolymer contains amino groups and was employed for cations adsorption in water depollution, it formed a positively charged electrolyte once dissolved in acetic acid. Chitosan can be obtained under the form of particles, gels, beads, and more. Due to this property, it was used particularly in the elaboration of beads for the adsorption of various water pollutants.

Specifically, for the removal of ions contaminants from wastewater, the anionic exchange using LDHs and the adsorption process using chitosan and GO demonstrated good results. To research the effectiveness of this combination in terms of the adsorption of pollutants and the investigation of the parameter controlling this process, the combination of these three adsorbents has to be performed and improved.

In order to study the capture process on various anionic pollutants (sulfate, nitrate, and nitrite) and cationic pollutants (zinc), pure and effective adsorbent must be synthesized, characterized, and combined with chitosan matrix under the form of beads for industrial applications.

VII. References

[1] A. M.k, I. S, R. S, H. M, and I. M.m, 'Heavy Metals In Water, Sediment And Some Fishes Of Buriganga River, Bangladesh', vol. 4, no. 2, pp. 321–332, Jan. 2010.

[2] L. Wang, Y. Wang, C. Xu, Z. An, and S. Wang, 'Analysis and evaluation of the source of heavy metals in water of the River Changjiang', Environ. Monit. Assess., vol. 173, no. 1–4, pp. 301–313, Feb. 2011, doi: 10.1007/s10661-010-1388-5.

[3] H. Karadede and E. Ünlü, 'Concentrations of some heavy metals in water, sediment and fish species from the Atatürk Dam Lake (Euphrates), Turkey', Chemosphere, vol. 41, no. 9, pp. 1371–1376, Nov. 2000, doi: 10.1016/S0045-6535(99)00563-9.

[4] A. Demirak, F. Yilmaz, A. Levent Tuna, and N. Ozdemir, 'Heavy metals in water, sediment and tissues of Leuciscus cephalus from a stream in southwestern Turkey', Chemosphere, vol. 63, no. 9, pp. 1451–1458, Jun. 2006, doi: 10.1016/j.chemosphere.2005.09.033.

[5] J. M. Bubb and J. N. Lester, 'The impact of heavy metals on lowland rivers and the implications for man and the environment', Sci. Total Environ., vol. 100, pp. 207–233, Mar. 1991, doi: 10.1016/0048-9697(91)90379-S.

[6] W. Werner, 'Fertilizers, 6. Environmental Aspects', in Ullmann's Encyclopedia of Industrial Chemistry, John Wiley & Sons, Ltd, 2009. doi: 10.1002/14356007.n10_n05.

[7] H. J. M. van Grinsven, H. F. M. ten Berge, T. Dalgaard, B. Fraters, P. Durand, A. Hart, G. Hofman, B. H. Jacobsen, S. T. J. Lalor, J. P. Lesschen, B. Osterburg, K. G. Richards, A.-K. Techen, F. Vertès, J. Webb, and W. J. Willems, 'Management, regulation and environmental impacts of nitrogen fertilization in northwestern Europe under the Nitrates Directive; a benchmark study', Biogeosciences, vol. 9, no. 12, pp. 5143–5160, Dec. 2012, doi: 10.5194/bg-9-5143-2012.

[8] M. I. Ojovan, W. E. Lee, and S. N. Kalmykov, An Introduction to Nuclear Waste Immobilisation. Elsevier, 2019.

[9] J. G. Dean, F. L. Bosqui, and K. H. Lanouette, 'Removing heavy metals from waste water', Environ. Sci. Technol., vol. 6, no. 6, pp. 518–522, Jun. 1972, doi: 10.1021/es60065a006.

[10] N. Meunier, P. Drogui, C. Montané, R. Hausler, G. Mercier, and J.-F. Blais, 'Comparison between electrocoagulation and chemical precipitation for metals removal from acidic soil leachate', J. Hazard. Mater., vol. 137, no. 1, pp. 581–590, Sep. 2006, doi: 10.1016/j.jhazmat.2006.02.050.

[11] T. A. Kurniawan, G. Y. S. Chan, W.-H. Lo, and S. Babel, 'Physico–chemical treatment techniques for wastewater laden with heavy metals', Chem. Eng. J., vol. 118, no. 1, pp. 83–98, May 2006, doi: 10.1016/j.cej.2006.01.015.

[12] C. S. Lee, J. Robinson, and M. F. Chong, 'A review on application of flocculants in wastewater treatment', Process Saf. Environ. Prot., vol. 92, no. 6, pp. 489–508, Nov. 2014, doi: 10.1016/j.psep.2014.04.010.

[13] J. Bratby, Coagulation and Flocculation in Water and Wastewater Treatment. IWA Publishing, 2016.

[14] R. Yang, H. Li, M. Huang, H. Yang, and A. Li, 'A review on chitosan-based flocculants and their applications in water treatment', Water Res., vol. 95, pp. 59–89, May 2016, doi: 10.1016/j.watres.2016.02.068.

[15] T. Benvenuti, M. Rodrigues, A. Arenzon, A. M. Bernardes, and J. Zoppas-Ferreira, 'Toxicity effects of nickel electroplating effluents treated by photoelectrooxidation in the industries of the Sinos River Basin', Braz. J. Biol. Rev. Brasleira Biol., vol. 75, no. 2 Suppl, pp. 17–24, May 2015, doi: 10.1590/1519-6984.1113.

[16] C. Comninellis, 'Electrocatalysis in the electrochemical conversion/combustion of organic pollutants for waste water treatment', Electrochimica Acta, vol. 39, no. 11, pp. 1857–1862, Aug. 1994, doi: 10.1016/0013-4686(94)85175-1.

[17] M. Gattrell and D. Kirk, 'The electrochemical oxidation of aqueous phenol at a glassy carbon electrode', 1990, doi: 10.1002/CJCE.5450680615.

[18] Y. Awad and N. Abuzaid, 'Electrochemical treatment of phenolic wastewater: Efficiency, design considerations and economic evaluation', 1997, doi: 10.1080/10934529709376617.

[19] G. Rajalo and T. Petrovskaya, 'Selective Electrochemical Oxidation of Sulphides in Tannery Wastewater', Environ. Technol., vol. 17, no. 6, pp. 605–612, Jun. 1996, doi: 10.1080/09593331708616424.

[20] P. Drogui, J. Blais, and G. Mercier, 'Review of Electrochemical Technologies for Environmental Applications', 2007, doi: 10.2174/187221207782411629.

[21] S. Vasudevan and M. A. Oturan, ‘Electrochemistry: as cause and cure in water pollution—an overview’, Environ. Chem. Lett., vol. 12, no. 1, pp. 97–108, Mar. 2014, doi: 10.1007/s10311-013-0434-2.

[22] F. Pombo and A. Dutra, ‘Copper removal from diluted cyanide wastewater by electrolysis’, Environ. Prog. Sustain. Energy, vol. 32, Apr. 2013, doi: 10.1002/ep.10597.

[23] Y. Yang, Y. Li, and M. Pritzker, ‘Control of Cu2O Film Morphology Using Potentiostatic Pulsed Electrodeposition’, Electrochimica Acta, vol. 213, pp. 225–235, Sep. 2016, doi: 10.1016/j.electacta.2016.07.116.

[24] J. Lu, D. Dreisinger, and W. C. Cooper, ‘Thermodynamics of the aqueous copper–cyanide system’, Hydrometallurgy, vol. 66, pp. 23–36, Oct. 2002, doi: 10.1016/S0304-386X(02)00081-6.

[25] S. D. Alexandratos, ‘Ion-Exchange Resins: A Retrospective from Industrial and Engineering Chemistry Research’, Ind. Eng. Chem. Res., vol. 48, no. 1, pp. 388–398, Jan. 2009, doi: 10.1021/ie801242v.

[26] A. Clearfield, ‘Inorganic Ion Exchangers with Layered Structures’, Annu. Rev. Mater. Sci., vol. 14, no. 1, pp. 205–229, 1984, doi: 10.1146/annurev.ms.14.080184.001225.

[27] M. Meyn, K. Beneke, and G. Lagaly, ‘Anion-exchange reactions of layered double hydroxides’, Layer. Double Hydroxides, p. 7.

[28] M. Grassi, G. Kaykioglu, V. Belgiorno, and G. Lofrano, ‘Removal of Emerging Contaminants from Water and Wastewater by Adsorption Process’, in Emerging Compounds Removal from Wastewater: Natural and Solar Based Treatments, G. Lofrano, Ed., in SpringerBriefs in Molecular Science. Dordrecht: Springer Netherlands, 2012, pp. 15–37. doi: 10.1007/978-94-007-3916-1_2.

[29] M. Schmidt, A. Masson, H.-P. Cheng, and C. Bréchignac, ‘Physisorption and Chemisorption on Silver Clusters’, ChemPhysChem, vol. 16, no. 4, pp. 855–865, 2015, doi: 10.1002/cphc.201402726.

[30] A. H. Berger and A. S. Bhown, ‘Comparing physisorption and chemisorption solid sorbents for use separating CO2 from flue gas using temperature swing adsorption’, Energy Procedia, vol. 4, pp. 562–567, 2011, doi: 10.1016/j.egypro.2011.01.089.

[31] A. H. El-Sheikh, A. P. Newman, H. Al-Daffaee, S. Phull, N. Cresswell, and S. York, ‘Deposition of anatase on the surface of activated carbon’, Surf. Coat. Technol., vol. 187, no. 2–3, pp. 284–292, Oct. 2004, doi: 10.1016/j.surfcoat.2004.03.012.

[32] A. Naeem, P. Westerhoff, and S. Mustafa, ‘Vanadium removal by metal (hydr)oxide adsorbents’, Water Res., vol. 41, no. 7, pp. 1596–1602, Apr. 2007, doi: 10.1016/j.watres.2007.01.002.

[33] W. J Walter, Physicochemical processes for water quality control. New York: Wiley-Interscience, 1972.

[34] O. Hamdaoui, ‘Batch study of liquid-phase adsorption of methylene blue using cedar sawdust and crushed brick’, J. Hazard. Mater., vol. 135, no. 1–3, pp. 264–273, Jul. 2006, doi: 10.1016/j.jhazmat.2005.11.062.

[35] B. B. Johnson, ‘Effect of pH, temperature, and concentration on the adsorption of cadmium on goethite’, Environ. Sci. Technol., vol. 24, no. 1, pp. 112–118, Jan. 1990, doi: 10.1021/es00071a014.

[36] G. E. Millward, ‘The adsorption of cadmium by iron(III) precipitates in model estuarine solutions’, Environ. Technol. Lett., vol. 1, no. 8, pp. 394–399, Aug. 1980, doi: 10.1080/09593338009383993.

[37] Z. Bekçi, Y. Seki, and M. K. Yurdakoç, ‘Equilibrium studies for trimethoprim adsorption on montmorillonite KSF’, J. Hazard. Mater., vol. 133, no. 1–3, pp. 233–242, May 2006, doi: 10.1016/j.jhazmat.2005.10.029.

[38] Y. Onal, C. Akmil-Başar, and C. Sarici-Ozdemir, ‘Elucidation of the naproxen sodium adsorption onto activated carbon prepared from waste apricot: kinetic, equilibrium and thermodynamic characterization’, J. Hazard. Mater., vol. 148, no. 3, pp. 727–734, Sep. 2007, doi: 10.1016/j.jhazmat.2007.03.037.

[39] H. Otker and I. Balcioğlu, ‘Adsorption and Degradation of Enrofloxacin, a Veterinary Antibiotic on Natural Zeolite’, J. Hazard. Mater., vol. 122, pp. 251–8, Aug. 2005, doi: 10.1016/j.jhazmat.2005.03.005.

[40] M. Ahmaruzzaman, ‘Industrial wastes as low-cost potential adsorbents for the treatment of wastewater laden with heavy metals’, Adv. Colloid Interface Sci., vol. 166, no. 1–2, pp. 36–59, Aug. 2011, doi: 10.1016/j.cis.2011.04.005.

[41] A. K. Bhattacharya, S. N. Mandal, and S. K. Das, ‘Adsorption of Zn(II) from aqueous solution by using different adsorbents’, Chem. Eng. J., vol. 123, no. 1, pp. 43–51, Oct. 2006, doi: 10.1016/j.cej.2006.06.012.

[42] E. Malkoc and Y. Nuhoglu, ‘Investigations of nickel(II) removal from aqueous solutions using tea factory waste’, J. Hazard. Mater., vol. 127, no. 1, pp. 120–128, Dec. 2005, doi: 10.1016/j.jhazmat.2005.06.030.

[43] Benício, L. P. F. ; Silva, R. A. ; Lopes, J. A. ; Eulálio, D. ; Santos, R. M. M. dos ; Aquino, L. A. de ; Vergütz, L. ; Novais, R. F. ; Costa, L. M. da ; Pinto, F. G. ; Tronto, J, 'Layered double hydroxides: nanomaterials for applications in agriculture', Rev. Bras. Ciênc. Solo, vol. 39, no. 1, pp. 1–13, Feb. 2015, doi: 10.1590/01000683rbcs2015081.

[44] P. Vialat, F. Leroux, and C. Mousty, 'Electrochemical properties of layered double hydroxides containing 3d metal cations.', J. Solid State Electrochem., vol. 19, pp. 1975–1983, 2015, doi: 10.1007/s10008-014-2671-0.

[45] K. Yan, Y. Liu, Y. Lu, J. Chai, and L. Sun, 'Catalytic application of layered double hydroxide-derived catalysts for the conversion of biomass-derived molecules', Catal. Sci. Technol., vol. 7, no. 8, pp. 1622–1645, Apr. 2017, doi: 10.1039/C7CY00274B.

[46] K.-H. Goh, T.-T. Lim, and Z. Dong, 'Application of layered double hydroxides for removal of oxyanions: A review', Water Res., vol. 42, no. 6, pp. 1343–1368, Mar. 2008, doi: 10.1016/j.watres.2007.10.043.

[47] F. Cavani, F. Trifirò, and A. Vaccari, 'Hydrotalcite-type anionic clays: Preparation, properties and applications.', Catal. Today, vol. 11, no. 2, pp. 173–301, 1991, doi: 10.1016/0920-5861(91)80068-K.

[48] H. F. W. Taylor, 'Crystal structures of some double hydroxide minerals', Mineral. Mag., vol. 39, no. 304, pp. 377–389, Dec. 1973, doi: 10.1180/minmag.1973.039.304.01.

[49] S. Marappa, S. Radha, and P. V. Kamath, 'Nitrate-Intercalated Layered Double Hydroxides – Structure Model, Order, and Disorder', Eur. J. Inorg. Chem., vol. 2013, no. 12, pp. 2122–2128, Apr. 2013, doi: 10.1002/ejic.201201405.

[50] R. Shivaramaiah and A. Navrotsky, 'Energetics of Order–Disorder in Layered Magnesium Aluminum Double Hydroxides with Interlayer Carbonate', Inorg. Chem., vol. 54, no. 7, pp. 3253–3259, Apr. 2015, doi: 10.1021/ic502820q.

[51] A. V. Radha, P. V. Kamath, and C. Shivakumara, 'Conservation of Order, Disorder, and "Crystallinity" during Anion-Exchange Reactions among Layered Double Hydroxides (LDHs) of Zn with Al', J. Phys. Chem. B, vol. 111, no. 13, pp. 3411–3418, Apr. 2007, doi: 10.1021/jp0684170.

[52] M. Chen, R. Zhu, X. Lu, J. Zhu, and H. He, 'Influences of Cation Ratio, Anion Type, and Water Content on Polytypism of Layered Double Hydroxides', Inorg. Chem., vol. 57, no. 12, pp. 7299–7313, Jun. 2018, doi: 10.1021/acs.inorgchem.8b00949.

[53] G. Mishra, B. Dash, and S. Pandey, ‘Layered double hydroxides: A brief review from fundamentals to application as evolving biomaterials’, Appl. Clay Sci., vol. 153, pp. 172–186, Mar. 2018, doi: 10.1016/j.clay.2017.12.021.

[54] J. He, M. Wei, B. Li, Y. Kang, D. G. Evans, and X. Duan, ‘Preparation of Layered Double Hydroxides’, in Layered Double Hydroxides, X. Duan and D. G. Evans, Eds., in Structure and Bonding. Berlin, Heidelberg: Springer, 2006, pp. 89–119. doi: 10.1007/430_006.

[55] J. He, M. Wei, B. Li, Y. Kang, D. G. Evans, and X. Duan, ‘Preparation of Layered Double Hydroxides’, in Layered Double Hydroxides, X. Duan and D. G. Evans, Eds., in Structure and Bonding, vol. 119. Berlin/Heidelberg: Springer-Verlag, 2006, pp. 89–119. doi: 10.1007/430_006.

[56] F. Prinetto, G. Ghiotti, P. Graffin, and D. Tichit, ‘Synthesis and characterization of sol–gel Mg/Al and Ni/Al layered double hydroxides and comparison with co-precipitated samples’, Microporous Mesoporous Mater., vol. 39, no. 1, pp. 229–247, Sep. 2000, doi: 10.1016/S1387-1811(00)00197-9.

[57] S. K. Yun and T. J. Pinnavaia, ‘Water Content and Particle Texture of Synthetic Hydrotalcite-like Layered Double Hydroxides’, Chem. Mater., vol. 7, no. 2, pp. 348–354, Feb. 1995, doi: 10.1021/cm00050a017.

[58] M. Z. Hussein, M. Y. Ghotbi, A. Yahya, and M. Z. Ab. Rahman, ‘Synthesis and characterization of (zinc-layered-gallate) nanohybrid using structural memory effect’, Mater. Chem. Phys., vol. 113, no. 1, Art. no. 1, Jan. 2009.

[59] S. H. Hwang, Y. S. Han, and J. H. Choe, ‘Intercalation of Functional Organic Molecules with Pharmaceutical, Cosmeceutical and Nutraceutical Functions into Layered Double Hydroxides and Zinc Basic Salts’, Bull. Korean Chem. Soc., vol. 22, no. 9, pp. 1019–1022, 2001, doi: 10.5012/bkcs.2001.22.9.1019.

[60] S.-Y. Kwak, Y.-J. Jeong, J.-S. Park, and J.-H. Choy, ‘Bio-LDH nanohybrid for gene therapy’, Solid State Ion., vol. 151, no. 1, pp. 229–234, Nov. 2002, doi: 10.1016/S0167-2738(02)00714-2.

[61] V. Ambrogi, G. Fardella, G. Grandolini, L. Perioli, and M. C. Tiralti, ‘Intercalation compounds of hydrotalcite-like anionic clays with anti-inflammatory agents, II: Uptake of diclofenac for a controlled release formulation’, AAPS PharmSciTech, vol. 3, no. 3, pp. 77–82, Sep. 2002, doi: 10.1007/BF02830624.

[62] S. Aisawa, S. Takahashi, W. Ogasawara, Y. Umetsu, and E. Narita, 'Direct Intercalation of Amino Acids into Layered Double Hydroxides by Coprecipitation', J. Solid State Chem., vol. 162, no. 1, pp. 52–62, Nov. 2001, doi: 10.1006/jssc.2001.9340.

[63] V. R. L. Constantino and T. J. Pinnavaia, 'Basic Properties of Mg2+1-xAl3+x Layered Double Hydroxides Intercalated by Carbonate, Hydroxide, Chloride, and Sulfate Anions', Inorg. Chem., vol. 34, no. 4, pp. 883–892, Feb. 1995, doi: 10.1021/ic00108a020.

[64] W. Feitknecht and M. Gerber, 'Zur Kenntnis der Doppelhydroxyde und basischen Doppelsalze III. Über Magnesium-Aluminiumdoppelhydroxyd', Helv. Chim. Acta, vol. 25, no. 1, pp. 131–137, 1942, doi: 10.1002/hlca.19420250115.

[65] W. Feitknecht and A. Berger, 'Über die Bildung eines Nickel- und Kobaltsilicates mit Schichtengitter', Helv. Chim. Acta, vol. 25, no. 7, pp. 1543–1547, 1942, doi: 10.1002/hlca.19420250715.

[66] M. C. Gastuche, G. Brown, and M. M. Mortland, 'Mixed magnesium-aluminiun hydroxides. I. Preparation and characterization of compounds formed in dialysed systems', Clay Miner., vol. 7, no. 2, pp. 177–192, Dec. 1967, doi: 10.1180/claymin.1967.007.2.05.

[67] U. Costantino, F. Marmottini, M. Nocchetti, and R. Vivani, 'New Synthetic Routes to Hydrotalcite-Like Compounds − Characterisation and Properties of the Obtained Materials', Eur. J. Inorg. Chem., vol. 1998, no. 10, pp. 1439–1446, 1998, doi: https://doi.org/10.1002/(SICI)1099-0682(199810)1998:10<1439::AID-EJIC1439>3.0.CO;2-1.

[68] M. Ogawa and H. Kaiho, 'Homogeneous Precipitation of Uniform Hydrotalcite Particles', Langmuir, vol. 18, no. 11, pp. 4240–4242, May 2002, doi: 10.1021/la0117045.

[69] Y. Israëli, C. Taviot-Guého, J.-P. Besse, J.-P. Morel, and N. Morel-Desrosiers, 'Thermodynamics of anion exchange on a chloride-intercalated zinc–aluminum layered double hydroxide: a microcalorimetric study', J. Chem. Soc. Dalton Trans., no. 5, pp. 791–796, Jan. 2000, doi: 10.1039/A906346C.

[70] R. P. Bontchev, S. Liu, J. L. Krumhansl, J. Voigt, and T. M. Nenoff, 'Synthesis, Characterization, and Ion Exchange Properties of Hydrotalcite Mg6Al2(OH)16(A)x(A')2-x·4H2O (A, A' = Cl-, Br-, I-, and NO3-, 2 ≥ x ≥ 0) Derivatives', Chem. Mater., vol. 15, no. 19, pp. 3669–3675, Sep. 2003, doi: 10.1021/cm034231r.

[71] KunWei Li, Nobuhiro Kumada, Yoshinori Yonesaki, Takahiro Takei, Nobukazu Kino mura, Hao Wang, Chao Wang, 'The pH effects on the formation of Ni/Al nitrate form layered double hydroxides (LDHs) by chemical precipitation and hydrothermal method', Mater. Chem. Phys, vol. 1–2, no. 121, pp. 223–229, 2010, doi: 10.1016/j.matchemphys.2010.01.026.

[72] J. S. Valente, E. Lima, J.A. Toledo-Antonio, M.A. Cortes-Jacome, L. Lartundo-Rojas, R. Montiel, J. Prince, 'Comprehending the Thermal Decomposition and Reconstruction Process of Sol−Gel MgAl Layered Double Hydroxides', ACS Publications, Jan. 12, 2010. https://pubs.acs.org/doi/pdf/10.1021/jp910538r (accessed Oct. 13, 2022).

[73] 'Characterization of Repeatedly Reconstructed Mg−Al Hydrotalcite-like Compounds: Gradual Segregation of Aluminum from the Structure | Chemistry of Materials'. https://pubs.acs.org/doi/abs/10.1021/cm980478q (accessed Oct. 13, 2022).

[74] B. Gregoire, C. Ruby, and C. Carteret, 'Structural Cohesion of MII-MIII Layered Double Hydroxides Crystals: Electrostatic Forces and Cationic Polarizing Power', Struct. Cohes. MII-MIII Layer. Double Hydroxides Cryst. Electrost. Forces Cationic Polarizing Power, vol. 12, no. 9, pp. 4324–4333, 2012.

[75] K. Abderrazek, N. Frini Srasra, and E. Srasra, 'Synthesis and Characterization of [Zn-Al] Layered Double Hydroxides: Effect of the Operating Parameters: Synthesis and Characterization of [Zn-Al] LDH', J. Chin. Chem. Soc., vol. 64, no. 3, pp. 346–353, Mar. 2017, doi: 10.1002/jccs.201600258.

[76] A. A. A. Ahmed, Z. A. Talib, M. Z. bin Hussein, and A. Zakaria, 'Zn-Al layered double hydroxide prepared at different molar ratios: Preparation, characterization, optical and dielectric properties', J. Solid State Chem. Fr., vol. 191, pp. 271–278, Jul. 2012, doi: 10.1016/j.jssc.2012.03.013.

[77] A. Seron and F. Delorme, 'Synthesis of layered double hydroxides (LDHs) with varying pH: A valuable contribution to the study of Mg/Al LDH formation mechanism', J. Phys. Chem. Solids, vol. 69, no. 5–6, pp. 1088–1090, May 2008, doi: 10.1016/j.jpcs.2007.10.054.

[78] J. Olanrewaju, B. L. Newalkar, C. Mancino, and S. Komarneni, 'Simplified synthesis of nitrate form of layered double hydroxide', Mater. Lett., vol. 45, no. 6, pp. 307–310, Oct. 2000, doi: 10.1016/S0167-577X(00)00123-3.

[79] C. Morcos, ‘procédé de captage et libération du CO2 assiste par l'électrolyse en utilisant des matériaux de type brucitiques, http://www.theses.fr, Dec. 13, 2021. http://www.theses.fr/s294216 (accessed Jun. 14, 2022).

[80] Z. P. Xu, G. Stevenson, C.-Q. Lu, and G. Q. (Max) Lu, ‘Dispersion and Size Control of Layered Double Hydroxide Nanoparticles in Aqueous Solutions’, J. Phys. Chem. B, vol. 34, no. 110, pp. 16923–16929, 2006, doi: 10.1021/jp062281o.

[81] Y. Zhao, J. Liang, F. Li, and X. Duan, ‘Selectivity of crystal growth direction in layered double hydroxides’, Tsinghua Sci. Technol., vol. 9, no. 6, pp. 667–671, Dec. 2004.

[82] F. Delorme, A. Seron, B. Vergnaud, P. Galle-Cavalloni, V. Jean-Prost, and J. Manguin, ‘Evidence of the influence of the cationic composition on the anionic affinity of layered double hydroxides’, J. Mater. Sci., vol. 48, no. 15, pp. 5273–5279, Aug. 2013, doi: 10.1007/s10853-013-7318-5.

[83] A. O. V, P. V. I, P. O. V, and G. V. V, ‘Phase formation under conditions of sefl-organization of particle growth restrictions in the reaction system’, Наносистемы Физика Химия Математика, vol. 13, no. 2, Art. no. 2, 2022.

[84] J.-H. Choy, ‘Intercalative route to heterostructured nanohybrid☆’, J. Phys. Chem. Solids, vol. 65, no. 2, pp. 373–383, Mar. 2004, doi: 10.1016/j.jpcs.2003.10.047.

[85] Y. Li, D. Sun, X. Pan, and B. Zhang, ‘Kaolinite intercalation precursors’, Clays Clay Miner., vol. 57, no. 6, pp. 779–786, Dec. 2009, doi: 10.1346/CCMN.2009.0570610.

[86] S. O’Leary, D. O’Hare, and G. Seeley, ‘Delamination of layered double hydroxides in polar monomers: new LDH-acrylate nanocomposites’, Chem. Commun., no. 14, pp. 1506–1507, Jul. 2002, doi: 10.1039/B204213D.

[87] M. Adachi-Pagano, C. Forano, and J.-P. Besse, ‘Delamination of layered double hydroxides by use of surfactants’, Chem. Commun., no. 1, pp. 91–92, Jan. 2000, doi: 10.1039/A908251D.

[88] W. Chen, L. Feng, and B. Qu, ‘Preparation of Nanocomposites by Exfoliation of ZnAl Layered Double Hydroxides in Nonpolar LLDPE Solution’, Chem. Mater., vol. 16, no. 3, pp. 368–370, Feb. 2004, doi: 10.1021/cm0303484.

[89] Q. Wu, A. Olafsen, Ø. B. Vistad, J. Roots, and P. Norby, ‘Delamination and restacking of a layered double hydroxide with nitrate as counter anion’, J. Mater. Chem., vol. 15, no. 44, pp. 4695–4700, 2005, doi: 10.1039/B511184F.

[90] Q. Wang, H.H Tay, D. Jia Wei Ng, L. Chen, Y. Liu, J. Chang, Z. Zhong, J. Luo, A. Borgna, ‘The effect of trivalent cations on the performance of Mg-M-CO(3) layered

double hydroxides for high-temperature CO(2) capture', ChemSusChem, vol. 3, no. 8, pp. 965–973, Aug. 2010, doi: 10.1002/cssc.201000099.

[91] M. Dadwhal, T. W. Kim, M. Sahimi, and T. T. Tsotsis, 'Study of CO 2 Diffusion and Adsorption on Calcined Layered Double Hydroxides: The Effect of Particle Size', Ind. Eng. Chem. Res., vol. 16, no. 47, pp. 6150–6157, 2008, doi: 10.1021/ie701701d.

[92] Y. Gao, Z. Zhang, J. Wu, X. Yi, A. Zheng, A. Umar, D. O'Hare and Q. Wang , 'Comprehensive investigation of CO2 adsorption on Mg–Al–CO3 LDH-derived mixed metal oxides', J. Mater. Chem. A, vol. 1, no. 41, pp. 12782–12790, Oct. 2013, doi: 10.1039/C3TA13039H.

[93] N. N. A. H. Meis, J. H. Bitter, and K. P. de Jong, 'Support and Size Effects of Activated Hydrotalcites for Precombustion CO2 Capture', Ind. Eng. Chem. Res., vol. 3, no. 49, pp. 1229–1235, Feb. 2010, doi: 10.1021/ie901114d.

[94] L. C. Santos, A. F. da Silva, P. V. dos Santos Lins, J. L. da Silva Duarte, A. H. Ide, and L. Meili, 'Mg-Fe layered double hydroxide with chloride intercalated: synthesis, characterization and application for efficient nitrate removal', Environ. Sci. Pollut. Res., vol. 27, no. 6, pp. 5890–5900, Feb. 2020, doi: 10.1007/s11356-019-07364-4.

[95] Q. Zhang, F. Ji, T. Zhao, Q. Shen, D. Fang, L. Kuang, L. Jiang, S. Ding, 'Systematic screening of layered double hydroxides for phosphate removal and mechanism insight', Appl. Clay Sci., vol. 174, pp. 159–169, Jun. 2019, doi: 10.1016/j.clay.2019.03.030.

[96] A. U. Kura, M. Z. Hussein, S. Fakurazi, and P. Arulselvan, 'Layered double hydroxide nanocomposite for drug delivery systems; bio-distribution, toxicity and drug activity enhancement', Chem. Cent. J., vol. 8, no. 1, p. 47, Aug. 2014, doi: 10.1186/s13065-014-0047-2.

[97] K. Sugano, M. Kansy, P. Artursson, A. Avdeef, S. Bendels, L. Di, G. F. Ecker, B. Faller, H. Fischer, G. Gerebtzoff, H. Lennernaes and F. Senner, 'Coexistence of passive and carrier-mediated processes in drug transport', Nat. Rev. Drug Discov., vol. 9, no. 8, Art. no. 8, Aug. 2010, doi: 10.1038/nrd3187.

[98] B. Saifullah, M. Z. Hussein, S. H. Hussein-Al-Ali, P. Arulselvan, and S. Fakurazi, 'Antituberculosis nanodelivery system with controlled-release properties based on para-amino salicylate–zinc aluminum-layered double-hydroxide nanocomposites', Drug Des. Devel. Ther., vol. 7, pp. 1365–1375, Nov. 2013, doi: 10.2147/DDDT.S50665.

[99] W. Xie, Z. Li, M. Shao, and M. Wei, 'Layered double hydroxide-based core-shell nanoarrays for efficient electrochemical water splitting', Front. Chem. Sci. Eng., vol. 12, Jun. 2018, doi: 10.1007/s11705-018-1719-6.

[100] M. Jayalakshmi and K. Balasubramanian, 'Cyclic Voltammetric Behavior of Copper Powder Immobilized on Paraffin Impregnated Graphite Electrode in Dilute Alkali Solution', Int J Electrochem Sci, vol. 3, p. 11, 2008.

[101] I. Alon, H. Jiao, and Y. Cui, 'Environmental dynamism, Innovation and dynamic capabilities: the case of China', Fac. Publ., Jan. 2010, doi: 10.1108/17506201111131550.

[102] R. A. Fisher, M. R. Watt, and W. J. Ready, 'Functionalized Carbon Nanotube Supercapacitor Electrodes: A Review on Pseudocapacitive Materials', ECS J. Solid State Sci. Technol., vol. 2, no. 10, p. M3170, Oct. 2013, doi: 10.1149/2.017310jss.

[103] B. Zhao, D. Chen, X. Xiong, B. Song, R. Hu, Q. Zhang, B. H. Rainwater, G. H. Waller, D. Zhen, Y. Ding, Y. Chen, C. Qu, D. Dang, C.P Wong, M. Liu., 'A high-energy, long cycle-life hybrid supercapacitor based on graphene composite electrodes', Energy Storage Mater., vol. 7, pp. 32–39, Apr. 2017, doi: 10.1016/j.ensm.2016.11.010.

[104] D. R. Dreyer, S. Park, C. W. Bielawski, and R. S. Ruoff, 'The chemistry of graphene oxide', Chem. Soc. Rev., vol. 39, no. 1, pp. 228–240, 2010, doi: 10.1039/B917103G.

[105] Y. Zhu, D. K. James, and J. M. Tour, 'New Routes to Graphene, Graphene Oxide and Their Related Applications', Adv. Mater., vol. 24, no. 36, pp. 4924–4955, 2012, doi: 10.1002/adma.201202321.

[106] J. Kim, L. J. Cote, and J. Huang, 'Two dimensional soft material: new faces of graphene oxide', Acc. Chem. Res., vol. 45, no. 8, pp. 1356–1364, Aug. 2012, doi: 10.1021/ar300047s.

[107] L. Sun, 'Structure and synthesis of graphene oxide', Chin. J. Chem. Eng., vol. 27, no. 10, p. 2251, 2019.

[108] G. Ruess 'Über das Graphitoxyhydroxyd (Graphitoxyd) doi:10.1007/BF00898987 (accessed Jul. 07, 2022).

[109] W. Scholz and H. Boehm 'Untersuchungen am Graphitoxid. VI. Betrachtungen zur Struktur des Graphitoxids - Scholz - 1969 - Zeitschrift für anorganische und allgemeine Chemie (accessed Jul. 07, 2022).

[110] T. Szabó, O. Berkesi, P. Forgó, K. Josepovits, Y. Sanakis, D. Petridis, and I. Dékány, 'Evolution of Surface Functional Groups in a Series of Progressively Oxidized Graphite Oxides', Chem. Mater., vol. 18, no. 11, pp. 2740–2749, May 2006, doi: 10.1021/cm060258+.

[111] D. R. Dreyer, A. D. Todd, and C. W. Bielawski, 'Harnessing the chemistry of graphene oxide', Chem. Soc. Rev., vol. 43, no. 15, pp. 5288–5301, Jul. 2014, doi: 10.1039/C4CS00060A.

[112] B. C. Brodie, ‘XIII. On the atomic weight of graphite’, Philos. Trans. R. Soc. Lond., vol. 149, pp. 249–259, Jan. 1859, doi: 10.1098/rstl.1859.0013.

[113] L. Staudenmaier, ‘Verfahren zur Darstellung der Graphitsäure’, Berichte Dtsch. Chem. Ges., vol. 31, no. 2, pp. 1481–1487, May 1898, doi: 10.1002/cber.18980310237.

[114] W. S. Hummers and R. E. Offeman, ‘Preparation of Graphitic Oxide’, J. Am. Chem. Soc., vol. 80, no. 6, pp. 1339–1339, Mar. 1958, doi: 10.1021/ja01539a017.

[115] A. M. Dimiev and J. M. Tour, ‘Mechanism of Graphene Oxide Formation’, ACS Nano, vol. 8, no. 3, pp. 3060–3068, Mar. 2014, doi: 10.1021/nn500606a.

[116] P. Yu, Z. Tian, S. E. Lowe, J. Song, Z. Ma, X. Wang, Z. J. Han, Q. Bao, G. P. Simon, D. Li and Y. L. Zhong, ‘Mechanically-Assisted Electrochemical Production of Graphene Oxide’, Chem. Mater., vol. 28, no. 22, pp. 8429–8438, Nov. 2016, doi: 10.1021/acs.chemmater.6b04415.

[117] S. Pei, Q. Wei, K. Huang, H.-M. Cheng, and W. Ren, ‘Green synthesis of graphene oxide by seconds timescale water electrolytic oxidation’, Nat. Commun., vol. 9, no. 1, Art. no. 1, Jan. 2018, doi: 10.1038/s41467-017-02479-z.

[118] A. Ambrosi and M. Pumera, ‘Electrochemically Exfoliated Graphene and Graphene Oxide for Energy Storage and Electrochemistry Applications’, Chem. – Eur. J., vol. 22, no. 1, pp. 153–159, 2016, doi: 10.1002/chem.201503110.

[119] C. Zhu, L. Liu, M. Fan, L. Liu, B. Dai, J. Yang, D. Sun, ‘Microbial oxidation of graphite by Acidithiobacillus ferrooxidans CFMI-1’, RSC Adv., vol. 4, no. 98, pp. 55044–55047, Oct. 2014, doi: 10.1039/C4RA09827G.

[120] C. Zhu, Q. Hao, Y. Huang, J. Yang, and D. Sun, ‘Microbial oxidation of dispersed graphite by nitrifying bacteria 2011.2’, Nanoscale, vol. 5, no. 19, pp. 8982–8985, Sep. 2013, doi: 10.1039/C3NR02069J.

[121] L. Liu, C. Zhu, M. Fan, C. Chen, Y. Huang, Q. Hao, J. Yang, H. Wang and D. Sun, ‘Oxidation and degradation of graphitic materials by naphthalene-degrading bacteria’, Nanoscale, vol. 7, no. 32, pp. 13619–13628, Aug. 2015, doi: 10.1039/C5NR02502H.

[122] C. Kiang Chua and M. Pumera, ‘Chemical reduction of graphene oxide: a synthetic chemistry viewpoint’, Chem. Soc. Rev., vol. 43, no. 1, pp. 291–312, 2014, doi: 10.1039/C3CS60303B.

[123] S. Park and R. S. Ruoff, ‘Chemical methods for the production of graphenes’, Nat. Nanotechnol., vol. 4, no. 4, Art. no. 4, Apr. 2009, doi: 10.1038/nnano.2009.58.

[124] D. Chen, H. Feng, and J. Li, ‘Graphene Oxide: Preparation, Functionalization, and Electrochemical Applications’, Chem. Rev., vol. 112, no. 11, pp. 6027–6053, Nov. 2012, doi: 10.1021/cr300115g.

[125] S. Park, J. An, I. Jung, R. D. Piner, S. J. An, X. Li, A. Velamakanni, and R. S. Ruoff, ‘Colloidal Suspensions of Highly Reduced Graphene Oxide in a Wide Variety of Organic Solvents’, Nano Lett., vol. 9, no. 4, pp. 1593–1597, Apr. 2009, doi: 10.1021/nl803798y.

[126] S. N. Alam, N. Sharma, and L. Kumar, ‘Synthesis of Graphene Oxide (GO) by Modified Hummers Method and Its Thermal Reduction to Obtain Reduced Graphene Oxide (rGO)’, Graphene, vol. 06, no. 01, Art. no. 01, 2017, doi: 10.4236/graphene.2017.61001.

[127] J. Song, X. Wang, and C.-T. Chang, ‘Preparation and Characterization of Graphene Oxide’, J. Nanomater., vol. 2014, pp. 1–6, 2014, doi: 10.1155/2014/276143.

[128] C. K. Chua, Z. Sofer, and M. Pumera, ‘Graphite oxides: effects of permanganate and chlorate oxidants on the oxygen composition’, Chem. Weinh. Bergstr. Ger., vol. 18, no. 42, pp. 13453–13459, Oct. 2012, doi: 10.1002/chem.201202320.

[129] R. Al-Gaashani, A. Najjar, Y. Zakaria, S. Mansour, and M. A. Atieh, ‘XPS and structural studies of high quality graphene oxide and reduced graphene oxide prepared by different chemical oxidation methods’, Ceram. Int., vol. 45, no. 11, pp. 14439–14448, Aug. 2019, doi: 10.1016/j.ceramint.2019.04.165.

[130] J. Zhang, H. Yang, G. Shen, P. Cheng, J. Zhang, and S. Guo, ‘Reduction of graphene oxide via l - ascorbic acid’, Chem. Commun., vol. 46, no. 7, pp. 1112–1114, 2010, doi: 10.1039/B917705A.

[131] D. C. Marcano, D. V. Kosynkin, J. M. Berlin, A. Sinitskii, Z. Sun, A. S. Slesarev, L. B. Alemany, W. Lu, and J. M. Tour, ‘Correction to Improved Synthesis of Graphene Oxide’, ACS Nano, vol. 12, no. 2, pp. 2078–2078, Feb. 2018, doi: 10.1021/acsnano.8b00128.

[132] H. L. Poh, F. Šaněk, A. Ambrosi, G. Zhao, Z. Sofer, and M. Pumera, ‘Graphenes prepared by Staudenmaier, Hofmann and Hummers methods with consequent thermal exfoliation exhibit very different electrochemical properties’, Nanoscale, vol. 4, no. 11, pp. 3515–3522, May 2012, doi: 10.1039/C2NR30490B.

[133] S. Park, K.-S. Lee, G. Bozoklu, W. Cai, S. T. Nguyen, and R. S. Ruoff, ‘Graphene Oxide Papers Modified by Divalent Ions—Enhancing Mechanical Properties via Chemical Cross-Linking’, ACS Nano, vol. 2, no. 3, pp. 572–578, Mar. 2008, doi: 10.1021/nn700349a.

[134] G. Wallace, R. B. Kaner, M. Muller, S. Gilje, and D. Li, 'Processable aqueous dispersions of graphene nanosheets', Fac. Sci. - Pap. Arch., pp. 101–105, Jan. 2008, doi: 10.1038/nnano.2007.451.

[135] P. Šimek, Z. Sofer, O. Jankovský, D. Sedmidubský, and M. Pumera, 'Oxygen-Free Highly Conductive Graphene Papers', Adv. Funct. Mater., vol. 24, no. 31, pp. 4878–4885, 2014, doi: 10.1002/adfm.201304284.

[136] F. Baskoro, C-B. Wong, S. R. Kumar, C-W. Chang, C-H. Chen, D. W. Chen, S.J. Lue, 'Graphene oxide-cation interaction: Inter-layer spacing and zeta potential changes in response to various salt solutions', J. Membr. Sci., vol. 554, pp. 253–263, May 2018, doi: 10.1016/j.memsci.2018.03.006.

[137] B. Konkena and S. Vasudevan, 'Understanding Aqueous Dispersibility of Graphene Oxide and Reduced Graphene Oxide through p K_a Measurements', J. Phys. Chem. Lett., vol. 3, no. 7, pp. 867–872, Apr. 2012, doi: 10.1021/jz300236w.

[138] J. Zhao, G. Chen, W. Zhang, P. Li, L. Wang, Q. Yue, H. Wang, R. Dong, X. Yan, and J. Liu., 'High-Resolution Separation of Graphene Oxide by Capillary Electrophoresis', Anal. Chem., vol. 83, no. 23, pp. 9100–9106, Dec. 2011, doi: 10.1021/ac202136n.

[139] N. Morimoto, T. Kubo, and Y. Nishina, 'Tailoring the Oxygen Content of Graphite and Reduced Graphene Oxide for Specific Applications', Sci. Rep., vol. 6, no. 1, p. 21715, Apr. 2016, doi: 10.1038/srep21715.

[140] Y. Shi and L.-J. Li, 'Chemically modified graphene: flame retardant or fuel for combustion?', J. Mater. Chem., vol. 21, no. 10, pp. 3277–3279, Feb. 2011, doi: 10.1039/C0JM02953J.

[141] A. Ambrosi, C. Chua, B. Khezri, Z. Sofer, R. Webster, and M. Pumera, 'Chemically reduced graphene contains inherent metallic impurities present in parent natural and synthetic graphite', Proc. Natl. Acad. Sci. U. S. A., vol. 109, pp. 12899–904, Jul. 2012, doi: 10.1073/pnas.1205388109.

[142] A. Ambrosi, S. Y. Chee, B. Khezri, R. D. Webster, Z. Sofer, and M. Pumera, 'Metallic impurities in graphenes prepared from graphite can dramatically influence their properties', Angew. Chem. - Int. Ed., vol. 51, no. 2, pp. 500–503, Jan. 2012, doi: 10.1002/anie.201106917.

[143] G. Zhao, X. Ren, X. Gao,b Xiaoli Tan, J. Li, C. Chen, Y. Huang and X. Wang, 'Removal of Pb(II) ions from aqueous solutions on few-layered graphene oxide nanosheets', Dalton Trans., vol. 40, no. 41, pp. 10945–10952, Oct. 2011, doi: 10.1039/C1DT11005E.

[144] H. Kinoshita, Y. Nishina, A. A. Alias, and M. Fujii, 'Tribological properties of monolayer graphene oxide sheets as water-based lubricant additives', Carbon, vol. 66, pp. 720–723, Jan. 2014, doi: 10.1016/j.carbon.2013.08.045.

[145] R. L. White, C. M. White, H. Turgut, A. Massoud, and Z. R. Tian, 'Comparative studies on copper adsorption by graphene oxide and functionalized graphene oxide nanoparticles', J. Taiwan Inst. Chem. Eng., vol. 85, pp. 18–28, Apr. 2018, doi: 10.1016/j.jtice.2018.01.036.

[146] X. Wang, Z. Chen, and S. Yang, 'Application of graphene oxides for the removal of Pb(II) ions from aqueous solutions: Experimental and DFT calculation', J. Mol. Liq., vol. 211, pp. 957–964, Nov. 2015, doi: 10.1016/j.molliq.2015.08.020.

[147] J. H. Chen, H.T. Xing, X. Sun, Z. B. Su, Y. H. Huang, W. Weng, S. R. Hu, H. X. Guo, W. B. Wu, Y. S. He, 'Highly effective removal of Cu(II) by triethylenetetramine-magnetic reduced graphene oxide composite', Appl. Surf. Sci., vol. 356, pp. 355–363, Nov. 2015, doi: 10.1016/j.apsusc.2015.08.076.

[148] M. Rinaudo, 'Chitin and chitosan: Properties and applications', Prog. Polym. Sci., vol. 31, no. 7, pp. 603–632, Jul. 2006, doi: 10.1016/j.progpolymsci.2006.06.001.

[149] S.-K. Kim and E. Mendis, 'Bioactive compounds from marine processing byproducts – A review', Food Res. Int., vol. 39, no. 4, pp. 383–393, May 2006, doi: 10.1016/j.foodres.2005.10.010.

[150] I. Aranaz, M. Mengibar; R. Harris, I. Panos, B. Miralles, N. Acosta, G. Galed and A. Heras, 'Functional Characterization of Chitin and Chitosan', Curr. Chem. Biol., vol. 3, no. 2, pp. 203–230, May 2009, doi: 10.2174/187231309788166415.

[151] D. Xu, S. Hein, and K. Wang, 'Chitosan membrane in separation applications', Mater. Sci. Technol., vol. 24, no. 9, pp. 1076–1087, Sep. 2008, doi: 10.1179/174328408X341762.

[152] M. Elimelech and W. A. Phillip, 'The future of seawater desalination: energy, technology, and the environment', Science, vol. 333, no. 6043, pp. 712–717, Aug. 2011, doi: 10.1126/science.1200488.

[153] B. Kırıl Mert, N. Özengin, E. Can, and C. Aydıner, 'Efficient Removal Approach of Micropollutants in Wastewater Using Membrane Bioreactor', 2018. doi: 10.5772/intechopen.75183.

[154] C. Charcosset, 'Preparation of emulsions and particles by membrane emulsification for the food processing industry', J. Food Eng., vol. 92, no. 3, pp. 241–249, 2009.

[155] J. Roy, F. Salaün, S. Giraud, A. Ferri, J. Guan, and G. Chen, 'Solubility of Chitin: Solvents, Solution Behaviors and Their Related Mechanisms', 2017. doi: 10.5772/intechopen.71385.

[156] N. Acosta, C. Jiménez, V. Borau, and A. Heras, 'Extraction and characterization of chitin from crustaceans', Biomass Bioenergy, vol. 5, no. 2, pp. 145–153, Jan. 1993, doi: 10.1016/0961-9534(93)90096-M.

[157] K. F. K. Oyedeko, A. S. A. Akinyanju, J. Akinbomi, M. K. Lasisi, and A. A. Adesina, 'Preparation and characterization of synthetic chitosan using bio-waste (snail shell)', Eng. Technol. Res. J., vol. 4, pp. 38–46, Sep. 2019, doi: 10.47545/etrj.2019.4.2.071.

[158] S. (Gabriel) Kou, L. M. Peters, and M. R. Mucalo, 'Chitosan: A review of sources and preparation methods', Int. J. Biol. Macromol., vol. 169, pp. 85–94, Feb. 2021, doi: 10.1016/j.ijbiomac.2020.12.005.

[159] K. L. B. Chang, G. Tsai, J. Lee, and W.-R. Fu, 'Heterogeneous N-deacetylation of chitin in alkaline solution', Carbohydr. Res., vol. 303, no. 3, pp. 327–332, Sep. 1997, doi: 10.1016/S0008-6215(97)00179-1.

[160] J.-H. Pa and T. L. Yu, 'Light scattering study of chitosan in acetic acid aqueous solutions', Light Scatt. Study Chitosan Acetic Acid Aqueous Solut., vol. 202, no. 7, pp. 985–991, 2001.

[161] I. Aranaz, R. Harris, and A. Heras, 'Chitosan Amphiphilic Derivatives. Chemistry and Applications', Curr. Org. Chem., vol. 14, no. 3, pp. 308–330, Feb. 2010, doi: 10.2174/138527210790231919.

[162] H. El Knidri, R. Belaabed, A. Addaou, A. Laajeb, and A. Lahsini, 'Extraction, chemical modification and characterization of chitin and chitosan', Int. J. Biol. Macromol., vol. 120, no. Pt A, pp. 1181–1189, Dec. 2018, doi: 10.1016/j.ijbiomac.2018.08.139.

[163] B. Sellergren and L. Andersson, 'Molecular recognition in macroporous polymers prepared by a substrate analogue imprinting strategy', Mol. Recognit. Macroporous Polym. Prep. Substrate Analog. Imprinting Strategy, vol. 55, no. 10, pp. 3381–3383, 1990.

[164] J. Zhang, W. Xia, P. Liu, Q. Cheng, T. Tahirou, W. Gu, and B. Li, 'Chitosan modification and pharmaceutical/biomedical applications', Mar. Drugs, vol. 8, no. 7, pp. 1962–1987, Jun. 2010, doi: 10.3390/md8071962.

[165] I. Hamed, F. Özogul, and J. M. Regenstein, 'Industrial applications of crustacean by-products (chitin, chitosan, and chitooligosaccharides): A review', Trends Food Sci. Technol., vol. C, no. 48, pp. 40–50, 2016, doi: 10.1016/j.tifs.2015.11.007.

[166] K. Kofuji, C.-J. Qian, M. Nishimura, I. Sugiyama, Y. Murata, and S. Kawashima, 'Relationship between physicochemical characteristics and functional properties of chitosan', Eur. Polym. J., vol. 11, no. 41, pp. 2784–2791, 2005, doi: 10.1016/j.eurpolymj.2005.04.041.

[167] C. C, 'Chitosan film mechanical and permeation properties as affected by acid, plasticizers, and storage', J Food Sci, vol. 63, pp. 1049–1053, 1998.

[168] Y.-W. Cho, J. Jang, C. R. Park, and S.-W. Ko, 'Preparation and Solubility in Acid and Water of Partially Deacetylated Chitins', Biomacromolecules, vol. 1, no. 4, pp. 609–614, Dec. 2000, doi: 10.1021/bm000036j.

[169] A. V. Il'ina and V. P. Varlamov, 'Hydrolysis of Chitosan in Lactic Acid', Appl. Biochem. Microbiol., vol. 40, no. 3, pp. 300–303, May 2004, doi: 10.1023/B:ABIM.0000025956.98250.30.

[170] Z. Zakaria, Z. Izzah, M. Jawaid, and A. Hassan, 'Effect of degree of deacetylation of chitosan on thermal stability and compatibility of chitosan-polyamide blend', BioResources, vol. 7, no. 4, Art. no. 4, Sep. 2012.

[171] M. Jiang et al., 'Removal of heavy metal chromium using cross-linked chitosan composite nanofiber mats', Int. J. Biol. Macromol., vol. 120, pp. 213–221, Dec. 2018, doi: 10.1016/j.ijbiomac.2018.08.071.

[172] M. Chandrasekaran, K. D. Kim, and S. C. Chun, 'Antibacterial Activity of Chitosan Nanoparticles: A Review', Processes, vol. 8, no. 9, Art. no. 9, Sep. 2020, doi: 10.3390/pr8091173.

[173] J. Berger, M. Reist, J. M. Mayer, O. Felt, and R. Gurny, 'Structure and interactions in chitosan hydrogels formed by complexation or aggregation for biomedical applications', Eur. J. Pharm. Biopharm., vol. 57, no. 1, pp. 35–52, Jan. 2004, doi: 10.1016/s0939-6411(03)00160-7.

[174] M. Raa, 'Amphoteric derivatives of chitosan and their biological significance', Chitin Chitosan, pp. 87–99, 1989.

[175] G. Crini, 'Recent developments in polysaccharide-based materials used as adsorbents in wastewater treatment', Prog. Polym. Sci., vol. 1, no. 30, pp. 38–70, 2005, doi: 10.1016/j.progpolymsci.2004.11.002.

[176] E. Guibal, 'Interactions of metal ions with chitosan-based sorbents: a review', Sep. Purif. Technol., vol. 1, no. 38, pp. 43–74, 2004, doi: 10.1016/j.seppur.2003.10.004.

[177] R. A. Muzzarelli and O. Tubertini, 'Chitin and chitosan as chromatographic supports and adsorbents for collection of metal ions from organic and aqueous solutions and sea-

water', Talanta, vol. 16, no. 12, pp. 1571–1577, Dec. 1969, doi: 10.1016/0039-9140(69)80218-3.

[178] X. Zhang, X. Shi, L. Ma, X. Pang, and L. Li, 'Preparation of Chitosan Stacking Membranes for Adsorption of Copper Ions', Polymers, vol. 11, no. 9, Art. no. 9, Sep. 2019, doi: 10.3390/polym11091463.

[179] P. Karthikeyan and S. Meenakshi, 'Fabrication of hybrid chitosan encapsulated magnetic-kaolin beads for adsorption of phosphate and nitrate ions from aqueous solutions', Int. J. Biol. Macromol., vol. 168, pp. 750–759, Jan. 2021, doi: 10.1016/j.ijbiomac.2020.11.132.

[180] W. S. W. Ngah, S. Ab Ghani, and A. Kamari, 'Adsorption behaviour of Fe(II) and Fe(III) ions in aqueous solution on chitosan and cross-linked chitosan beads', Bioresour. Technol., vol. 96, no. 4, pp. 443–450, Mar. 2005, doi: 10.1016/j.biortech.2004.05.022.

[181] T. S. Vo, T. T. B. C. Vo, J. W. Suk, and K. Kim, 'Recycling performance of graphene oxide-chitosan hybrid hydrogels for removal of cationic and anionic dyes', Nano Converg., vol. 7, no. 1, p. 4, Feb. 2020, doi: 10.1186/s40580-019-0215-0.

[182] M. A. M. Khraisheh, M. A. Al-Ghouti, S. J. Allen, and M. N. Ahmad, 'Effect of OH and silanol groups in the removal of dyes from aqueous solution using diatomite', Water Res., vol. 39, no. 5, pp. 922–932, Mar. 2005, doi: 10.1016/j.watres.2004.12.008.

[183] K. C. Lai, LY Lee, BYZ Hiew, TCK Yang and GT Pan, 'Utilization of eco-friendly and low cost 3D graphene-based composite for treatment of aqueous Reactive Black 5 dye: Characterization, adsorption mechanism and recyclability studies', J. Taiwan Inst. Chem. Eng., vol. 114, pp. 57–66, Sep. 2020, doi: 10.1016/j.jtice.2020.09.024.

[184] M. Zhang, G. Ma, L. Zhang, H. Chen, L. Zhu, C. Wang and X. Liu, 'Chitosan-reduced graphene oxide composites with 3D structures as effective reverse dispersed solid phase extraction adsorbents for pesticides analysis', Analyst, vol. 144, no. 17, pp. 5164–5171, Aug. 2019, doi: 10.1039/C9AN00927B.

[185] G. Ünsoy, 'The Synthesis and characterization of doxorubicin and bortezomib loaded magnetic nanoparticles for targeting tumor cells', Kanser hücrelerinin hedeflenmesi için doksorubisin ve bortezomib yüklü manyetik nanoparçacıkların sentezlenmesi ve karakterizasyonu., 2013, Accessed: Apr. 07, 2023. [Online]. Available: https://open.metu.edu.tr/handle/11511/22857

[186] M. Rasoulzadehzali and H. Namazi, 'Facile preparation of antibacterial chitosan/graphene oxide-Ag bio-nanocomposite hydrogel beads for controlled release of

doxorubicin', Int. J. Biol. Macromol., vol. 116, pp. 54–63, Sep. 2018, doi: 10.1016/j.ijbiomac.2018.04.140.

[187] R. Justin and B. Chen, 'Characterisation and drug release performance of biodegradable chitosan–graphene oxide nanocomposites', Carbohydr. Polym., vol. 103, pp. 70–80, Mar. 2014, doi: 10.1016/j.carbpol.2013.12.012.

[188] M. Rasoulzadeh and H. Namazi, 'Carboxymethyl cellulose/graphene oxide bio-nanocomposite hydrogel beads as anticancer drug carrier agent', Carbohydr. Polym., vol. 168, pp. 320–326, Jul. 2017, doi: 10.1016/j.carbpol.2017.03.014.

[189] W. Zhu, X. Jiang, F. Liu, F. You, and C. Yao, 'Preparation of Chitosan—Graphene Oxide Composite Aerogel by Hydrothermal Method and Its Adsorption Property of Methyl Orange', Polymers, vol. 12, no. 9, Art. no. 9, Sep. 2020, doi: 10.3390/polym12092169.

[190] K. Hristovski, A. Baumgardner, and P. Westerhoff, 'Selecting metal oxide nanomaterials for arsenic removal in fixed bed columns: from nanopowders to aggregated nanoparticle media', J. Hazard. Mater., vol. 147, no. 1–2, pp. 265–274, Aug. 2007, doi: 10.1016/j.jhazmat.2007.01.017.

[191] J. Sargent-Michaud, K. J. Boyle, and A. E. Smith, 'Cost effective arsenic reductions in private well water in Maine', Cost Eff. Arsen. Reduct. Priv. Well Water Maine, vol. 42, no. 5, pp. 1237–1245, 2006.

[192] J. S. Yamani, A. W. Lounsbury, and J. B. Zimmerman, 'Adsorption of selenite and selenate by nanocrystalline aluminum oxide, neat and impregnated in chitosan beads', Water Res., vol. 50, pp. 373–381, Mar. 2014, doi: 10.1016/j.watres.2013.10.054.

[193] G. J. CHURCHMAN, 'Formation of complexes between bentonite and different cationic polyelectrolytes and their use as sorbents for non-ionic and anionic pollutants', Form. Complexes Bentonite Differ. Cationic Polyelectrolytes Their Use Sorbents Non-Ion. Anionic Pollut., vol. 21, no. 3–4, pp. 177–189, 2002.

[194] J.-H. An and S. Dultz, 'Adsorption of tannic acid on chitosan-montmorillonite as a function of pH and surface charge properties', Adsorpt. Tann. Acid Chitosan-Montmorillonite Funct. PH Surf. Charge Prop., vol. 36, no. 4, pp. 256–264, 2007.

[195] J.-M. Li, X.-G. Meng, C.-W. Hu, and J. Du, 'Adsorption of phenol, p-chlorophenol and p-nitrophenol onto functional chitosan', Bioresour. Technol., vol. 100, no. 3, pp. 1168–1173, Feb. 2009, doi: 10.1016/j.biortech.2008.09.015.

[196] M. Li, A. Dopilka, A. N. Kraetz, H. Jing, and C. Chan, 'Layered Double Hydroxide/Chitosan Nanocomposite Beads as Sorbents for Selenium Oxoanions', Ind.

Eng. Chem. Res., vol. 57, no. 14, pp. 4978–4987, Apr. 2018, doi: 10.1021/acs.iecr.8b00466.

[197] F. Lyu, H. Yu, T. Hou, L. Yan, X. Zhang, and B. Du, 'Efficient and fast removal of Pb2+ and Cd2+ from an aqueous solution using a chitosan/Mg-Al-layered double hydroxide nanocomposite', J. Colloid Interface Sci., vol. 539, pp. 184–193, Mar. 2019, doi: 10.1016/j.jcis.2018.12.049.

Chapter 2: Materials and methods

This chapter describes the chemicals, experimental setups, and conditions used in this PhD project. In particular, the method of synthesis of Co/Fe layered double hydroxides, multilayered graphene oxide; pure chitosan and hybrid beads were presented. This chapter also describes the equipment and analytical conditions used to synthesize and characterize these materials.

VIII.1. Synthesis of Co^{II}/Fe^{III} LDHs with different cationic ratios by co-precipitation using the variable pH value method

VIII.1.1. Co^{II}/Fe^{III} co-precipitation step

Aqueous solutions, containing the appropriate ratio of cobalt nitrate salt (Acros, 99 % purity) and iron nitrate salt (Acros, 99% purity), were prepared in deionized water, in order to obtain Co^{II}/Fe^{III} LDHs with cationic ratios of 2/2, 4/2, 6/2, 8/2, and 10/2. Alkaline solutions were prepared by mixing 280 ml of 2.7 M sodium hydroxide (Acros NaOH pellets, 98.5 % purity) and 1000 ml of either 0.8 M Na_2CO_3 solution (Acros Na_2CO_3 solid, 99.6 % purity) or 0.8 M NaCl solution (Acros NaCl solid, 99 % purity). This method entails adding the alkaline solution ($NaOH/Na_2CO_3$ or NaOH/NaCl) to the metal salt solution ($Co(NO_3)_2$, $6H_2O$, $Fe(NO_3)_3$, $9H_2O$) or ($CoCl_2$, $6H_2O$, $FeCl_3$,$9H_2O$) contained in a 3-liter reactor, drop by drop, using a peristaltic pump, until the desired pH value of 8 was reached. Such pH value was chosen for the Co/Fe LDHs based on the acid-base titration curves. The slow addition of an alkaline solution will allow while continuously increasing the pH, the co-precipitation of Co and Fe in the form of LDHs. The 3-liter double-jacketed glass reactor was thermostated at 35°C with continuous stirring (900 rpm) during the Co/Fe co-precipitation. After the final pH value was reached, a maturation process was applied resulting in more crystalline LDHs with larger particle sizes. The suspension was aged at 60°C for 24 hours, the minimum aging time required to see an effect on the crystallinity and particle size of the LDHs. After the ageing process, the supernatant-solid phases were separated by centrifugation (Jouan CR412, 4500 rpm, 5 min).

VIII.1.2. Synthesis of LDHs with chosen interlayer anions

Co/Fe LDHs were synthesized using the coprecipitation method. The following paragraphs will discuss in details the synthesis conditions of the Co/Fe-CO_3 and Co/Fe-Cl LDHs.

VIII.1.2.a. Carbonated LDHs: Co^{II}/Fe^{III}-CO_3 LDHs

The synthesis of carbonated LDHs was carried out using $NaOH/Na_2CO_3$ as the alkaline solution. Since nitrate metal salts were used in the synthesis of Co/Fe LDHs, after co-precipitation, the initial interlayer anions were mainly nitrate. In order to elaborate, carbonate mono-anionic LDHs, the nitrate interlayer anions were exchanged by introducing the pristine NO_3-LDH slurry in a dialysis membrane MWCO (SpectraPor, 3.5 kD) into a 3 M sodium carbonate solution for 48 hours. To remove extra salts, the mono-anionic LDHs was washed by dialysis in a deionized water bath that was renewed every day for 5 days [1].The Co/Fe-CO_3 was dried at 60°C for 24 hours and finely ground with an agate mortar to obtain a fine LDH powder. The exchange process was verified afterwards using Fourier Transformer Infrared spectroscopy.

VIII.1.2.b. Chlorided LDHs: Co^{II}/Fe^{III}-Cl LDHs

To avoid carbonate contamination from the atmosphere, the synthesis of chloride LDHs was carried out in an abiotic glove box with inert N_2 gas flowing. These chloride LDHs were not matured, and the supernatant/solid phase separation was accomplished in the glove box through decantation for 24 hours. In addition to the use of chloride metal salts during the synthesis, synthesized LDHs were exchanged for 48 hours using a dialysis membrane MWCO (Spectrapor, 3.5 kD) into a 1M sodium chloride solution to obtain mono-anionic LDHs. To remove extra salts, the exchanged solid was washed by dialysis in a deionized water bath that was renewed every day for 5 days. A silver nitrate 1M solution was used to confirm the removal of chloride extra salts. The absence of a white precipitate (AgCl) indicates the complete removal of chlorides from the solution. The Co/Fe-Cl powder was obtained after freeze-drying. For this, the exchanged solid was frozen, using a freezer, at -41°C which is suitable for the freeze-drying process, for 24 hours, and then placed in specific jars for freeze-drying in the abiotic glove box to eliminate any CO_3^{2-} contamination. Finally, dried under vacuum with a freeze dryer (0.02 Pa

at -91°C). The anionic interlayer content of LDHs was also verified using the Fourier Transformer Infrared spectroscopy.

VIII.2. Synthesis of multilayered graphene oxide (MGO)

Multilayered graphene oxide was synthesized using Hummer's method [2]. It consists on dispersing 6g of graphene (Carl Roth) into a mixed solution of 720 ml of sulfuric acid (Aldrich purity 95–98%) and 80 ml of phosphoric acid (Al Chem purity 85%) for 10 minutes. Dispersing the graphene in an acidic medium allows the exfoliation of the graphene sheets. After that, the mixture was treated with 36 g of potassium permanganate ($KMnO_4$) (Aldrich purity 99%) to oxidize graphene sheets and obtain functional groups such as carboxylic, epoxy, and phenolic groups. The mixture, thermostated at 50°C by an oil bath, was stirred for 21 hours. The mixture was then allowed cooling at room temperature. After that, 6 ml of hydrogen peroxide (Roth 35%) mixed with 800 ml of cold deionized water were slowly added to the oxidized mixture resting in an ice bath. Hydrogen peroxide was added to reduce the excess of $KMnO_4$ used in the oxidation of graphene sheets. When the color of the suspension changes from black/purple to light brown, stirring was stopped and the suspension was left to decant for four days in a 3000 ml beaker. Then, the acidic aqueous phase was removed, and the settled solid was washed several times by suspending it in deionized water under stirring until a neutral pH was reached. After each wash, the liquid/solid phases were separated by centrifugation (Eppendorf centrifuge 5804 R, 500 rpm, 10 minutes).

To achieve dry MGO, the obtained solids were dried in an oven at 100 °C for two days. When the MGO was dry, it was ground into powder using a planetary mill (Retsch PM100, 500 rpm, 50 minutes). The obtained powder was sieved to yield MGOs with a grain size of 50 µm.

VIII.3. Synthesis of pure chitosan beads and hybrid beads

VIII.3.1 Pure chitosan beads

To make pure chitosan (CS) beads, chitosan gel was made by slowly adding 3 g of chitosan flakes (Mahtani chitosan MW 175 000 $g.mol^{-1}$) to 97 g of 0.5 M acetic acid solution (Aldrich 99 %) under continuous agitation. The viscous solution formed after total solvation of chitosan flakes has a high viscosity and thus cannot be used directly for the formation of the

desired beads. This is why the gel was kept at room temperature for three days. ***Figure.12*** represents the process of CS beads formation.

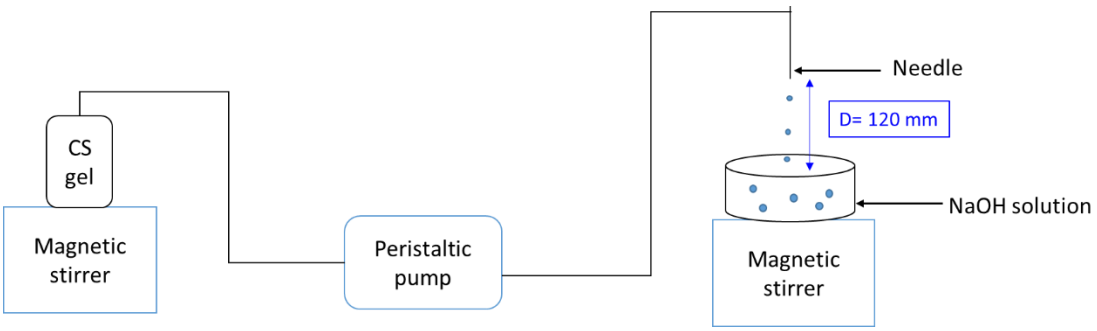

Figure.12. Elaboration process of pure chitosan beads

Such maturated chitosan solution (3wt.%) was then stirred again and transferred into an alkaline solution (NaOH 2.5 M) using a peristaltic pump (20 $mL.min^{-1}$), through tubes and syringe to elaborate the pure chitosan beads. Dropping the chitosan solution in alkaline solution kept at low agitation in the form of droplets with a 1.2 mm diameter syringe allows the biopolymer to gel, resulting in mechanically resistant beads. The distance between the surface of the alkaline solution and the tip of the needle was 120 mm. Following the gelation of chitosan gel in NaOH solution, the beads were recovered and washed for at least 5 times with deionized water under low agitation until neutral pH was reached. After the washing process, pure chitosan beads were stored in deionized water at a neutral pH.

VIII.3.2. Hybrid beads

CS/LDH beads

Pure chitosan gel was made by solvating 3 g of chitosan flakes in 97 g of diluted acetic acid (0.5M). Then, the metal salts in the appropriate proportion to achieve the desired Co^{II}/Fe^{III} ratio were dissolved in 100 mL of deionized water and slowly added to the chitosan gel under agitation until the mixture was completely homogenized. The hybrid beads were made by dropping the gel obtained after mixing in NaOH (2.5M) in the same way as the pure chitosan beads (***Figure 1***). After gelation, the beads are washed with deionized water until neutral pH, and then stored in deionized water at pH = 7 for a minimum of 24 hours before use.

CS 3% /MGO 1.5% beads

Using an ultra-sonication bath, 1.35 g of multilayered graphene oxide, corresponding to half of the total mass of chitosan (2.7g), were dispersed in 45.5 g of diluted acetic acid (0.5 M). The chitosan flakes were solvated in 20 g of diluted acetic acid (0.5 M), and then the ultra-sonicated MGO was added to the chitosan gel. To retrieve the remaining MGO, the final 20 g of diluted acetic acid were used. The gel was then kept agitated, and the remaining chitosan flakes were slowly added to the mix until full homogenization. Hybrid beads were obtained using this gel and washed in the same way as the pure chitosan and chitosan/LDH beads.

CS 3% /MGO 1.5%/LDH beads

A chitosan/MGO primary gel was formed in the manner described in the preceding paragraph. Then, 100 ml of metal salt solution (Co, Fe LDHs precursors) with the appropriate concentration, was added to the gel to obtain, the desired Co/Fe ratio, and the entire mixture was stirred until homogenization.

As previously reported (***Figure.12***), beads were made by transferring the hybrid gels to an alkaline solution (NaOH 2.5 M) using tubes and a 1.2 mm diameter needle. In contrast to the case of pure chitosan, for the two and three components beads, the distance between the surface of the alkaline solution and the tip of the needle was raised up to 220 mm instead of 120 mm.

VIII.4. Determination of the physico-chemical properties

The effect of the Co/Fe ratio and the final pH value on the purity, structure, and morphology of the LDHs were investigated.

Purity and crystallinity of the LDH samples

The purity and crystallinity of the synthesized LDHs were controlled by XRD analysis on Co/Fe-CO_3 samples synthesized at pH 8.0 and 11.5 as well as on the Co/Fe-Cl LDHs powder synthesized at pH 8.0. This technique allowed the identification of the synthesized crystalline phases as well as the control of the crystallinity based on the intensity and the full width of half-maximum (FWHM) of the (00l) peaks which were highly characteristic of the LDH structure. Before XRD analysis was performed, LDH powders were dispensed over a sample holder and

the surface was slightly smoothed carefully using a glass slide to prevent particles orientation. The divergent X-rays were generated using a cathode tube and directed towards the sample (Bragg-Brentano geometry). The interaction between the sample and the X-rays will create constructive interferences as well as diffracted rays when the conditions respect Bragg's Law:

$$n\lambda = 2d \sin \theta$$

λ: wavelength of the incident K_α radiation

d : inter-reticular distance between hkl plan

θ: Bragg angle (half angle between the incident and the refracted X-ray)

n: interference order n = 1

The diffracted X-rays were then detected, processed and counted. Following the Bragg's law, the peaks obtained were function of d-spacing of the mineral allowing the identification of the sample. For these measurements, a SiemensD5000 diffractometer with Cu K radiation was used. Operating at 40 kV and 30 mA at room temperature, powder XRD patterns were obtained. With a step size of 0.03° and a step time of 288 seconds, the scans were recorded from 4° to 76° (2θ).

Interlayer anions identification

Interlayer anions were identified using Fourier Transform Infrared Spectroscopy (FTIR). The concept of this technique was based on the absorption of different frequencies depending on the structure of the molecules. This method was used for semi-quantification or identification of chemical compounds, specifically in the case of LDHs for the defining of interlayer anions, based on the vibration of chemical bonds correlated to bands at different wavenumbers. The carbonates bonds were identified at wavenumber around 1350 cm^{-1} since it was an active molecule in infrared spectroscopy. However, chloride anions do not contain active infrared bonds; this is why it was not detected using infrared spectroscopy. In order to analyze LDHs using infrared spectroscopy, the powdered sample was embedded in KBr (Acros 99% KBr IR grade), a medium that does not absorb in the mid-IR. A homogeneous mixture of 0.5 mg of sample and 150 mg of KBr powders was prepared and finely ground in an agate mortar. Pellets (13mm in diameter and about 1mm thick) were then made by compressing the powder mixture at 10 kPa. To quantify and compare carbonate bands between different Co/Fe LDHs ratios, an internal standard potassium ferricyanide (Aldrich, 99% purity) was introduced

in the previous mixture before palletization. The analysis was recorded using an Equinox55 (Bruker, Germany) FTIR spectrometer over a range of 300-4000 cm^{-1} with a resolution of 4 cm^{-1}.

Metal ratios determination in LDHs

The determination of the chemical composition of the synthesized solids (LDHs and LDHs containing beads) requires the dissolution of the synthesized materials in acid medium in order to perform elemental analysis by atomic absorption spectroscopy. A micropipette was used to collect 1 mL of LDH suspension which was added to 9 mL of nitric acid (Aldrich, 65% purity).The meld was well mixed until the LDH suspension was completely dissolved, and then it was filtered through 0.45 µm and 0.1µm filters (Sodipro, Nylon, d=13 mm). Following that, AAS was used to examine the filtered solutions (Varian AA 200).

Solutions containing dissolved cobalt and iron elements were atomized in an acetylene/air flame for the analysis. The atoms were exposed to the light of a cathode lamp specific to the metals concerned, which allows them to transit from their fundamental state to excited electronic states. The incident intensity I_0 and transmitted intensity I_T were measured by the detector to determine the weight concentration of the chemical elements to be measured, which is proportional to log (I_0/I_T).

AAS method was used to determine the associated Co/Fe ratios of carbonated and chlorided LDHs.

Structure and morphology examination

A variety of materials was characterized using electron microscopes. The transmission electron microscope (TEM) and the scanning electron microscope (SEM) were the main types. The main difference between the two techniques was that SEM uses reflected electrons to create images, which provides information about the surface and chemical composition of the sample, whereas TEM uses transmitted electrons, which means electrons pass through the sample, providing much valuable information about the inner structure of the sample, such as crystal structure and morphology. Energy-dispersive X-ray spectroscopy (EDX) examination can be integrated with TEM and SEM techniques. This technique was based on the use of an electron beam that interacts with the atoms of a material (*e.g.* LDH) and ionizes them. The electromagnetic energies emitted by the ionized atoms, when they return to equilibrium (X-ray

fluorescence), were characteristic of the elements and allow the determination of the chemical composition of the solid. TEM examination was applied on the Co/Fe-CO_3 LDHs powder to observe the structure, and determine the cationic ratios, and chemistry of the LDHs particles using EDX analysis. A PHILIPS CM20 microscope with a 200 kV voltage was used to conduct these measures. One drop of the LDH suspension was deposited on the carbon membrane of the microscope grid, and then the solvent was evaporated at room temperature to obtain the preparations to be studied.

SEM observations were carried out on a TESCAN Mira3XMU (Brno, Czech Republic) FEG (Field Emission Gun, high resolution) SEM equipped with an EDS microanalysis system (Energy Dispersive X-ray Spectrometry, EDAX TEAM, SDD detector without liquid nitrogen, EDAX XPP). Images were captured using a secondary electron detector "In Beam" (IBSE) at 10 kV and EDS spectra at 15 kV in high vacuum. The powder LDH samples were coated with a 2 nm coating of platinum-palladium before observations to make them conductive for studying the morphology of the generated product.

Cryo-SEM analysis was used to study pure CS and hybrid beads maintained at neutral pH. It allowed the characterization of the homogeneity of the adsorbent distribution inside the chitosan matrix by observations and chemical EDX analysis. This technique differs from the classical SEM analysis by the preparation of the samples. The samples were glued on the sample holder with carbon based glue (which improves the conductivity between the sample holder and the sample). After that, they were immersed in slush nitrogen at -210°C and under high vacuum, pressure near 0. The cryo-preparation module was the model PP3010 from QUORUM. A vacuum was applied using a pump. 5 min later, the temperature in the chamber had decreased to a minimum of -210°C and the pressure was reduced to approximately 0 bars, resulting in the liquid nitrogen being transformed into a slush state. Slush nitrogen has a lower internal temperature without vaporization, and provides higher rates of cooling. The samples were then transferred to the cryopreparation chamber where the cryo platinum temperature: -140°C and the chamber pressure: 4.10^{-7} mbar.

The beads were fractured with a knife and then sublimated at -90°C for 10 minutes, this will allow the conservation of the beads porous network. Then a Pt metallization (by sputtering) was done during 45s at 5mA. The sample holder was transferred to the FEG Jeol JSM IT800-SHL SEM on a cryo stage also cooled to -140°C. The samples were then observed at 5kV and 15kV. The EDS detector was an Oxford SDD Ultim Max 100.

Cations valence and chemical bonds determination

The study by X-ray photoelectron spectroscopy was based on the interaction between an X-ray beam and a material (*e.g.* MGO). When the electrons of chemical elements constituting the material absorb sufficient energy, they were ejected with different kinetic energies depending on their electronic orbital. These energies were measured with a detector. The XPS method can be used to determine the chemical environment as well as the composition of the materials. XPS were utilized to determine the bonds and group surface formed during the synthesis of MGO. Pellets were made by compressing MGO powder dried under a vacuum at 100 °C. The equipment used to perform such analysis was a thermos electron 2000 with an X-Ray monochromator in Al, and a spot size of 900 microns diameter. Survey spectrum was recorded with a pass energy of 50 eV and a step size of 3.5 eV.

Thermal Degradation

Thermogravimetric analysis was based on a gradual rising of the temperature of a sample placed in a furnace while its weight was measured using an analytical balance. The mass variations were observed when a thermal increase was imposed, this will illustrate the transitions obtained illustrating the transition of the material and its decomposition. Thermogravimetry analysis (TGA) was performed with Jupiter NETZSCH STA449-F5 equipment. The temperature program employed was 1°C/min in the range of 20°C-900°C, and the mass used was around 14 mg for LDHs and 40 mg for chitosan-based beads. TGA analysis was used to determine the stages of LDH and chitosan based beads degradation , as well as the amount of solid present in the chitosan based beads.

Pore volume and specific surface determination

The specific surface of a solid is the total surface area per unit of mass that is accessible to gas molecules. The detection method relies on the adsorption and desorption of an inert gas (for example, nitrogen) on porous particles. The various processes that use physical gas adsorption at low temperatures are based on the work of Brunauer, Emmett, and Teller (BET). The LDH powder was kept in the oven at 50°C for 2 days before being introduced into the equipment.

The obtained isotherm can be used to calculate various parameters that characterize the surface of the powder. In fact, the device calculates the specific surface of a sample using the volume

of gas that forms a monomolecular layer on the surface of the particles. The capillary condensation allows for the measurement of pores volume. Adsorption-desorption measurements of N_2 at 77 K were performed on Co/Fe LDHs using gas manometry (Quantachrome, Autosorb 1). The measurements were carried out after 72 hours of degassing the samples at 80 °C under vacuum (10^{-2} mbars).

From the isotherm data, the BET surface area was calculated by applying the BET equation in the P/P_0 range from 0.05 to 0.3. By fitting the isotherm curve using DFT equation (slit pore, NLDFT equilibrium model), the volumes of micropores (0.7 – 2 nm) and mesopores (2 – 50 nm) were determined.

Quantification of carbon, hydrogen, nitrogen and oxygen

Elemental analysis was used for the quantification of materials composition in C, H and N using flash combustion and pyrolysis for O analysis. This equipment was formed of two independent furnaces (950°C for the C, H, and N analysis and 1070°C for the O analysis) and the separation was done using gas chromatography. The C was quantified under the form of CO_2, H and O under H_2O, and N under the form of NO_x. 1 mg of LDHs was measured in a tin vessel (C and N) or a silver vessel (O) and then analyzed using a flash2000 analyzer (thermo scientific) with an electronic flow meter for the control of O_2 and H_2 gas. An automatic injector/sample changer MAS200R with sample tray for up to 32 samples was used and the EAGERxperience piloted the control of the whole analysis.

Determination of oxygenated groups

Exfoliating and oxidizing graphene sheets lead to the creation of functional groups on the surface of the graphene oxide. In order to quantify these groups, potentiometric titration based on acid-base titration was used where 100 mg of multilayered graphene oxide was combined with 50 ml of sodium nitrate (0.01M), outgassed for 1 hour in an ultrasonic bath. For 48 hours, the mixture was stirred constantly. After that, a NaOH (0.1M) solution was used to titrate the group surface of the MGO. The titration was performed using methrom 848 Titrino plus equipment and the data were first obtained under the form of acid-basic curve with different inflection points. After that, the data were processed using excel sheets and the inflection points were converted to pKa values corresponding to different surface groups.

VIII.5. Study of the pollutants trapping properties

VIII.5.1. Cations trapping: application for Zinc (Zn^{2+})

One of the objectives of this work was to determine the metal trapping capabilities of the synthesized hybrid beads. Zinc was chosen as the metallic cation for this study since it is rejected in the environment by different industries. Adsorption tests were done on pure MGO, CS/MGO and CS/MGO/HDL beads. The adsorption kinetics (amount of Zn adsorbed per gram of adsorbent as a function of time) was studied from a suspension obtained as follows: Under agitation, 100 mg of MGO or 1100 mg of beads were dispersed in 50 ml of deionized water; the pH of the suspension was adjusted to a value of 5 using NaOH (0.1M) or HNO_3 (0.1M) solutions. After the pH has been stabilized, 50 mL of Zn $(NO_3)_2$ was added (1.5 mM). Following the addition of the zinc solution, the pH was re-adjusted to 5. During 2 hours, a sample of 100 µl was taken every 10 minutes for MGO materials and for 420 minutes, a sample of 100 µl was taken for chitosan-based beads. The samples were diluted in 5 mL deionized water, then filtered through 0.22 µm filters (Sodipro, Nylon, d=13 mm) before being treated with 4.9 mL of nitric acid (Aldrich 65% purity, 10% dilution). Analysis of the Zn^{2+} concentration was performed in duplicates using AAS (principle of the method reminded in ***Metal ratios determination***)).

VIII.5.2. Anionic exchange: application for major anions

The ability of LDHs to release their initial anion and capture another informs the solution in a specified concentration and affinity was one of their most essential properties. The experimental method described in this paragraph was carried out using the synthesized Co/Fe-CO_3 and Co/Fe-Cl LDHs with various cationic ratios to investigate the influence of the Co/Fe ratio on anionic exchange capacity and affinity as well as the study of the anionic exchange capacity of the CS/LDH and CS/LDH/MGO beads.

Unlike chlorides, which are easily exchanged, LDHs have a strong affinity for carbonates [5]. As a result, the carbonate anions were exchanged with chlorides prior to any anion exchange experiments with LDH-CO_3^{2-} samples. The chloride exchange was performed using a dialysis method into a 3M chloride solution. Concerning the Co/Fe-Cl LDHs, the same procedure as the carbonated LDHs was followed. For these LDHs, the exchange process was carried out in the abiotic glove box in order to prevent any CO_3^{2-} contamination. The anionic exchange capacity

research was then conducted using the swapped LDH suspension. The anion salts were used to make anionic solutions including sulfates, nitrates, and nitrites.

For the Co/Fe LDHs, the number of monovalent exchangeable anions was theoretically equal to the number of iron cations in the octahedral sheets. Measurements of Fe concentration by AAS (paragraph VIII) were used to calculate the charge to be compensated by interlayer anions. Then, the quantity of anions salts to be used was fixed considering 1.33 anionic exchange capacity (AEC) in order to have an excess of each anion participating in the exchange process.

10 ml of LDH suspension were added to 100 ml of anionic solution containing sulfates, nitrites, and nitrates. The mixture was stirred for 24 hours. Following that, 10 mL of solution was taken and filtered through 0.45 µm and 0.1 µm filters (Sodipro, Nylon, d=13 mm). The ion chromatography was used to analyze the major anions in the filtrate. This technique consists on separating ions based on how they interact with the stationary phase (column in resin: quaternary ammonium) and eluent (mobile phase: KOH). The ions will flow at varying speeds through the column depending on their affinity for the stationary phase and will be distinguished based on their charge and size. Because the eluent will flow through the stationary phase, the ions having a weaker affinity for the resin will be eluted first, followed by the ions with a strong affinity for the column. The ions were detected with a conductivity detector, which generates chromatograms displaying conductivity versus retention time. Because the height and position (retention period) were proportional to the concentration and nature of the ions tested, the concentration of ions can be determined. For this study, the use of Metrohm ion chromatography was used with ammonium quaternary as stationary phase and KOH as eluent. The manipulation was done in triplicates.

VIII.6. Kinetic adsorption models

At a given adsorbent quantity, temperature, flow rate, and pH, adsorption kinetics is a curve that indicates the rate of retention or release of a solute from an aqueous environment to solid-phase interface. For this, two main pseudo orders were used to determine the kinetic absorption models.

The pseudo first order (equation (1)) and pseudo second order (equation (2)) models were tested to fit the kinetic experimental curves:

$$Q(e) = Q_m.(1 - e^{-k_1 t}) \qquad (1)$$

$$Q(e) = \frac{k_2.Q_m^2.t}{1 + (k_2.Q_m.t)} \qquad (2)$$

Where Q(t) (mmol.g^{-1}) was the adsorbed amount of Zn^{2+} as a function of time (t), Q_m was the maximum adsorbed amount of Zn^{2+} (mmol.g^{-1}) in the experimental conditions, k_1 (min^{-1}) and k_2 (g.mmol^{-1}.min^{-1}) were the velocity constants for the first order and second order equations, respectively.

Additionally to both kinetic orders, the intra particle diffusion was also determined using the intra particle diffusion model equation: $q_t = kt^{1/2}$

Where q_t represents the adsorbed quantity of pollutants (mg.g^{-1}), k is the intra particle diffusion constant (mg.g^{-1}/minutes$^{1/2}$) and t is the time (mins). The adsorbed quantity q_t (mg.g^{-1}) versus the square root of time (mins) will allow the obtainment of a linear curve. If the curve obtained was linear and passed through the origin point, the adsorption process was controlled by the diffusion process.

VIII.7. References

[1] C. Morcos, “Procede de captage et de liberation du CO2 assiste par l'electrolyse utilisant des materiaux de type brucitiques,” *http://www.theses.fr*, Dec. 13, 2021. http://www.theses.fr/s294216 (accessed Jun. 14, 2022).

[2] W. S. Hummers and R. E. Offeman, “Preparation of Graphitic Oxide,” *J. Am. Chem. Soc.*, vol. 80, no. 6, pp. 1339–1339, Mar. 1958, doi: 10.1021/ja01539a017.

[3] N. Louvain, J. Peyroux, M. Dubois, W. Simond, and F. Leroux, “Efficient Fluorinating Agent through Topochemical Fluorination of Co−Fe Layered Double Hydroxides.,” *Inorganic Chemistry*, vol. 53, pp. 852–860, 2014, doi: 10.1021/ic402193x.

[4] Y. Kuang, L. Zhao, S. Zhang, F. Zhang, M. Dong, and S. Xu, “Morphologies, Preparations and Applications of Layered Double Hydroxide Micro-/Nanostructures,” *Materials (Basel)*, vol. 3, no. 12, pp. 5220–5235, Dec. 2010, doi: 10.3390/ma3125220.

[5] F. Delorme, A. Seron, B. Vergnaud, P. Galle-Cavalloni, V. Jean-Prost, and J. Manguin, “Evidence of the influence of the cationic composition on the anionic affinity of layered double hydroxides,” *Journal of Materials Science*, vol. 48, no. 15, pp. 5273–5279, Aug. 2013, doi: 10.1007/s10853-013-7318-5.

Chapter 3: Results and discussion

IX.1. Optimization of synthesis conditions and characterization of Co^{II}/Fe^{III} LDHs

IX.1.1. Determination of the pH values for Co^{II}/Fe^{III} LDH synthesis

Co/Fe LDH were synthesized under high supersaturation conditions. As explained in the above paragraph (VII.1.2), this procedure consists in adding an alkaline aqueous solution (2.80 M NaOH and 0.78 M Na_2CO_3 or NaCl) into a cationic solution containing Co^{II} and Fe^{III} in specific ratio until the final pH was reached to allow the formation of LDHs with x ratio between 0.50 and 0.17 (**Table *3***)

Table 3.Co and Fe concentrations used to obtain the desired cationic ratios

Co/Fe ratio	**Cobalt (II) concentration (M)**	**Iron (III) concentration (M)**
2/2 (x=0.50)	0.090	0.090
4/2 (x=0.33)	0.120	0.060
6/2 (x=0.25)	0.135	0.045
8/2 (x=0.2)	0.144	0.036
10/2(x=0.17)	0.150	0.030

Figure 13 shows the pH titration curves of the different Co^{II}/Fe^{III} solutions. The first plateau, which was noticed at a pH value between 2.4 and 3, was related to the Fe^{III} precipitation as ferrihydrite in agreement with Morcos *et al.*[1]. The continuous modulated addition of alkaline solution increases the pH value of the suspension to reach a second plateau in the pH range 6.5-7.5 where co-precipitation of Co/Fe LDH occurs [1].

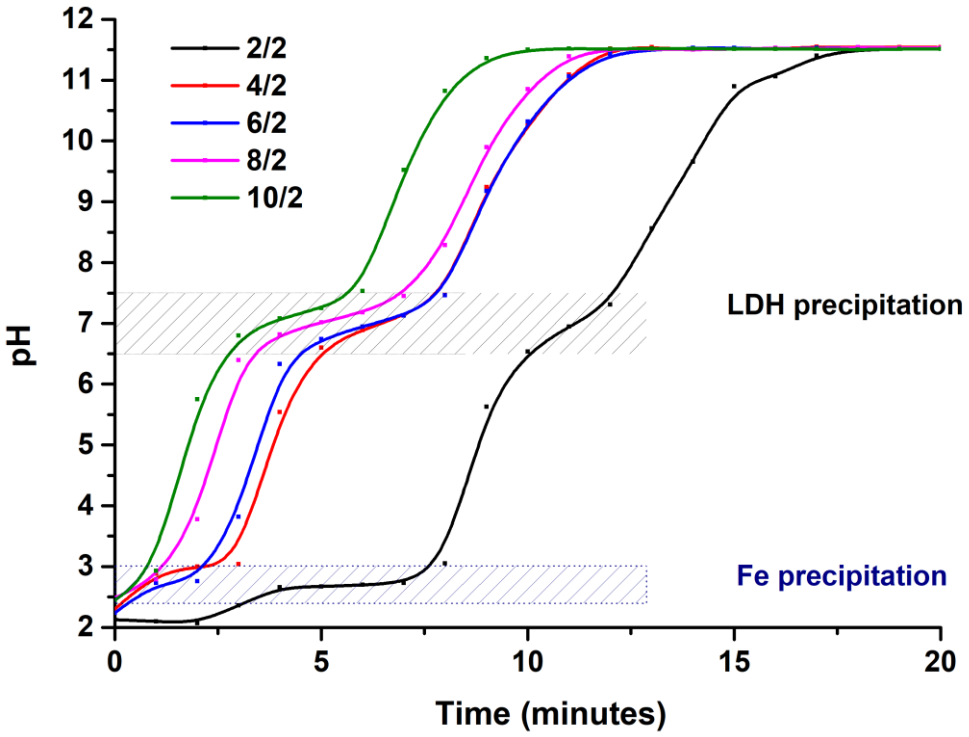

Figure 13. Acid-base titration curves of Co^{II}/Fe^{III} solutions with different cationic ratios using NaOH and Na_2CO_3.

Co-precipitation of cobalt and iron starts at a pH around 6.5 and slows down at pH 7.5. Consequently, a first LDH synthesis pH value of 8.0 was chosen. In the present work, synthesis at a pH value of 11.5 was also performed, as publications showed that higher pH value induces the increase of crystallinity of some LDH compositions [2]–[4]. The third plateau, at a pH value of 11.5, was in agreement with the pH value of the alkaline solution used for the synthesis of LDHs at a final pH value of 11.5.

The synthesized LDHs were described (crystallinity, morphology, and purity) at both pH values, and the results were discussed in the following paragraph.

IX.1.2. Crystallinity and purity of Co^{II}/Fe^{III}-CO_3 LDHs

Synthesis of carbonated LDHs

First, crystallinity and purity of Co/Fe-CO_3 LDHs synthesized at pH values of 8.0 and 11.5 was studied.

Figure 14 a and b show the diffractograms of the maturated Co/Fe-CO_3 LDHs at pH values of 11.5 and 8.0 respectively (section VII.1).

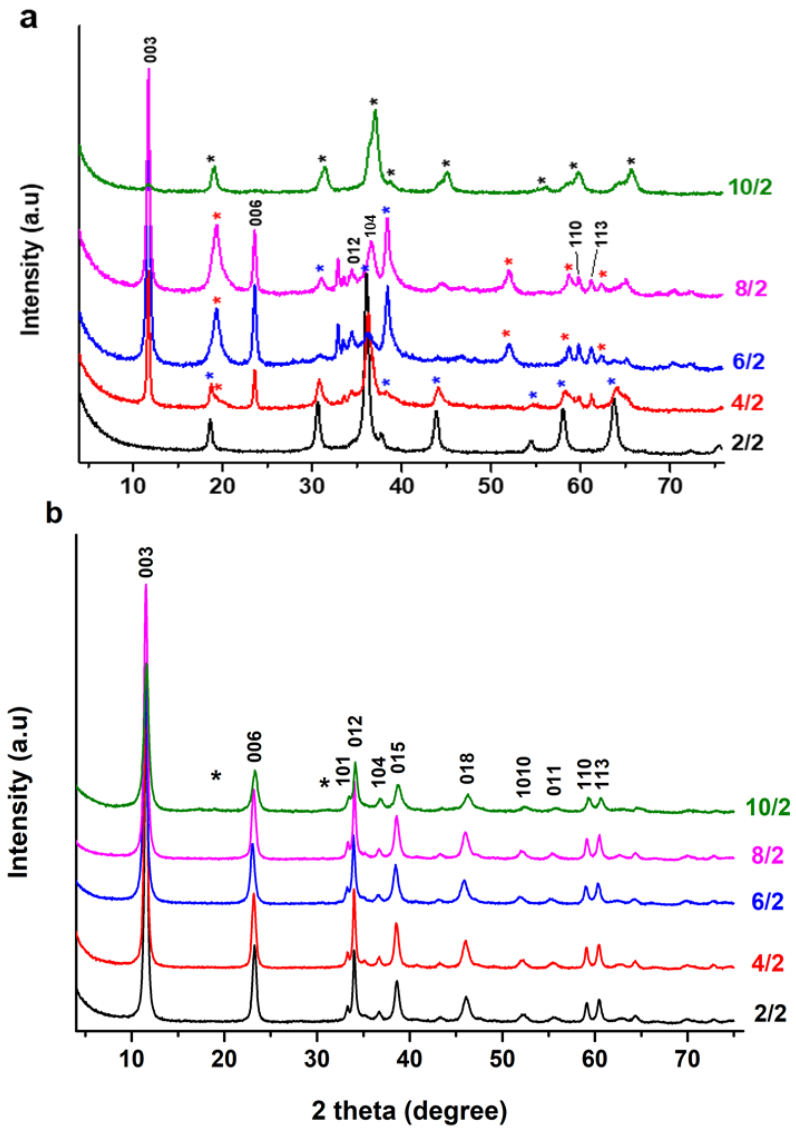

Figure 14.XRD patterns of 2/2, 4/2, 6/2, 8/2 and 10/2 materials synthesized at a pH value of (a) 11.5 and (b) 8.0

Identified crystalline phases are (*): Co $(OH)_2$, (*): Fe_2O_3, (*):Co_3O_4

Except for the 2/2 Co/Fe ratio at pH value of 11.5, whatever the synthesis pH value, strong and narrow diffraction peaks observed at 2θ values 11°; 23°, 34°; 38.5°; 59° and 61°are characteristic of (003), (006), (012), (015), (110), (113) families of reticular plans of Co/Fe-CO_3 LDHs [5], [6] (JCPDS 04-017-8816). The peaks appearing at medium angles, around (2θ= 30 - 50°) corresponding to the h0l and 0kl positions, depend on the polytype and were affected by the stacking defects. The XRD peaks of the synthesized Co/Fe-CO_3 LDH were characteristic of a mixture of rhombohedral 3R-1 and 3R-2 polytypes [7]. Indeed, the two polytypes show similar reflections at the same XRD positions and can only be distinguished using the intensity of the h0l and the 0kl reflections. The 3R-1 polytype was characterized by the presence of strong 0kl reflections while the 3R-2 polytype exhibits intense h0l reflections [8]. The sharpness of the peaks proves that the synthesized LDHs obtained after the ageing process are well crystallized [7].

At the synthesis pH value of 11.5 **(*Figure 14 a*)**, peaks indexed with red and blue asterisks were respectively attributed to cobalt hydroxide (α-$Co(OH)_2$) (JCPDS 74-1057) and maghemite (Fe_2O_3) (JCPDS 83-0112) impurities, for Co/Fe ratio higher or equal to 4/2 and lower or equal to 8/2.

Considering, 10/2, traces of LDH phases were detected as demonstrated through the small (003) peak while for Co/Fe 2/2, the (003) peak was not detected clearly showing no formation of crystalline LDH phases. In both products, the reflection peaks at **18.0**, **30.5, 35.5, 37.0, 43.5, 53.5, 63.0,** 71.5 and 75.0° (JCPDS 39-1346) are characteristic of Co-doped maghemite spinel structure. The 2-theta angles indicated in bold corresponds to the peaks found in the diffractograms indexed with black asterisk. The other peaks were missing due to the low orientation of the aggregates. This result is in agreement with Gregoire *et al.*[9] who demonstrated that at x values lower than 0.33 (4/2 ratio), too much of M^{III} ions are present, which leads to M^{III}-(O)-M^{III} interactions belonging to neighboring octahedral sites. Such interactions induce strong electrostatic repulsions, which was reported in the complete absence of LDH phases compared to other ratios. Those observed at 19.0, 31.0, 37.0, 38.5, 45.0, 56.0, 59.5° are characteristic of a Fe-doped Co_3O_4 spinel structure (JCPDS 09-0418) which is the major phase.

From solids synthesized at pH 8.0 (***Figure 14 b***), the XRD patterns exhibit the characteristic reflections of LDH materials for all the investigated Co/Fe ratios. Well-crystallized LDHs were observed for Co/Fe ratio lower than 10/2. For the Co/Fe 10/2 ratio, traces of cobalt based impurity, respectively detected at 17.0 and 19.0°, were attributed to Co_3O_4 (JCPDS card

No.01.080.1533). The other bands characteristic of those impurities were not detectable due to the overlaying of the Co_3O_4 characteristic bands with those of LDH phases.

From data provided by XRD analysis performed on the solids synthesized at pH 8.0 and 11.5, the formation of impurities can be related to the pH value used during the co-precipitation method. In comparison with the data obtained at pH 8.0, it can be assumed that the high pH value 11.5 lead to the simultaneous dissolution of the formed LDH and reprecipitation of iron oxide and cobalt oxyhydroxide (**Figure *14***).

The XRD study clearly shows the obtainment of well-crystallized LDH phases synthesized at a pH value close to 8.0 for Co/Fe ratio between 2/2 and 8/2.

Table 4.XRD data extracted from the patterns for Co/Fe-CO3 LDH obtained at pH 8.0.

Co/Fe ratio	**2/2**	**4/2**	**6/2**	**8/2**	**10/2**
$2\theta_{(003)}$ (°)	11.68	11.52	11.44	11.52	11.53
$2\theta_{(110)}$ (°)	59.24	59.09	59.05	59.14	59.25
d_{003} (Å)	7.56	7.67	7.73	7.67	7.66
d_{110} (Å)	1.55	1.56	1.56	1.56	1.56
"a" (Å)	3.10	3.12	3.12	3.12	3.12
"c" (Å)	22.68	23.01	23.19	23.01	22.98
Particle thickness (Å)	178 ± 12	202 ± 16	163 ± 10	183 ± 13	125 ± 6
Full width at half maximum ± 0.03 (°)	0.44	0.39	0.48	0.43	0.61

Table *4*. presents the $2\theta_{(003)}$ and $2\theta_{(110)}$ positions, the full width at half maximum (FWHM) (003), the d_{003} (Å) and d_{110} (Å) as well as the lattice parameters "c" and the unit cell parameter "a" calculated from the positions of the (003) and (110) reflections in the XRD patterns of Co/Fe-CO_3 LDHs synthesized at pH 8.0 (**Figure *14 b***). Particle thickness is determined using XRD data and Scherrer equation [10] using 003 lines with a K value of 0.89.

For Co/Fe ratio lower than 10/2, well-crystalized LDHs were characterized by high (003) intensities (**Figure *14*** b), with a full width at half-maximum (FWHM) between 0.39 and 0.48° ± 0.03°(standard error is related to step size used for the measurement) and particle thickness between 163 ± 10 Å and 202 ± 16 Å. From 2/2 to 8/2 Co/Fe ratios, mean FWHM value is 0.44°, therefore showing homogeneous average particle thickness around 180 Å related with the stacking of 8 layers. A less crystallized structure was observed for Co/Fe 10/2 with smaller (003) intensities, higher FWHM (0.61°) and smaller particle thickness of 125 Å, related with the stacking of approximately 6 layers.
Whatever the Co/Fe ratio, the lattice parameter "a" remains constant at 3.12 Å, in agreement with the close radii values of Co^{II} (0.89 Å) and Fe^{III} (0.79 Å) in high spin octahedral sites [11].

The two (00l) narrow symmetric peaks, at low angles (2θ= 11.5 and 23.2°) are linked to the basal spacing reflection which position mainly depends on the size of the intercalated anions. Considering the Co/Fe 2/2 ratio, the layer to layer spacing d(003) of 7.56 Å is in good agreement with an OH-based interlayered LDH [12] along with the presence of carbonate anions. The OH anions were provided by the sodium hydroxide alkaline solution, whereas the d(003) of 7.73 Å obtained for the Co/Fe 6/2 ratio is in good agreement with the predominance of CO_3^{2-} in the interlayer space [13],[14]. Although the Co/Fe ratio influences the nature and the content of the interlayered anions [12], [15], the results showing an impact was only observed for the 2/2 ratio, where interlayered OH^- and CO_3^{2-}anions were highlighted. For the ratios between 4/2 and 10/2, the layer to layer spacings close to 7.67 Å observed for the 4/2, 8/2 and 10/2 Co/Fe ratios were rather in accordance with the presence of CO_3^{2-} as predominant anion in the interlayer spacing [16].

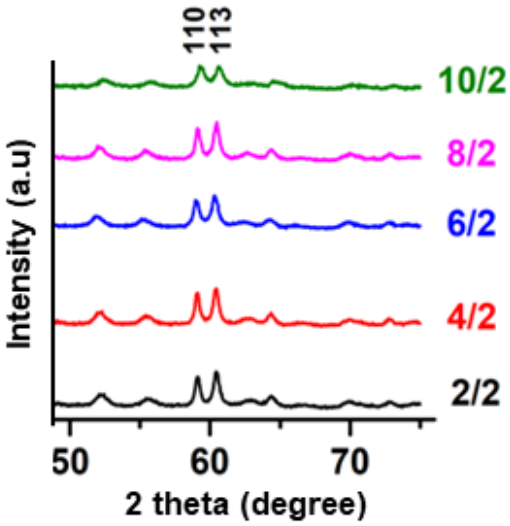

Figure 15. Highlights of the double peak of Co/Fe LDHs in the range of 55 - 70°

The peaks appearing in the range from 55 to 65° in 2θ were characteristic of the structural organization inside the layers and their positions depend on the nature of the cations constituting the LDH sheets [17]. From Co/Fe 6/2 to 10/2 ratios, a slight shift to higher angles observed for (110) and (113) is in good agreement with the increase in Co content in the LDH structure whose radii in high spin octahedral site Co^{II} (0.89 Å) slightly higher than that of iron Fe^{III} (0.79 Å) [11].

IX.1.3. Morphological and textural studies of Co^{II}/Fe^{III}-CO_3 LDHs

The morphological and the textural studies of the synthesized Co/Fe-CO_3 LDHs were determined using SEM and TEM analyses. The SEM images (**Figure *16***) showed that whatever the investigated Co/Fe ratio, the LDH particles were roughly hexagonal shaped and arranged in the form of platelets-like sheets. This morphology results from the natural growth of well-crystallized LDHs [18].

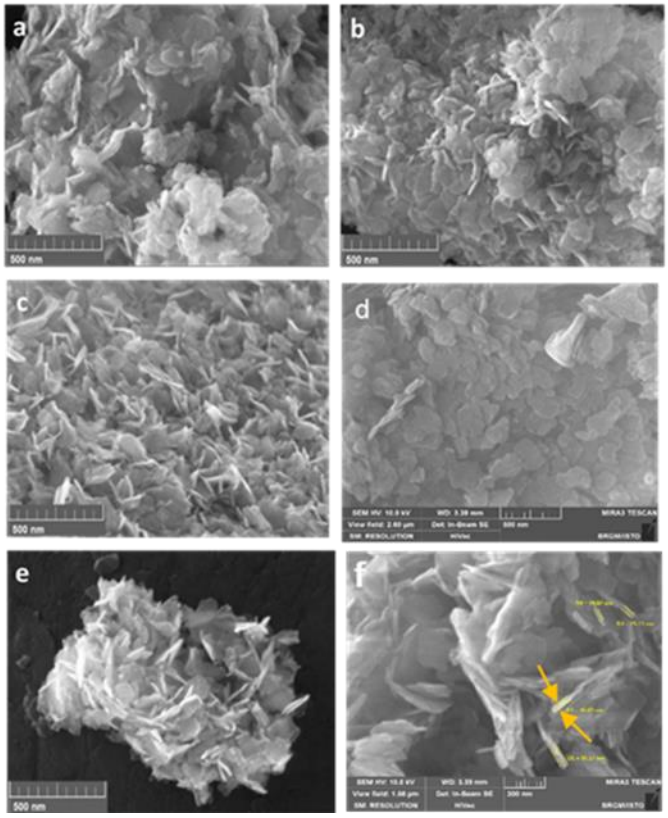

Figure 16.SEM images of Co/Fe-CO_3 LDHs a) 2/2, b) 4/2, c) 6/2 d) 8/2, e) 10/2 and f) particles thickness of 8/2

The well-defined lamellar particles in the 2/2 to 8/2 Co/Fe ratios have a random particle size (diagonal of the hexagon) between 200 and 500 nm. They are distributed randomly. In accordance with Zhang *et al.* [19], SEM images of the 2/2 Co/Fe ratio revealed particle sizes between 400 and 500 nm comparable with those 4/2 ratio controlled between 300 and 400 nm. However, the particle size of the Co/Fe 6/2 and 8/2 ratios showed similarity, ranging from 200 to 300 nm. The increase of the Co/Fe ratio up to 10/2 (**Figure *16***.e) sharply decreases both LDH crystallinity and particle size (less than 200 nm), in agreement with XRD data.

In agreement with Zhang et al. [19], the increase in Co versus Fe leads to more rounded morphology instead of sharp hexagonal particles (**Figure *16.d***, Co/Fe 8/2 LDH). SEM images also allow the determination of the mean thickness of ratios of 2/2 to 8/2 particles in the range of 19 to 40 nm (***Figure 16.f***) this thickness was obtained based on the observation of the particles placed in a perpendicular way to the observation plane.

On the other hand, the TEM images (**Figure *17***) showed hexagonal shape with random sized particles, which were consistent with the SEM observations.

To avoid the dehydration of the solid samples deposited on a simple grid, placed under vacuum and electron beam, the stabilization the LDH particles must be performed by embedding the LDH in a resin before TEM analysis.

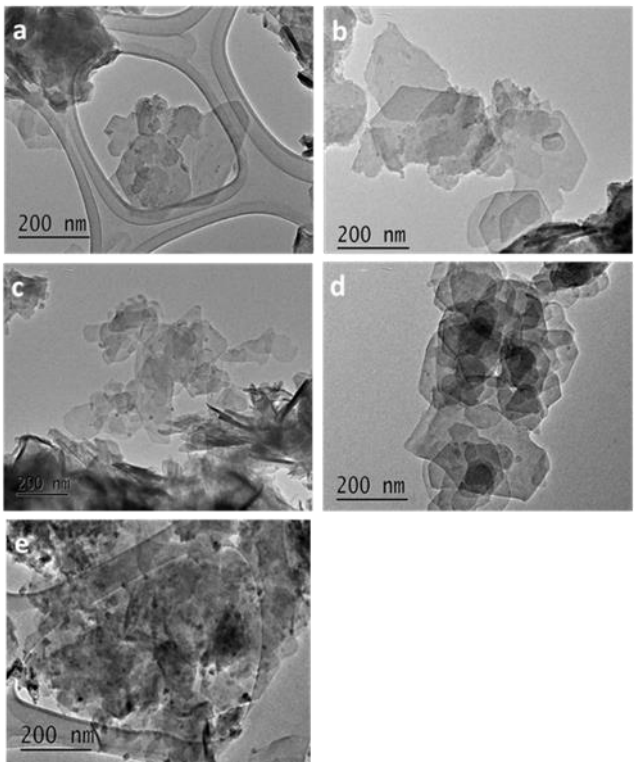

Figure 17.TEM observations of Co/Fe LDHs with ratios: a) 2/2, b) 4/2, c) 6/2, d) 8/2 and e) 10/2

Energy dispersive X-Ray analysis (EDX) was used on single particles of each Co/Fe LDH to better investigate the distribution of the Co/Fe ratios (results are presented in the next paragraph). On the surface of the LDH from Co/Fe 2/2 to 8/2 a few, small other particles containing iron or cobalt were observed. These particles were much more numerous on the 10/2 Co/Fe sample. They can be attributed to some spinel impurities that have been detected and identified by XRD analysis in the 10/2 Co/Fe ratio.

IX.1.4. Chemical study of Co^{II}/Fe^{III}-CO_3 LDHs

Comparative study of LDH Co^{II}/Fe^{III} ratios determined from bulk (AAS) and local (EDX) measurements

By comparing the Co/Fe experimental ratios, obtained using the AAS analysis and the expected ones based on the amount of Co and Fe salts used for the synthesis, only a slight

difference is observed with measured ratio. The measured ratios were slightly below the expected ones which means that a small part of Co did not precipitate during acid-base titration (**Table *5***). For Co/Fe 6/2 and 8/2 ratios, this shift versus the expected values was 3.4 and 5.3% respectively but reaches 8.7% for the 10/2 ratio.

Table 5. Comparison of data obtained by AAS from dissolved Co/Fe LDHs suspension and EDX from different particles of each LDH synthesized at pH value of 8.0

Co/Fe LDHs	**Introduced ratio**	**Co/Fe molar ratio (AAS)**	**Co/Fe molar ratio (EDX)**
2/2	1.0	1.0	2.1
4/2	2.0	2.0	2.2
6/2	3.0	2.9	2.9
8/2	4.0	3.8	3.2
10/2	5.0	4.6	4.0

For a better insight into the Co/Fe ratios, energy dispersive X-Ray analysis (EDX) were performed on few individual particles of each LDH. Data were compared to those acquired by AAS. It appears from EDX analysis on few single particles that the ratios range from 2.1 to 4.0 (**Table *5***) instead of 1 to 5. For the 2/2 introduced ratio, EDX showed particles having ratios of 0.94 and in a lesser content 1.88. This may be caused by the trivalent cations becoming first cationic neighbors leading to a sensitive increase of the electrostatic repulsion in the cationic layer [9] thus giving rise to a 4/2 Co/Fe ratio. For the 10/2, EDX showed co-precipitated particles having ratios of 8/2 and in a lesser content Co enriched nanoparticles, as Co_3O_4 spinel type ones (XRD). For both the 2/2 and 10/2 introduced ratio, the difference between the expected ratio and the experimental one measured using EDX could be attributed to, respectively for 2/2 and 10/2, iron and cobalt rich amorphous nanoparticles in agreement with XRD. On the other hand, the 4/2, 6/2 and in a lesser extent, 8/2 Co/Fe ratios were well established ratios encountered in well crystalline Co/Fe LDHs. As shown in **Table *5***, as the quantity of cobalt increases, the shift from the expected ratio tends to increase. For the 8/2 ratio, the limited ageing period (24 hours) of the suspension after coprecipitation may be responsible for the diverse particle ratios differing from those expected. A longer ageing period may be required to achieve more homogenous particles in terms of cationic ratios. EDX analysis was

performed on specified particles present in the LDH sample which were different from the others and special attention should be taken when discussing the 2/2, 8/2 and 10/2 ratios since these particles were not representative of average of the overall samples. This may be the reason why the obtained ratios using the EDX analysis were not the same as those determined using AAS analysis. However, the 4/2 and 6/2 ratios showed the absence of these particles leading to the obtainment of Co/Fe ratios in agreement with AAS analysis.

Determination of the nature of the interlayer anions

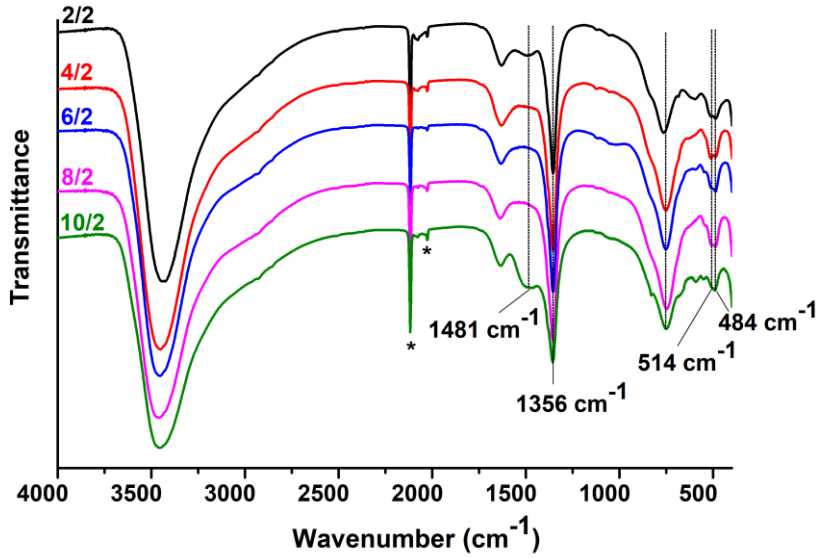

Figure 18. Overlay of Co/Fe-CO_3 LDHs/ Potassium ferricyanide FTIR spectrum of Co/Fe ratios 2/2, 4/2, 6/2, 8/2 and 10/2. (*): potassium ferricyanide bands

FTIR measurements were performed on LDH samples to investigate the purity of the material as well as to identify interlayer anions. The presence of a broad band at 3450 cm^{-1} is essentially related to the O-H stretching vibrational mode of interlayered and adsorbed water molecules [20]–[22]. The bending mode band of water molecules is observed at 1638 cm^{-1} (***Figure 19***)

[4], [23], [24]. Highlights of the FTIR spectra in the 1200-1700 cm^{-1}, 600-1000 cm^{-1} and 450-600 cm^{-1} regions are shown in ***Figure 19 a, b and c***.

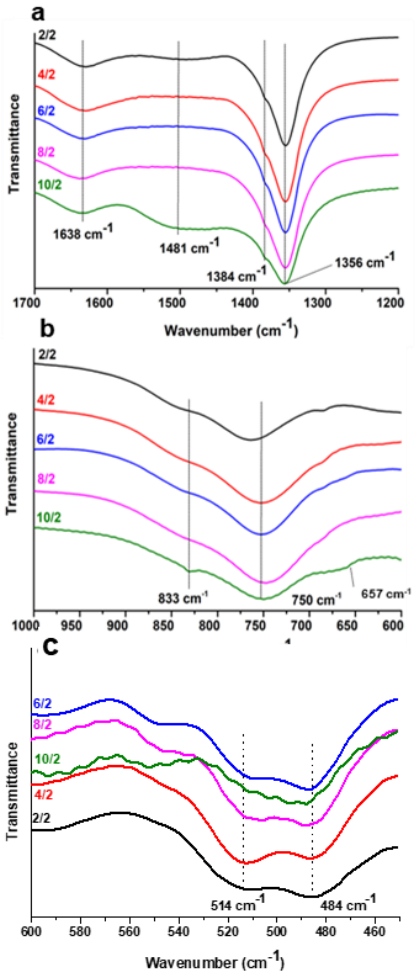

Figure 19. FTIR spectra of Co/Fe-CO_3 LDHs: highlight of interlayer anions (a, b) and structural metal-oxygen bonds (c)

The presence of carbonate anions in the interlayer space is clearly shown by the band at 1356 cm^{-1} related to the asymmetric stretching vibration of C-O bond of carbonates [25]. The narrow band observed at 1384 cm^{-1} (***Figure 19***) demonstrates the presence of nitrate anions in the interlayer space [26], [27] as traces remaining after the anion exchange process. At wavenumber lower than 1000 cm^{-1}, bands at 833 cm^{-1} and at 750 cm^{-1} (***Figure 19***) were attributed to metal (Co^{II} and Fe^{III})-carbonates bonds [28]–[31].

For the Co/Fe 2/2 and 10/2 ratios, the additional presence of a wide band at 1481 cm^{-1} could be caused by the presence of HCO_3^- anions already highlighted in the literature [32]. The double band at 514 - 484 cm^{-1} is attributed to Co-O and Fe-O bonds from LDH structure respectively [33]. The weak band at 544 cm^{-1} is characteristic of Co-OH vibration mode in LDH based materials [34].

For the 10/2 Co/Fe ratio, the band at 657 cm^{-1} is attributed to Co_3O_4 impurity [35], in agreement with XRD analysis. For all samples, FTIR demonstrates the obtainment of carbonate-based LDHs.

Table 6. Elemental analysis of Co/Fe-CO3 LDHs with different cationic ratios

Co/Fe ratio	**Fe (mol) .10-6**	**LDH phase Co/Fe ratio**	**C (mol) ± 0.001 .10-6**	**HCO3- (mol) .10-6**	**CO32- (mol) .10-6**	**R=Fe3+ /C**	**H2O (mol)**
2/2	3.9	3.2/2* **4/2**	**1.4**	0.0 **0.7**	1.0 **0.6**	**2.8**	4.3 **6.4**
4/2	2.3	**4/2**	**1.2**	**0.4**	**0.8**	**1.9**	**5.5**
6/2	1.8	**6/2**	**1.9**	**1.8**	**0.1**	**1.0**	**6.9**
8/2	1.7	**6/2** 7.6/2**	**1.7**	**1.3**	**0.3**	**1.0**	**7.7** 6.1
10/2	1.6	**8/2** 9.3/2**	**1.9**	**1.8** 1.8	**0.1** 0.1	**0.8**	**4.1** 2.8

Values represented in bold correspond to stoichiometry determined by the combination of elemental analysis and local analysis (TEM/EDX).

Values with asterisks correspond to stoichiometry determined by elemental analysis.

*3.2/2 is the lowest ratio that can tolerate an LDH structure including all carbon as CO_3^{2-} and/or HCO_3^- in the interlayer space

**7.6/2 and 9.3/2 are the highest ratios that can tolerate LDH structure including all carbon as CO_3^{2-} and/or HCO_3^- in the interlayer space. However, TEM/EDX analyses, showed Co-enriched impurities simultaneously with LDH particles thus the 9.3/2 ratio is not possible.

The results of elemental analysis of the Co/Fe-CO_3 LDHs are presented in **Table *6***. Based on the flash pyrolysis of the samples with different Co/Fe ratios, this technique provided the mass content of carbon, which was converted to a mole number for comparison with the amount of iron present in each LDH. Because carbonates are twice negatively charged while each mole of Fe^{3+} generates one exceeding positive charge, a half of CO_3^{2-} is required to compensate the excess charge generated by one Fe^{3+}. If all of the carbon in the surroundings was in the form of carbonates, the R ratio, which is the mole number of Fe^{3+} over the mole number of carbon (R= Fe^{3+}/C), should be equal to 2.

The R ratio (2.8) for Co/Fe 2/2 (**Table *6***), indicates that the amount of Fe was higher than the amount compensated by CO_3^{2-}. Since FTIR, examination revealed the absence of any other interlayer anion aside carbonates ($0.6.10^{-6}$ mol) and hydrogenocarbonates ($0.7.10^{-6}$ mol), the extra charge may be balanced by the hydroxide anions. It is consistent with the d spacing of 7.56 Å determined by using XRD analysis, which is smaller than that of pure carbonated LDHs but coherent with that of partially hydroxylated ones. The presence of HCO_3^- in the interlayer region in in good agreement with the FTIR analysis were the presence of a band at 1450 cm^{-1} was observed.

Considering 4/2 Co/Fe ratio, the R= 1.9 was close to 2.0, indicating that the Co/Fe LDH was mostly carbonated with a slightly higher mole number of carbon than the Fe^{3+} mole number suggesting the presence of a mix of CO_3^{2-}($0.8.10^{-6}$) and HCO_3^- ($0.4.10^{-6}$) with a higher proportion of carbonates compared to HCO_3^- as calculated using the total mole number of carbon. In the case of the Co/Fe 6/2, 8/2, and 10/2 ratios, R= 1.0, and 0.8, respectively, lower than two, indicating the presence of more carbon than required for charge neutrality. The R ratio equal or close to 1.0, indicates that the carbon species are under the form of HCO_3^-. Since the d(003) values calculated using XRD results (**Table *4***) agreed well with pure carbonated LDHs, and furthermore the presence of CO_3^{2-} in the interlayer region was confirmed by FTIR analysis except for the 10/2, where the presence of the band at 1450 cm^{-1} was observed, these values of R lower than 2 were probably due to the evolving of the LDH structure inside the suspension. Whatever the Co/Fe cationic ratio, the presence of HCO_3^- and CO_3^{2-} coexist.

Since elemental analysis showed the presence of HCO_3^- in different proportions in the interlayer region along with carbonates anions for all cationic ratio, the FTIR analysis was performed on the 6/2 ratio for the comparison between the spectrum of Co/Fe 6/2 obtained directly after synthesis and the one obtained after 1 year of storing the LDH under the form of suspension.

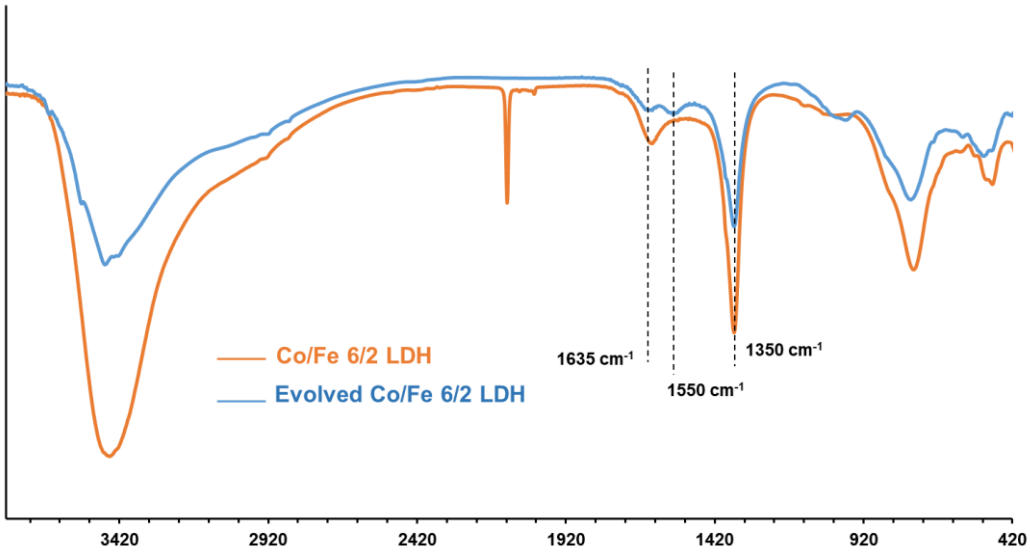

Figure 20. Overlay of FTIR spectrum of Co/Fe 6/2 LDHs directly after synthesis (orange one) and after one year of storing (bleu one).

It is obvious that the evolved 6/2 LDH showed an additional band at 1550 cm^{-1} (***Figure 20***) which may be caused by the presence of HCO_3^- in the interlayer region. A decrease in the carbonates band at 1350 cm^{-1} was also observed for the evolved 6/2 LDH in comparison with the Co/Fe 6/2 LDH directly analyzed after synthesis. These results are in good agreement with the elemental analysis data. The band at 1635 cm^{-1} was attributed to the vibrational mode of water molecules.

The elemental examination revealed no nitrogen in the samples. This confirms that the presence of nitrate, highlighted by the band observed in the FTIR technique at 1380 cm^{-1} was correlated to traces.

IX.1.5.Thermal degradation, pore volume and surface area study

The thermal degradation and the determination of the specific surface area of Co/Fe-CO_3 LDHs with different cationic ratios was performed using TGA analysis and S_{BET} techniques respectively.

The obtained results using thermal degradation were investigated and compared to those provided by CHON analyses in order to attempt the determination of the LDH formula.

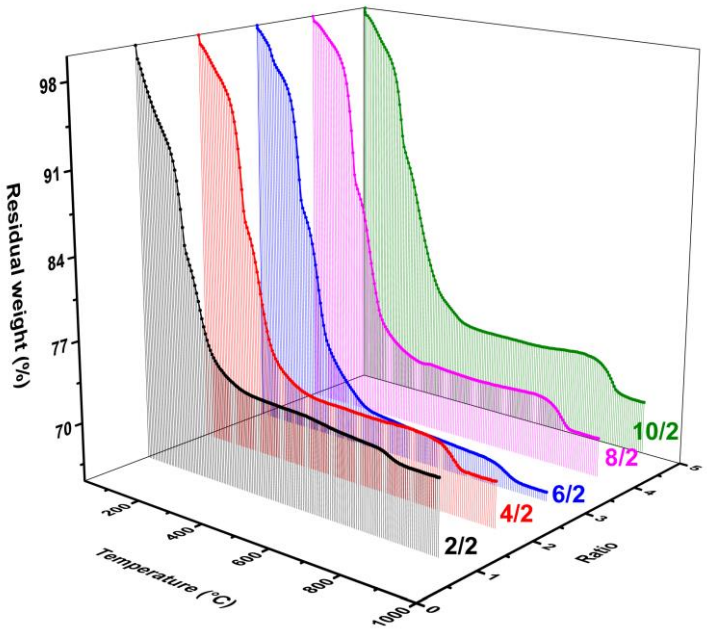

Figure.21.TGA curves of Co/Fe LDHs with the different cationic ratio

In order to compare the thermal degradation of the investigated Co/Fe LDHs, the thermal behavior of LDHs was studied using TGA analysis (***Figure.21***). In agreement with Morcos [36], who investigated the thermal degradation of Co/Fe LDHs using high temperature XRD (HTXRD) and thermogravimetric analysis coupled to gas chromatography, TGA curves showed three main degradation stages [36]. The first one in the range from room temperature to 100 ºC is linked to the departure of physisorbed water molecules. This observation agrees with the results of HTXRD data obtained by Morcos *et al.* [39] which shows that the $d_{(003)}$ parameter remained constant throughout this temperature range. It should be noted, however, that below 100 ºC, the variation of physisorbed water content regarding the different samples (**Table *7***) can be attributed to the sample preparation before analysis.

In the range from 104 to 165 ºC, de-hydroxylation of LDH structure and release of interlayer water molecules occurred along with, in a lesser extent, the removal of a fraction of carbonates interlayer anions [36].

During the third stage (165 ºC - 360 ºC), the residual loss is caused, in accordance to the work of Morcos [36], by the removal of carbonate ions which continues slowly. In this range of temperature, de-hydroxylation of cobalt oxyhydroxide also occurred for powders containing such impurities [36].

Table 7. Carbon content speciation and water molecules content of the different synthetized Co/Fe LDHs

Co/Fe ratio	**Co/Fe ratio in LDH phase**	**HCO_3^- (mole)**	**CO_3^{2-} (mole)**	**H_2O (mole)**
2/2	**4/2** 3.2/2*	**0.0** 0.6	1.0 0.7	1.6 1.5
4/2	4/2	0.4	0.8	2.6
6/2	**6/2**	**1.8**	**0.1**	**5.0**
8/2	**6/2** 7.6/2**	**1.2** 1.1	**0.4** 0.4	**3.5** 5.4
10/2	8/2	0.2	0.9	3.3

According to the work of Morcos, spinel phase is obtained from the decomposition of the LDH Co/Fe structure. For each synthesized ratio, the residual mass obtained on the plateau, located between 200 and 600° C, corresponds to the mass of spinel. For each synthesized LDH, an AB_2O_4 type spinel was considered. For each spinel, whose mass can be calculated, the Co/Fe ratio considered was the one obtained using AAS analysis carried out on the synthesized products. A pure LDH structure generates, using thermal decomposition, a spinel structure whose ratio is identical to that of heat-treated LDH. An LDH associated with spinel type impurities generates by thermal decomposition a spinel whose ratio is equal to the initial ratio determined by AAS analysis of the elaborated solid. From the loss of mass leading to the formation of the spinel phase, the initial mass of hydrated LDH was determined. In the presence of impurities, the mass of the latter was subtracted from the final residual mass to determine, via the overall mass loss, the initial mass of hydrated LDH. For the Co/Fe 2/2 ratio, the Fe_2O_3 impurity was not considered in the mass loss calculations since this phase thermally decomposes only above 1000°C. The mass of interlayer water is determined graphically (**Figure.*21***) between 100 and 150°C. The mass relative to the loss of structural OH is determined by calculation, taking into account the quantities of Co and Fe that constitute the LDH structure. The loss of mass relative to the dehydroxylation of the LDH structure is the difference between the mass of the OH groups constituting the LDH sheets and the mass of the oxygen keeped in the residual spinel. The subtraction of the mass of interlayer water as well as the mass related to the dehydroxylation of LDHs made it possible to determine the loss of mass linked to carbonates and bicarbonates anions. This last treatment made it possible to determine the speciation of the carbonaceous species in the interlayer space, by balancing the charges of

the carbonaceous species with the excess charges brought by the iron constituent of the structure of the LDHs.

The calculated results obtained from TGA data are in good agreement with those obtained by the elemental (CHON) analysis. The speciation of carbonaceous anionic species evolves within LDHs whose Co/Fe ratio is between 3.2/2 and 8/2, with an increase in the amount of HCO_3^- in agreement with the increase in the Co/Fe ratio. This result tends to predict interesting perspectives for the mutual trapping of bivalent and monovalent anions using Co/Fe LDHs.

S_{BET} techniques was used to analyze the specific surface area and the porosity of the synthesized LDHs, which could influence trapping of anions pollutants. N_2 adsorption/desorption measurements were carried out to determine the specific surface areas of the synthesized LDHs with different cationic ratios. The N_2 adsorption/desorption isothermal curves were shown in **Figure.22.**

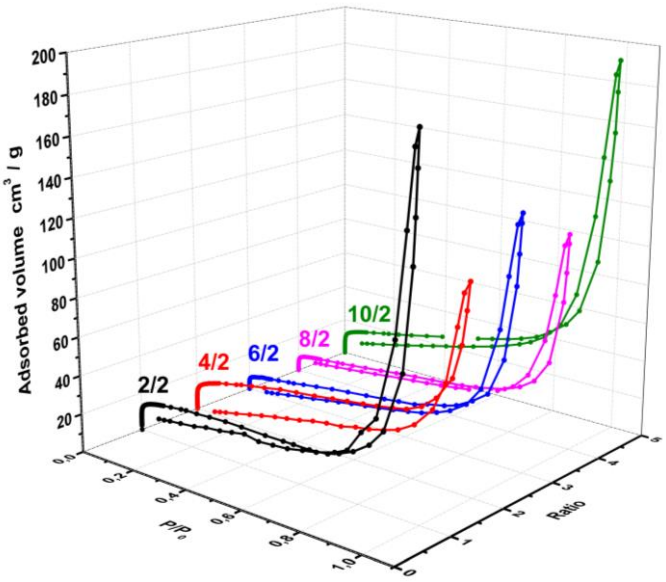

Figure.22.N_2 adsorption-desorption isotherms of Co/Fe-CO_3 LDHs with different cationic ratios

All five samples presented typical type I isotherm characteristic of non-porous samples. Hysteresis loops at high P/P_0 values, higher than 0.8, suggest a mesoporous structure (type IV) [37]. The specific surface areas calculated by the Brunauer–Emmett–Teller (BET) method were shown in **Table *8***.

Table 8. Pore volumes and specific surface area of synthesized LDHs

LDHs	**2/2**	**4/2**	**6/2**	**8/2**	**10/2**
Vmicro (cm^3/g)	0.010	0.010	0.002	0.005	0.003
Vmeso (cm^3/g)	0.260	0.099	0.168	0.135	0.232
S_{BET} (m^2/g)	67	68	35	40	60

According to IUPAC rules, mesoporous materials contain pores with diameters between 2-50 nm while microporous materials have pores smaller than 2 nm and, macroporous one has pores higher than 50 nm in diameter.

Comparison of the mesoporous volumes with the microporous ones clearly shows that synthesized LDHs contain a small amount of mesopores originated from the random distribution of the 2D particles. For low P/P0 values, it appears that the nitrogen desorption curves were slightly below the adsorption curves in relation with the low amount of nitrogen adsorbed due to non-porous samples containing very few micropores.

Co/Fe LDHs showed low BET surface areas ranging from 35 to 68 m^2/g (**Table *8***) as expected when considering literature, 148.1 m^2/g for Mg/Al-CO_3 LDH [38], and 46.9 m^2/g for Fe/Al LDHs [39]. BET surface areas of different synthesized samples were expected to differ depending on the particle size linked to the synthesis process and the platelet arrangement after the drying step. These results are in agreement with SEM observations (**Figure *16***) which show that the LDHs synthesized for the 2/2 and 4/2 ratios have particle sizes close to and larger than those of the 6/2 and 8/2 ratios.

IX.1.6. Synthesis of chloride LDHs

The Co/Fe LDHs showed high affinity for carbonate anions due to the high interaction between the positively charged sheets of the Co/Fe LDHs and the carbonate anions present in the interlayer region, this was proven by Morcos *et al.*[1]. However, the low affinity of LDHs towards chloride anions was demonstrated for different LDH composition, leading to easier anionic exchange process with other anions such as sulfates, nitrates and nitrites. This is why the synthesis of Co/Fe-Cl LDHs at a pH value of 8.0 using the coprecipitation at high supersaturation method with NaOH (2.78M) and NaCl (0.78M) alkaline solution was

conducted. In order to prevent the contamination of the synthesized chloride Co/Fe LDHs by atmospheric CO_2, such synthesis was thus performed in an abiotic glove box under N_2 atmosphere. The synthesized Co/Fe-Cl LDHs did not follow any ageing process, to allow comparison purposes between the anionic exchange capacity of the synthesized chloride LDHs and the chitosan-based beads containing LDHs which will be discussed later on.

The diffractograms of Co/Fe-Cl LDHs with cationic ratio x between 0.17 and 0.50 were presented in ***Figure.23***

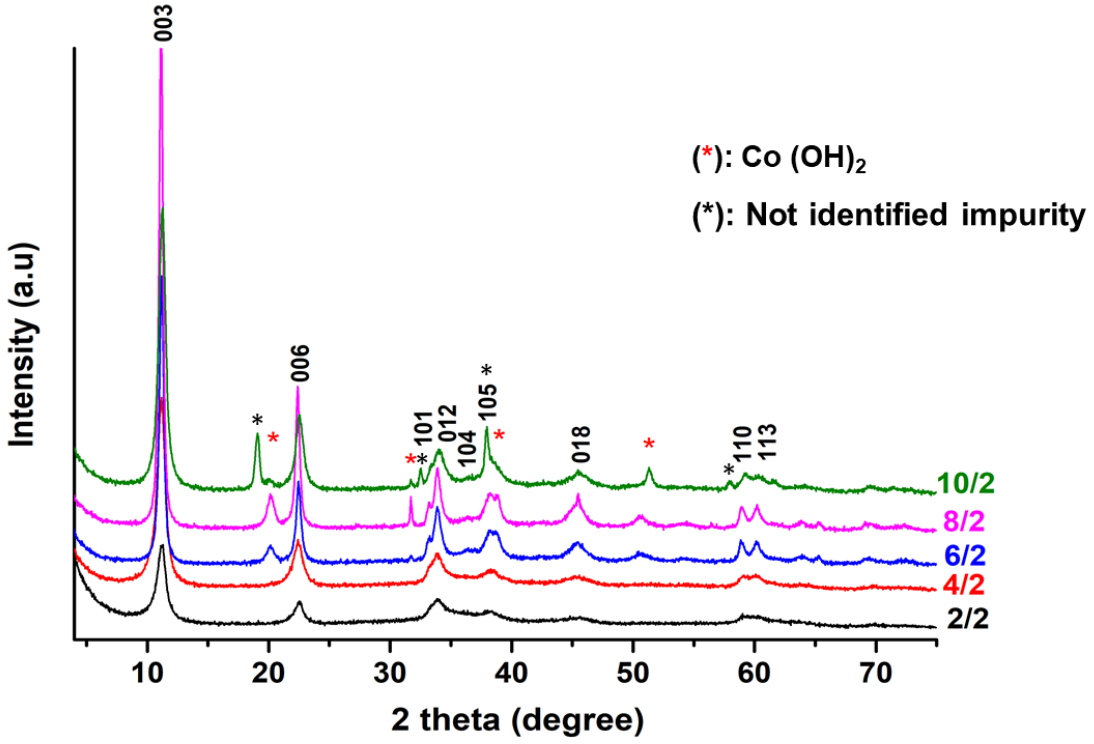

Figure.23. XRD patterns of materials synthesized at a pH value of 8.0 using NaOH/NaCl alkaline solution from 2/2, 4/2, 6/2, 8/2 and 10/2 Co/Fe solution

For all cationic ratios, the presence of peaks corresponding to 11.2°; 22.5°, 34.1°; 38.5°; 58.4° and 60.1° were characteristic of (003), (006), (012), (015), (110), (113) of LDH reticular plans (JCPDS 04-017-8816). The 2/2 and 4/2 cationic ratios showed the absence of the peaks corresponding for α-$Co(OH)_2$ phase. However, these ratios have lower crystallinity than the 6/2, 8/2 and 10/2 ratios. The increase of cationic ratio lead to the increase of the cobalt quantity leading to the formation of α-$Co(OH)_2$ impurity (JCPDS no. 46-0605). For ratios higher than 4/2, the presence of the peaks at 9.6°, 19.3°, 33.4°, and 59.6° correspond to the lattice distances of (003), (006), (012), and (110) planes of α- $Co(OH)_2$ structure (JCPDS no. 46-0605). For the 10/2 ratio, the presence of an additional phase was observed at 19° and 33° which could not be attributed because of the low intensity of the peaks. Indeed, chloride LDHs did not follow any

ageing process which could favor the dissolution of impurities (α-$Co(OH)_2$) and consequently the insertion of resulting free Co^{2+} into the LDH structure. Note that the impact of ageing process can be explained by the Ostwald growth, which consists on dissolving the small particles of LDHs and reprecipitation of constituting chemical elements into bigger ones to generate larger and more crystalline LDH particles [40].

Table *9*.presents the $2\theta_{(003)}$ and $2\theta_{(110)}$ positions, the full width at half maximum (003), the d_{003} (Å) and d_{110} (Å) as well as the lattice parameters "c" and the unit cell parameter "a" calculated from the positions of the (003) and (110) reflections in the XRD patterns of Co/Fe-Cl LDHs synthesized at pH 8.0 (***Figure.23***). Particle thickness was determined using the 003 lines provided by XRD through Scherrer equation with a K value of 0.89 [10].

Table 9.XRD data extracted from the patterns for Co/Fe-Cl LDH

Co/Fe LDH	**2/2**	**4/2**	**6/2**	**8/2**	**10/2**
$2\theta_{(003)}$ (°)	11.20	11.14	11.17	11.13	11.23
$2\theta_{(110)}$ (°)	59.22	59.10	58.94	58.97	59.22
d_{003} (Å)	7.89	7.93	7.89	7.93	7.87
d_{110} (Å)	1.56	1.56	1.56	1.56	1.56
"a" (Å)	3.13	3.13	3.13	3.13	3.13
"c" (Å)	23.67	23.79	23.67	23.79	23.61
Particle thickness (Å)	95 ± 7	101 ± 8	190 ± 27	211 ± 33	116 ± 10
Full width at half maximum (± 0.03) (°)	0.83	0.78	0.41	0.37	0.65

The Co/Fe-Cl LDHs with cationic ratios of 6/2 and 8/2 were better crystallized than 2/2, 4/2 and 10/2 ratios as shown by their more intense and narrower (003) peaks, with FWHM of 0.41° and 0.37° ± 0.03 respectively (standard error is related to the step size used for the measurement).

The particle thickness determined using the Scherrer equation and the data provided by XRD analysis, for the 6/2 and 8/2 cationic ratios were 190 ± 27 Å and 211 ± 33 Å respectively, which was greater than the particle size of the other Co/Fe ratios (**Table *9***). Although these LDHs were

not aged, they crystalized with particle thicknesses comparable to those of aged 6/2 and 8/2 Co/Fe-CO_3 LDHs (**Table *4***), even if the chloride anions were suspected to be less structuring than the carbonate ones. The 2/2 and 4/2 powders were characterized using XRD analysis directly after their synthesis contrarily to the 6/2, 8/2 and 10/2 ratios where a gap of one week between the synthesis and the XRD analysis was present. This may explain the intercalation of traces of CO_3^{2-} in the interlayer space of the cationic ratios higher than 4/2. Even though the synthesis was performed in an abiotic glove box, traces of carbon dioxide were present in the atmosphere, causing the intercalation of traces of CO_3^{2-}. This result is in good agreement with the FTIR analysis discussed later on (***Figure 24***). Additionally, an ageing process may occur during the storing of the LDH suspensions with a cationic ratio of 6/2, 8/2 and 10/2 in the abiotic glove box (T=25ºC) for one week prior to the analysis compared to the 2/2 and 4/2 cationic ratios.

Because of the lack of ageing, Co/Fe-Cl LDHs 2/2, 4/2, and 10/2 have less crystallized structures, compared to 6/2 and 8/2 cationic ratios, since smaller (003) intensities (***Figure.23***), higher FWHM (0.83, 0.78, and 0.65° ± 0.03), and smaller particle thickness of 95 ± 7 Å, 101 ± 8 Å, and 116 ± 10 Å, respectively were obtained.

Independently of the Co/Fe ratio, the lattice parameter "a" remains constant at 3.13 since it was related to the Co^{II} (0.89 Å) and Fe^{III} (0.79 Å) radii in high spin octahedral sites [11].

Although the Co/Fe ratio influences the nature and the content of the interlayered anions [13], [41], [42], the layer to layer spacing measured for the different Co/Fe-Cl^--LDHs (between 7.87 and of 7.93 Å) were in accordance with the presence of Cl^- as predominant anion in the interlayer spacing [43], [44].

The chemical composition of the synthesized Co/Fe-Cl LDHs was determined using the AAS analysis. **Table *10*** presents the comparison between the experimental ratios, obtained using the AAS analysis, and the expected ones based on the amounts of Co and Fe introduced during the synthesis.

Table 10.Comparison of data obtained by AAS from dissolved Co/Fe-Cl LDH suspension and the introduced Co/Fe ratios

Co/Fe LDHs	Expected Co/Fe ratio	Co/Fe molar ratio (AAS) ± 0.1
2/2	1.0	1.0
4/2	2.0	2.0
6/2	3.0	3.1
8/2	4.0	4.0
10/2	5.0	4.7

No significant differences, except for the Co/Fe 6/2 and 10/2 ratios, were observed. For the 6/2 cationic ratio, the value determined using the AAS analysis was slightly higher (3.1) than the expected one (3.0). The shift reached 3.3% could be correlated to the experimental error. However, the value determined for the ratio 10/2 (4.7) was slightly lower than the expected one (5.0), corresponding to a 6.0% shift. For this ratio, a small part of Co did not precipitate during acid-base titration due to the use of a high cobalt concentration compared to the other cationic ratios.

The study of the interlayer anions was performed using the Co/Fe-Cl LDHs powder using FTIR analysis. The spectrum showed in ***Figure 24***.

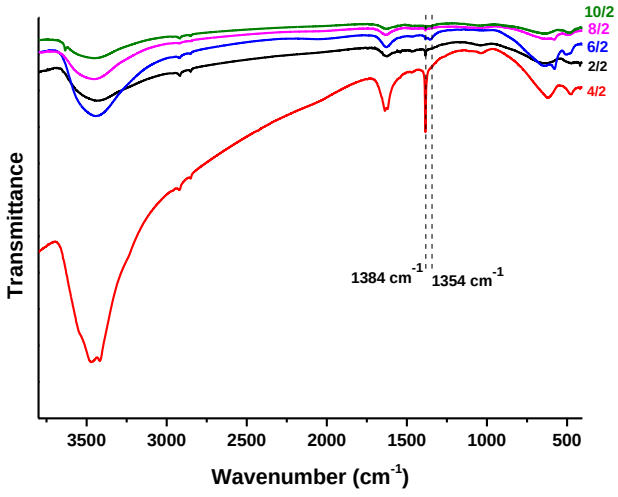

Figure 24. Overlay of Co/Fe-Cl LDHs FTIR spectra for 2/2, 4/2, 6/, 8/2 and 10/2 cationic ratios

The wide band seen at 3480 cm^{-1} can be attributed to the OH stretching vibrational mode of adsorbed water molecules and OH vibration of the LDH structure. The OH bending from H_2O was observed at 1600 cm^{-1} as well. Due to the presence of residues of nitrate from the reactor previously washed with nitric acid prior to each LDH synthesis, the band observed at 1384 cm^{-1} was attributed to the presence of nitrates. At 1354 cm^{-1}, carbonates were detected in traces for the 4/2, 6/2, and 8/2 ratios. That contamination may have occurred when the suspension was freeze-dried,

A highlight on the range of 700 cm^{-1} - 400 cm^{-1} was performed in order to identify the bands corresponding to metals oxygen bonds.

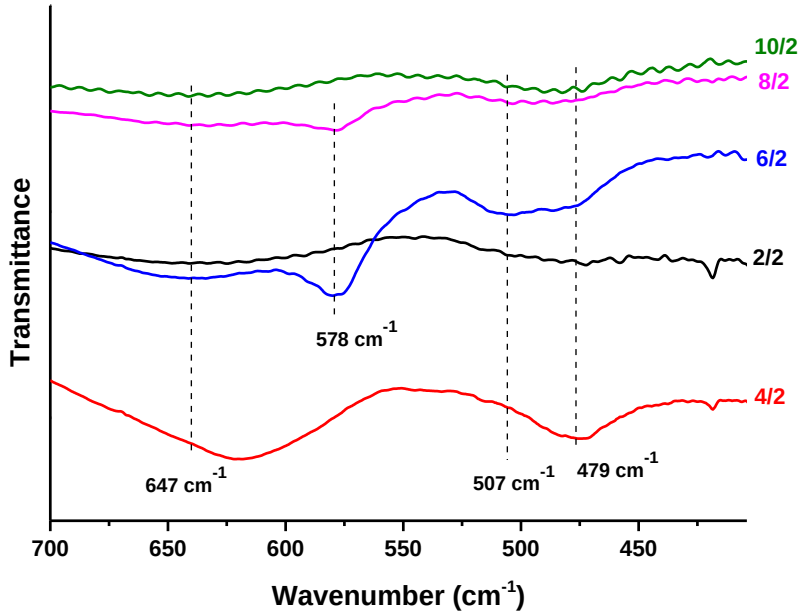

Figure 25. Highlights of the Co/Fe-Cl LDHs FTIR spectra on the range of 700-400 cm^{-1} for 2/2, 4/2, 6/, 8/2 and 10/2 cationic ratios

A very large band at 647 cm^{-1} was attributed to the Co-OH bond from the LDH structure. This band was shifted for the Co/Fe 2/2 and 4/2 ratios. For the 6/2 and 8/2 cationic ratios an additional band at 578 cm^{-1} is observed. This band can be attributed to the presence of α-$Co(OH)_2$ [45] phase in accordance with XRD data. For the 10/2 ratio, the band at 578 cm^{-1} could be present within the large band at 647 cm^{-1}. The double bands at 507 and 479 cm^{-1} were attributed to the Co-O and Fe-O of the LDH phases.

Conclusion

- Multiscale physico-chemical techniques allowed the fine characterization of LDH-based materials having a wide range of Co/Fe-CO_3 LDHs with cationic ratios between 2/2 and 10/2. The synthesis was performed by the co-precipitation with varying pH value method using NaOH and Na_2CO_3 alkaline solution, followed by a 24-hour ageing process at 60°C.
- A comparison of the purity and crystallinity of the products obtained at pH 8.0 and 11.5 was carried out by powder XRD study. Co/Fe LDH synthesis realized at pH 8.0 leads to the formation of crystalline LDH phases with an average particle thickness around 180 Å related with the stacking of 8 layers. For the 10/2 Co/Fe ratio, small amounts of spinel oxide were identified. The layer spacing is in good agreement with predominant CO_3^{2-} anion content for the LDH obtained for 4/2, 6/2, 8/2 and 10/2 Co/Fe ratio while for Co/Fe 2/2, interlayered OH^- predominates with the presence of some carbonate ions. This was confirmed by FTIR spectroscopy, elemental analysis and thermogravimetric analysis. The increase of the synthesis pH value up to 11.5 is responsible for the formation of impurities such as α-$Co(OH)_2$, Fe_2O_3, and Co_3O_4.
- The LDHs synthesized at pH value of 8.0 were made of quasi-hexagonal shaped particles with diagonal length between 200 and 500 nm. Global chemical analysis showed that average Co/Fe ratios were close to expected ones. Local chemical analysis demonstrated pure 4/2 and 6/2 ratios. For the 8/2 Co/Fe ratio, pure LDH with a ratio of 6/2 was obtained due to the lack of Co precipitation. While for 2/2, and 10/2 ratios, the presence of respectively few iron and cobalt enriched amorphous nano-particles was detected. The use of higher duration of ageing step or, in a lesser extent pH value slightly higher than 8 allowing full incorporation of cobalt into the LDH phases could allow reaching Co/Fe ratios closer to the expected ones.
- The characterization of chloride Co/Fe LDHs showed the presence of an additional phase of α-$Co(OH)_2$ along with the LDH phases for the Co/Fe cationic ratios higher than 6/2. The Co/Fe 4/2, 6/2 and 8/2 ratios showed the presence of nitrate impurities caused by the vessel washing process using nitric acid before each synthesis, as well as the presence of carbonate peaks caused by the contamination of the samples during the freeze-drying process. AAS proved the formation of LDHs with the desired cationic ratios except for the 10/2, having a Co/Fe ratio slightly lower than the expected one (4.7 ± 0.1).

- The use of the carbonates as interlayer anion lead to the formation of well-crystallized LDH phases for Co/Fe ratios between 2/2 and 10/2. On the other hand, the chloride LDHs showed α-$Co(OH)_2$ impurity for the cationic ratio higher than 4/2. The maturation process along with the nature of the interlayer anions were the two differences between the carbonated and the chloride LDHs. The maturation process allows the redissolution/reprecipitation of the Co^{2+} impurities under the form of LDH structure and the carbonates anions, based on the geometry and the charge of this anion, and reinforced the LDH structure having more stable structure than the impurity phases.

X.1. Optimization of the cationic composition of LDHs

X.1.1. Anionic exchange capacity of Co^{II}/Fe^{III} LDHs

Since Co/Fe LDHs showed high affinity towards carbonate anions, the synthesized Co/Fe-CO_3 LDHs followed a preliminary exchange process with chlorides, easily exchanged with other anions, prior to further anionic exchange study. Co/Fe-CO_3 LDH with different cationic ratios, were exchanged with 3M chloride solution for 2 days before being washed with deionized water for 5 times, with water renewed twice a day to eliminate the excess of chloride used for the exchange. Following that step, the obtained solid phases were characterized using FTIR spectroscopy in order to verify the success of the exchange process.

Prior to their use in the anionic exchange process, the example of the FTIR spectrum of the Co/Fe 4/2 LDH after chloride exchange was shown in ***Figure 26*** to verify the achievement of the elimination of carbonate anions.

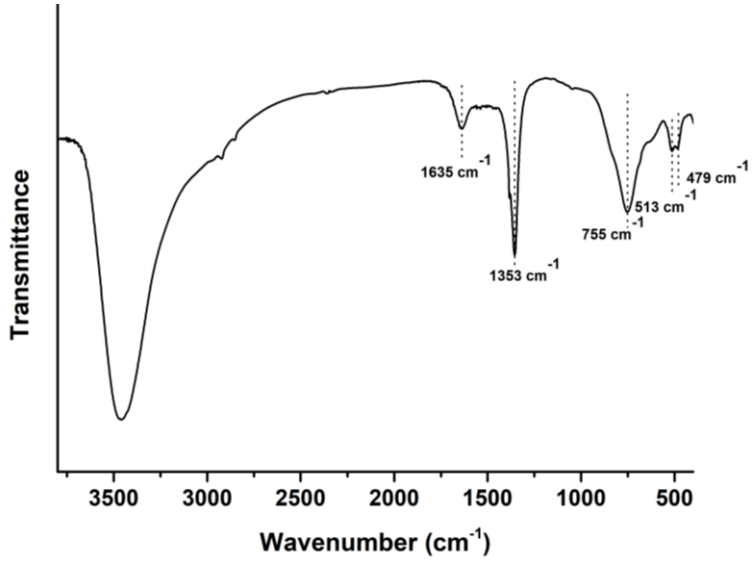

Figure 26. FTIR spectrum of 4/2 Co/Fe LDH after chloride exchange

Unfortunately, the band at 1353 cm^{-1} affirms the presence of carbonate anions indicating the non-accomplishment of the carbonate exchange process using chloride anions. The carbonated Co/Fe LDHs were eliminated and replaced by chloride LDHs.

This is why, to the investigation of the anionic exchange capacity of these LDHs using chloride anions was used, the chloride LDHs with varying Co/Fe cationic ratios synthesized in an abiotic glove box were used:

-First, the mole number of Fe constituting the LDH sheets were determined by dissolving the LDH from suspension in nitric acid and then analyzed using AAS analysis. Note that the excess positive charge on the LDH layers were caused by the presence of Fe. Since each Fe cation was responsible for one excess positive charge, the number of excess charges caused by Fe was equal to its mole number.

-Second, the anionic solutions were prepared based on the charge attributed to each anion prior to the exchange process. For example, SO_4^{2-} anions were responsible for two negative charges; however, NO_2^- and NO_3^- were responsible for one negative charge.

-Finally, the determined concentration of the desired sulfates, nitrates and nitrites anions was multiplied by 1.33 in order to have an excess amount of the present anions.

Thus, the determination of the concentration of different anions used for the exchanged process was performed based on the total excess positive charges generated by Fe^{3+} cations and the negative charge given by the anions to be exchanged.

An example of the calculation of the sulfate anions for the Co/Fe 6/2 ratio was detailed as follow: C_{Fe3+}= 7.25 g/L initial mass concentration of Fe determined using AAS considering the dilution made.

Vp =0.01L, volume of Co/Fe 6/2 suspension used for the exchange process. M_{Fe}=55.85 g/mol is the molecular weight of Fe.

Number of moles of Fe^{3+} ($nmol_{Fe}^{3+}$) = (C_{Fe3+} * Vp)/ M_{Fe}

= (7.25*0.01)/55.85 = 0.0013 mol of Fe present

As explained above, 1 mole of Fe generated 1 eq of excess positive charge which is compensated by the charge of intercalated anions.

For the SO_4^{2-}, $nmol_{SO42}^-$= $nmol_{Fe3+}$/2 = 0.0013/2 =0.0006 mol of sulfate to neutralize the total positive charge generated by Fe.

In order to have an excess of negative charge, $nmol_{SO42^-}$.1.33=0.0009 mol. This mole number was used to determine the corresponding SO_4^{2-} mass weighted for the preparation of the anionic solutions.

m_{SO42-}= $nmol_{SO42^-}$.1.33. M_{SO4}=0.0009*96=0.083 g/L

The total volume (Vt) of anionic solution was 0.1 L this leads to the Cm of SO_4^{2-}= m_{SO42-}/Vt

Cm=0.083/0.1 = 0.83 g/L=830 mg/L.

The same calculation procedure was followed for the nitrate and nitrite anions, as well as for the other Co/Fe cationic ratios.

Table *11* shows the obtained charges of exchanged anions in eq / mol of Fe with the variation of the cationic ratios.

Table 11.The variation of the exchanged anionic fractions (eq / mol of Fe) versus cationic ratios.

Anions (eq/mol of Fe)	**2/2**	**4/2**	**6/2**	**8/2**	**10/2**
Sulfates	0.4	0.5	0.5	0.8	0.6
Nitrates	0.2	0.2	0.3	0.5	0.4
Nitrites	0.2	0.2	0.2	0.3	0.3
Total negative charge	0.8	0.9	1.0	1.6	1.2

The anionic affinity of LDHs toward divalent anions (SO_4^{2-}) is usually higher than their anionic affinity towards monoanionic ones (NO_3^- and NO_2^-) [46]. This is also applied for the Co/Fe LDHs, where the results present in **Table *11*** clearly demonstrates the high affinity of these LDHs towards sulfate independently from the cationic ratio. A competition was observed between the nitrate and the nitrite anions. For the 2/2 and 4/2 ratios, the amount of nitrites exchanged was equal to the nitrate ones (0.2 eq / mol of Fe). However, the Co/Fe cationic ratios higher than 4/2 showed different behavior. The amount of nitrates (0.3, 0.5 and 0.4 eq / mol of Fe respectively) was higher than the nitrite ones (0.2, 0.3 and 0.3 eq / mol of Fe respectively) (**Table *11***).

To fully comprehend the involved phenomenon in exchange process of chloride LDHs, the amount of chloride initially present in the LDHs, the amount of chloride exchanged, the total

negative charges from the exchanged anions, all were determined using ion chromatography, and compared to the amount of iron initially present determined using AAS analysis.

Table 12. Comparison between the charges generated by different ions

Co/Fe ratio	Excess positive charge from Fe (AAS) (eq/mol of Fe)	Negative charge from LDH containing Cl^- (eq/mol of Fe)	Negative charge from exchanged Cl^-(eq/mol of Fe)	Negative charges from anions (eq/mol of Fe)
2/2	1.0	0.4	0.4	0.8
4/2	1.0	0.5	0.5	0.9
6/2	1.0	0.8	0.7	1.0
8/2	1.0	2.4	1.7	1.6
10/2	1.0	1.4	1.6	1.2

Since the synthesis of these LDHs was performed in an abiotic glove box, using chlorided metal salts, following an anionic exchange with chloride solution and based on the FTIR analysis performed (section **VIII.1.2.2.Synthesis of chlorided LDHs)**, the chlorided LDHs obtained contains mainly chloride and hydroxide anions in the interlayer region. The amount of excess charges provided by the iron for the 2/2, 4/2 and 6/2 ratios was greater than the initial concentration of chloride following the synthesis of the LDHs (**Table *12)***, this indicates that hydroxide anions were primarily responsible for counterbalancing the excess positive charge due to the presence of iron. However, the 8/2 and 10/2 cationic ratios showed an amount of excess charges provided by iron (1.0 eq / mol of Fe) lower than the initial concentration of chloride following the synthesis of the LDHs (2.4 and 1.4 eq / mol of Fe respectively) (**Table *12***). The increase in the exchange capacity of these LDHs can be attributed to the presence of structures having a deficit of OH^- anions such as α-$Co(OH)_2$ in agreement with bibliographical studies [47], [48], which leads to the intercalation of an excess of anions compared to the excess positive charge present in the LDH structure. The α-$Co(OH)_2$ phase was identified for the Co/Fe 8/2 and 10/2 ratios using XRD analysis (***Figure.23***).

A comparison between the exchanged chloride anions and the exchanged total anions (sulfates, nitrates and nitrites) was performed and the results were presented in ***table 12***. For the 2/2, 4/2 and 6/2 cationic ratios, the amount of anions exchanged (0.8, 0.9 and 1.0 eq / mol of Fe

respectively) was higher than the amount of chlorides exchanged (0.4, 0.5 and 0.7 eq / mol of Fe respectively). This is in a good agreement with the presence of OH^- anions in the interlayer region, which were being exchanged during the process. On the other hand, the 8/2 ratio showed similar amount of chlorides (1.7 eq / mol of Fe) and total anions exchanged (1.6 eq / mol of Fe), meaning that this ratio is chlorided and was able to exchange all its chloride anions.

Conclusion

The anionic exchange process of the Co/Fe LDHs was studied using the chlorideCo/Fe LDHs with cationic ratios between 2/2 and 10/2. The results obtained differed depending on the cationic ratio studied, for the 2/2, 4/2 and 6/2 ratios, the presence of OH^- along with chlorides anions in the interlayer region was observed since the amount of excess charges provided by the iron was greater than the initial concentration of chloride following the synthesis of the LDHs. The 8/2 and 10/2 ratios showed higher anionic exchange capacity which may be caused by the presence of α-$Co(OH)_2$ impurity.

XI.1. Characterization and adsorption properties of multilayered graphene oxide (MGO)

The modified Hummer's method was used to synthesize multilayered graphene oxide (MGO). Several synthesis were conducted in order to obtain an amount of MGO powder enough to be further introduced in the hybrid material. The resulting powders from two synthesis were named MGO_1 and MGO_2 respectively. The mix of the two MGOs was performed in order to obtain a more homogeneous mixture used to study the adsorption of zinc metal using MGO powder and the MGO containing hybrid materials. Different techniques were used to characterize the resulting MGO_1 and MGO_2 powders, to determine the oxygen content, the chemical nature and the quantity of the oxygenated functional groups as well as the number of available adsorption sites for Zn^{2+}. These techniques include pKa titration, elemental analysis, XPS analysis and FTIR spectroscopy. After the characterization of the obtained materials, adsorption kinetics of zinc was performed using the MGO mixture to study the efficiency of the available adsorption sites present on its surface towards this metal.

XI.1.1. Characterization of MGO and adsorption sites determination

The oxidation of graphene generates different oxygenated functional groups. These components are carboxylic, lactone, phenolic groups etc... The obtained MGO_1 and MGO_2 were firstly characterized using the elemental analysis technique in order to quantify the total amount of carbon, oxygen and hydrogen atoms present in each MGO sample. These results are given in mass percentage and are presented in the following table.

Table 13.Chemical composition of the MGO1 and MGO2 obtained using elemental analysis

Chemical composition (wt %)	**MGO_1**	**MGO_2**	**Average value**
Oxygen (O)	21.3	21.1	21.2
Carbon (C)	64.6	66.7	65.6
Hydrogen (H)	1.2	1.2	1.2
Sulfur (S)	2.9	3.5	3.2
Total percentage	90.0	92.5	91.3

Graphene sheets were used to synthesis both MGOs, this explains the presence of high content of carbon with 64.6 and 66.7 % for MGO_1 and MGO_2 respectively. The oxidation of graphene sheets using $KMnO_4$ in an acid mixture (H_2SO_4, H_3PO_4) will create different oxygenated groups on the surface of the graphene sheets. These groups can be attributed to hydroxyl, carboxylic and phenolic groups resulting in the presence of a low proportion of hydrogen atoms (1.2 wt %) for both MGOs. The presence of sulfur (2.9 and 3.5 %) was caused by the use of sulfuric acid during the synthesis of both MGOs. The high percentage of oxygen found by elemental analysis, which is 21.3 and 21.1 % for MGO_1 and MGO_2 respectively, demonstrates a good achievement of the oxidation process of graphene sheets into MGOs. The percentage of oxygen found was lower than the percentage found in the literature (was higher than 30 %) [49]. This difference may be caused by the synthesis procedure of MGOs applied, for example, the dispersion time in acid solutions or the contact time between the graphene sheets and the oxidant agent. The O/C ratio is an important factor for MGO materials. As explained in the literature review, this ratio indicates the degree of achievement of the oxidation process. The O/C ratio should be in the range of 0.67 to 0.4 in order to obtain MGO component rich in oxygen groups [50]. The O/C ratio calculated using the elemental analysis results is equal to 0.32, which is in the range of the minimum value of 0.4 obtained, which also indicates that the MGO obtained contains large amounts of oxygenated groups. The total percentage of different components obtained using the elemental analysis was lower than 100 %. It was caused by the presence of impurities such as potassium and manganese originated from the use of potassium permanganate as oxidizing agent.

Additionally, the determination of the nature of the functional groups present in the produced MGO_1 and MGO_2 samples were further examined using the XPS analysis.

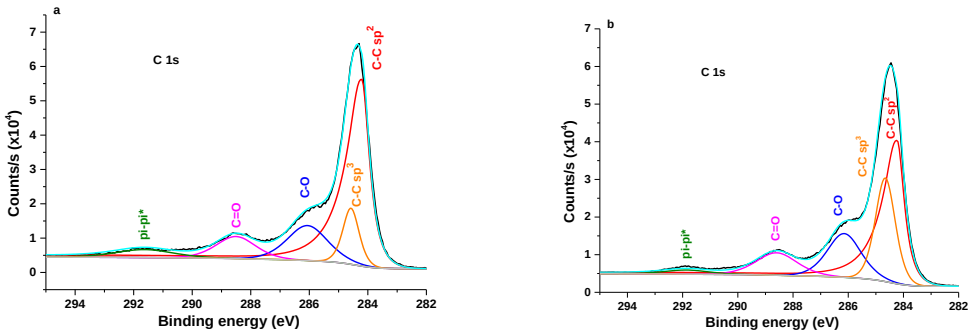

Figure 27. XPS deconvolution of C1s spectra of a) MGO_1 and b) MGO_2

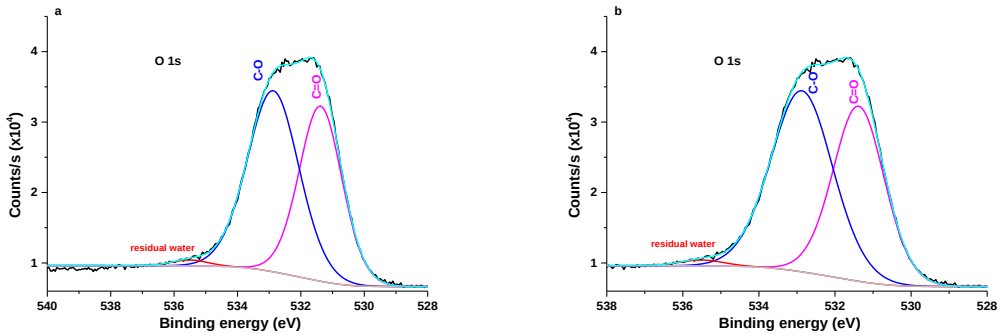

Figure 28. XPS deconvolution of O1s spectra of a) MGO_1 and b) MGO_2

Table 14. Determination of oxygenated groups using XPS analysis (atomic %)

Adsorbents	**O/C ratio**	**O_{1s} Binding energy (eV)**				**C_{1s} Binding energy (eV)**			
		O=C 531.4	**O-C 532.8**	**O-C/O=C ratio**	**C-C sp^2 284.2**	**C-Csp^3 284.7**	**C-O 286.2**	**C=O 288.6**	**C-O/C=O ratio**
MGO_1 (%)	0.5	44	55	1.3	60	10	15	9	1.7
Mass %					**66**		**34**		
MGO_2 (%)	0.5	45	53	1.2	47	25	17	11	1.5
Mass %					**68**		**31**		

The deconvolution of the XPS peaks of the C1s spectrum for MGO_1 and MGO_2 are represented in ***Figure 27***. The main oxygenated groups, in both MGOs, were C-O and C=O. The ratio of C-O/C=O determined using the C1s spectrum deconvolution was equal to 1.7 and 1.5 for MGO_1 and MGO_2 respectively. This means that the presence of C-O in terms of atomic percentage was higher than the C=O one.

The deconvolution of the C-C envelope into C-C sp^2 and C-C sp^3 allowed the redefinition of a new C-C skeleton containing new sp^3 function. The addition of both C-C sp^2 and C-C sp^3 peaks in term of atomic percentage for MGO_1 and MGO_2 were equal to 70 and 72 % respectively. The conversion of the atomic percentage into mass percentage will allow the comparison between the obtained results using XPS deconvolution and elemental analysis. The total carbon percentage was determined using the C-C sp^3 and C-C sp^2 percentages and the oxygen percentage was determined using the C=O and C-O total percentages. The mass percentage of carbon and oxygen are 66 and 34% for MGO_1 and 68 and 31 % for MGO_2. The carbon content

determined using XPS deconvolution peaks were equal to the carbon content determined using the CHONS analysis (average value 65.6%). On the other hand, the oxygen content was higher than the value determined using the elemental analysis (average value 21.2%). This was caused by the fact that XPS technique allows the analysis of the surface of the material. Whereas, the CHONS analysis allows the bulk analysis of the sample. This leads to the obtainment of O/C ratio determined using the conversion of the atomic percentage of the XPS analysis into mass percentage (0.5) which was higher than the O/C ratio determined using the mass percentage of the elemental analysis (0.3).

The presence of satellite peak represented by pi-pi* annotation on the C_{1s} spectrum (***Figure 27***), also called plasmon (292 eV), was caused by the conduction band of the C-C sp^2. When a core electron removed by photoionization interacts with a valence electron, the energy of the core electron was reduced causing a satellite structure.

The O_{1s} spectra showed in ***Figure 28*** also confirms the presence of the O=C and O-C functional groups. C-O atomic percentage was higher than the C=O one having O-C/O=C ratio of 1.3 and 1.2 for MGO_1 and MGO_2 respectively (**Table *14*).** These results are in good agreement with the ones found for the C_{1s} spectra. The addition peak observed at higher binding energy (535.5 eV) was attributed to the residual water present in the MGO samples.

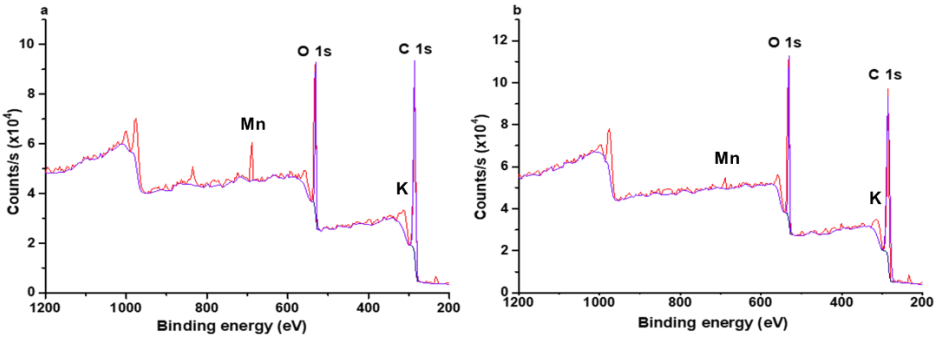

Figure 29. XPS survey of a) MGO_1 and b) MGO_2

The wide scan (***Figure 29***) clearly shows the presence of other elements identified using the corresponding binding energy (eV), Mn under the form of MnO_2 at 641.8 eV, MnO at 641.4 eV [51] and potassium $K2p_{3/2}$ at 292.9 eV [52]. This result is in good agreement with the elemental analysis, where the total loss of weight percentage was not equal to 100% due to the presence of these components.

Further characterization techniques were applied in order to confirm the presence of oxygenated groups. Since the synthesized MGO contains different oxygenated functional groups, and thus will be used for metallic cations adsorption, the functional groups able to deprotonate at low pKa values were to be considered. This is why; the determination of these groups will be performed using the acid-base titration method. The pKa determination approach can be used to quantify various functional groups present on the surface of the synthesized MGO. Because of the substantial amount of acidic oxygenated functional groups generated during the strong oxidation of graphene, the point of zero charge pH (pH_{PZC}) of the MGO was found to be pH_{PZC} = 3.2. The oxygenated groups can be divided into two categories, the first one consists of carboxylic groups or acid groups with pH values below 7.0 (neutral pH) and the second one is the phenolic groups (basic groups) with pH values above 7.0. Due to the existence of these oxygenated groups, the MGO has the ability to adsorb cationic species via electrostatic interactions. The adsorption of metallic cations was usually performed using the carboxylic groups at pH values lower than 7.0. Since the precipitation of the majority of metallic species usually occurs at high pH values (***Figure 30***, Eh/pH diagram), the use of phenolic groups for the adsorption process was difficult because they require pH values higher than 7 (close to 11.0) to deprotonate. The adsorption of Zn^{2+} using MGO was conducted at a pH value of 5.0 to prevent the precipitation of the Zn^{2+} under the form of $Zn(OH)_2$ (***Figure 30***). Therefore, the amount of oxygenated groups at pH values lower than 5.0 was determined

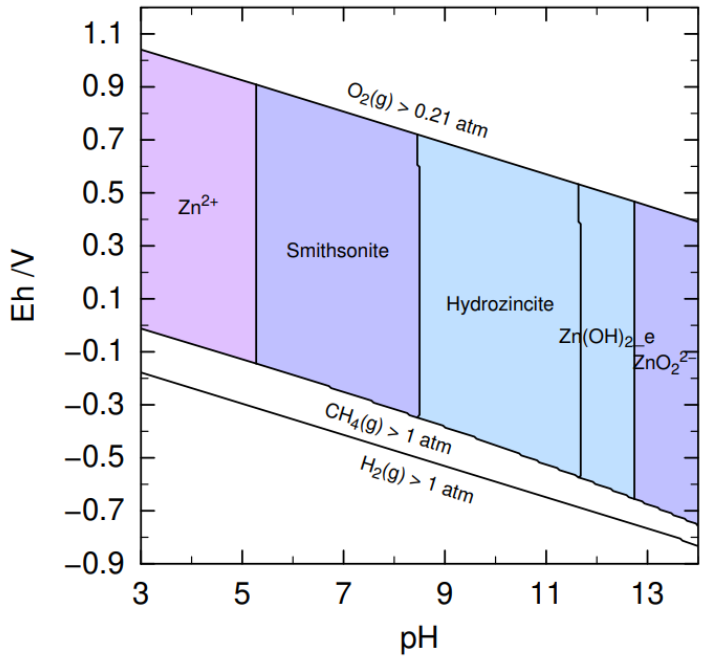

Figure 30. Eh/pH diagram of Zn^{2+} (1.48 mmol/L) at 25°C under atmosphere

The following figure (***Figure 31***) represents the quantification of the functional groups using acid-base titration system. The obtained peaks corresponding to the number of functional groups in function of the pKa values were used to quantify the oxygenated groups present on the surface of MGO_1 and MGO_2. The determination of the surface area of the peaks in a pKa range will generate the number of functional groups (in $mmol.g^{-1}$).

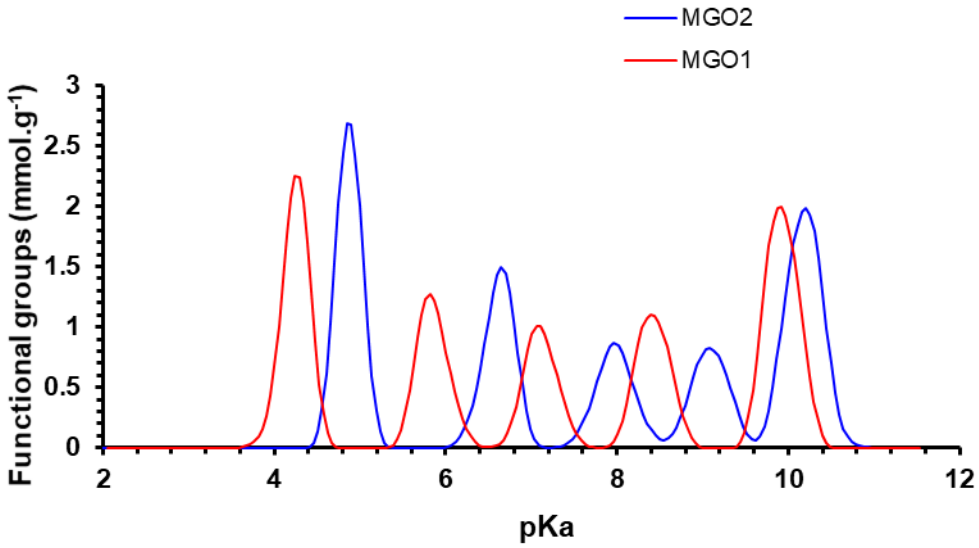

Figure 31. Amount of functional groups (mmol.g^{-1}) versus pKa values of (a) MGO_1 and (b) MGO_2

The different quantity of functional groups based on the pKa values were summarized in the following **Table *15***

Table 15. The amount of functional groups determined using the pKa titration

Adsorbent	**Functional groups having pKa lower than 5.0 (mmol.g^{-1})**	**Functional groups having pKa higher than 5.0 (mmol.g^{-1})**	**Total amount of functional groups**
MGO_1	0.92	2.72	3.60
MGO_2	1.00	2.70	3.80
Average	0.95	2.71	3.70

By comparing the results obtained for both MGOs, it is clear that no major differences between the two adsorbent materials was observed (**Table *15***). The total amount of the functional groups is equal to 3.60 and 3.80 mmol.g^{-1} for MGO_1 and MGO_2 respectively, but only 0.92 and 1.00 mmol.g^{-1} could be used during the adsorption process since the working pH value of 5 was chosen. This is in good agreement with the XPS results, where the C-O peaks can be attributed to the phenolic and carbonyl groups, are present in higher amounts (atomic percentage) than the C=O correlated to the carboxylic and lactones groups.

Based on the characterization of the MGO_1 and MGO_2 using XPS and elemental analysis, grossly, both materials synthesized using the Hummer's method were close in terms of

functional groups, percentage of carbon and oxygen, amount of functional sites used for the Zn^{2+} adsorption and O/C ratio. The mixture of both MGOs (50% of MGO_1 and 50% of MGO_2) was performed in order to have a homogeneous batch of similar MGO powder used for the Zn^{2+} adsorption experiments, with an amount of functional groups, mainly carboxylic groups, determined by acid-base titration and equal to 0.95 $mmol.g^{-1}$.

Once the combination of both MGOs was performed, the identification of the oxygenated functional groups was confirmed using FTIR analysis (***Figure 32***).

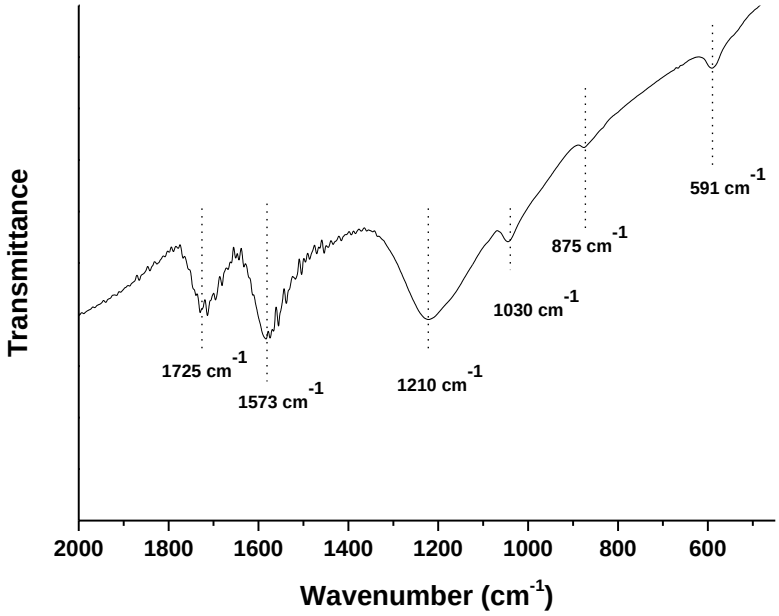

Figure 32. FTIR spectrum of MGOs

Table 16. Band attribution of MGO

Wavenumber (cm^{-1})	Attribution
1725	C=O of carboxyl groups
1573	C=C
1210	C-O of epoxy groups
1030 – 875	C-O of carbonyl and carboxyl groups
591	C=C

MGO exhibits standard FTIR analysis bands. The carboxyl group C=O was attributed to the band at 1725 cm^{-1}. The graphene planar bonds C=C was responsible of the band at 1573 cm^{-1} and 591 cm^{-1}. Additionally, the C-O of epoxy groups found on the surface of MGO were responsible for the peak at 1210 cm^{-1}. The vibration mode of the C-O of the carbonyl and carboxyl groups is responsible for the band that was identified at 1030 cm^{-1} and 875 cm^{-1}[54]–[56]. This technique was in good agreement with XPS analysis, where the identification of the oxygenated functional groups was performed and the existence of the C=O, C-O and C-C groups was confirmed.

XI.1.2. Adsorption kinetics of Zn^{2+} using MGO

The characterization of the synthesized MGO using the Hummer's method showed the presence of oxygenated functional groups such as epoxy, phenol, carboxylic, lactone etc… The acidic groups, having a pKa lower than 5.0, were deprotonated at acidic pH values leading to negatively charged components. Based on the Pourbaix diagram of Zinc (***Figure 30***), at the pH value of 5.0, Zn is under the form of Zn^{2+}, the adsorption process mainly occurs by the electrostatic attractions between the negatively charged functional groups of the MGO, mainly the carboxylic groups in proportion 0.95 $mg.g^{-1}$, and the positively charged Zn^{2+}. The adsorption experiment was performed using the combination of both MGO_1 and MGO_2, where MGO powder was mixed with Zn^{2+} solution. After sampling, AAS analysis was used for the determination of the concentration of Zn^{2+}. The adsorption curve (***Figure 33***) shows the amount of zinc that has been adsorbed in $mg.g^{-1}$ over time (min).

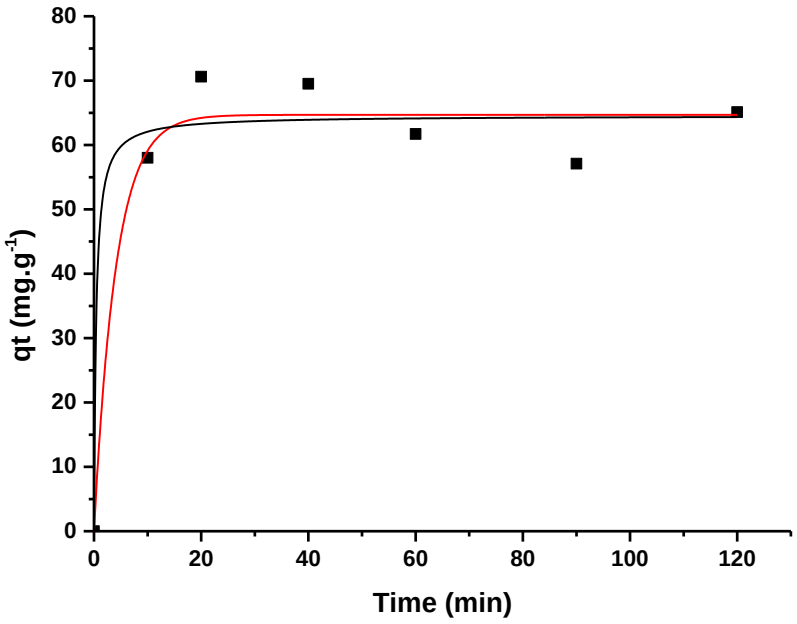

Figure 33. Adsorption kinetics of Zn^{2+} using MGO. The red and black curves correspond respectively to the pseudo first and second order fittings

Since MGO is a non-porous material, the adsorption mechanism was fast. The majority of the Zn^{2+} has been adsorbed within 10 minutes of contact time with the solution. After two hours, 65.1 mg (1.00 mmol.g^{-1}) of Zn^{2+} have been adsorbed for one gram of MGO. At a pH value of 5.0, 0.95 mmol.g^{-1} of active sites were available for adsorption identified using the pKa measurement. Therefore, each adsorption site adsorbed one Zn^{2+} cation. This result is in agreement with a good accessibility of all MGO available adsorption sites.

Table 17. Kinetic parameters of the fitting model for the adsorption of Zn^{2+} on MGO material

Kinetic order	**Kinetic parameters**		
	R^2	k_1 (min^{-1})	k_2 ($g.mg^{-1}.min^{-1}$)
1st	0.956	0.25 0.1	-
2nd	0.947	-	0.04 0.1

For the adsorption of Zn^{2+} using MGO powder, pseudo first order model is well fitting the experimental data (**Table *17***) since the R^2 (0.956) obtained using the pseudo first order model is closer to 1 as compared to the pseudo second order model (0.947). 70% of the initial quantity of Zn^{2+} is adsorbed onto MGO (q_e= 65 mg.g^{-1}).

Two types of electrostatically attractive interactions can be considered between carboxylic groups and Zn^{2+}: i) electrostatic attraction between COO^- groups and Zn^{2+} and ii) chelation bindings caused by the non-bonding electron pairs of the oxygen groups present *via* hydroxyl, epoxy and other functional groups.

XII.1. Elaboration, characterization and adsorption properties of the elaborated beads

XII.1.1. Synthesis method of hybrid CS-based beads

The elaboration of chitosan-based beads containing different adsorbents such as Co/Fe LDHs and/or MGO particles was challenging since the incorporation of the LDH structure and MGO material into the chitosan beads must be done while conserving the structure, anionic exchange properties, homogeneity, adsorption properties and porosity of these materials inside the desired beads. Especially, the synthesis of the chitosan beads requires at the same time low pH value for the dissolution of chitosan polymer and high pH value for the formation of the chitosan gel, while considering that, LDH structures are not compatible with acidic solutions having pH values below 4.0. The Co/Fe 6/2 ratio was chosen for the elaboration of LDH-based beads depended on the different characterization results obtained using the Co/Fe LDHs powder. The Co/Fe 6/2 ratio showed well crystallized LDH structure with the absence of impurities (***Figure 14***) with the desired global and local cationic ratio of 3 (**Table *6***). The anionic exchange capacity for the chloride form of Co/Fe 6/2 ratio reached 100% of its capacity. These were the reasons why Co/Fe 6/2 ratio was chosen. Based on the study performed by Li *et al.* [59] the elaboration of CS/LDH beads using two synthesis methods was done.

The first synthesis method, which was the most common one, consists in mixing the synthesized Mg/Al-LDHs [59] with the chitosan gel and dropping the mixture in NaOH alkaline solution to form chitosan/LDH beads. The elaboration of CS/LDH beads was performed using the described method but two problems were encountered: As generally known, LDHs are dissolved in acidic solutions. When combining Co/Fe LDHs with CS gel at pH values lower than 4.0 (initial pH value of CS gel was 3.4), the dissolution of LDHs occurs leading to the instability of the structure and the creation of impurities inside the CS gel. Usually, once the gel containing the dissolved LDHs was dropped in NaOH (2.5M) alkaline solution having a pH value of 14.0, the reformation of LDH phases should occurs, this was the case for the Mg/Al LDHs [59]. However, the Co/Fe LDHs behaved differently. As previously demonstrated when

Co/Fe-LDHs were synthesized using the coprecipitation method ***(VIII.1.2.Crystallinity and purity of Co/Fe-CO_3 LDHs)*** the final pH value of 11.5 leads to the creation of impurities that could also be synthesized during the beads formation.

The second method consists in mixing metals salts LDH precursors, with the CS gel. The initial gel formed contains dissolved LDH precursors ($Co(Cl)_2$ and $Fe(Cl)_3$) at an acidic pH of 3.0. After homogenization, the gel was dropped in an alkaline solution (NaOH 2.5 $mol.L^{-1}$) having a pH value of 14.0. However, the high pH value (11.5) caused again the obtainment of impurities. Co and Fe were also present as metal hydroxides (***Figure 34***). However, the washing process, using deionized water (in order to store the beads at neutral pH), caused a decrease in the pH value of the solution and thus a decrease of the pH value of the inner part of the bead. This pH decrease leads to the dissolution of the metal impurities formed at high pH value, and the re-precipitation of elements under the form of LDH phases (more stable form)(***Figure 35***). The LDHs formed inside the beads have a lower crystallinity compared to the synthesized LDHs using the co-precipitation method (***Figure 34***).

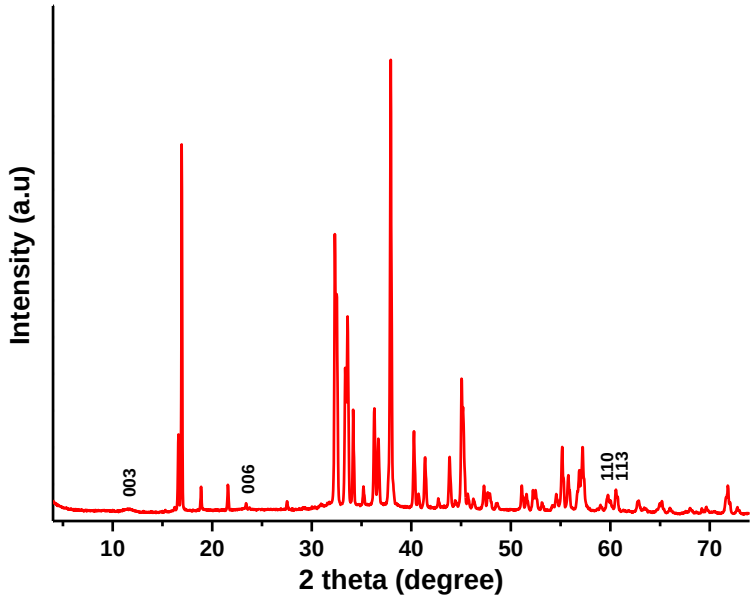

Figure 34. XRD patterns of CS/LDH beads formed at pH value of 14.0 before the washing process. Indexed peaks correspond to LDH phases.

After the optimization of the CS/LDH composite bead elaboration using the second method, the characterization of the elaborated beads was performed using dry powder obtained from beads for XRD analysis for the LDH phase identification, AAS analysis for the determination

of the Co/Fe average concentration present in LDH containing beads and TGA analysis to determine the thermal degradation and the amount of solid present in the beads. Finally, the observation of the structure (chitosan pore network) and homogeneity of the LDH distribution inside the beads were studied using the cryo-SEM technique.

XII.1.2. Characterization of chitosan-based beads

The CS/LDH and CS/LDH/MGO diffractograms ***(Figure 35***) affirm the presence of LDH structure inside the chitosan beads since the (003), (006), (110) and (113) peaks at 11, 23.5, 59 and 60.5° (2 theta) respectively were identified. The other characteristic peaks of LDH between 30 and 50º, are not very visible. The formation of LDH phases inside the chitosan-based beads was mainly obtained by re-dissolution of the $Co(OH)_2$ and $Fe(OH)_3$ phases and the re-precipitation of the free Co^{II} and Fe^{III} under the form of an LDH structure, as explained in the above paragraph. The difference in the intensities of the LDH reflection peaks between the Co/Fe LDH with cationic ratio of 6/2 and the LDH containing CS beads may be caused by the different orientation of the LDH particles inside the beads. The width of the LDH peaks in the CS/LDH/MGO is bigger than the width of the Co/Fe 6/2 LDH which indicates the low crystallinity of the obtained LDHs inside the chitosan beads.

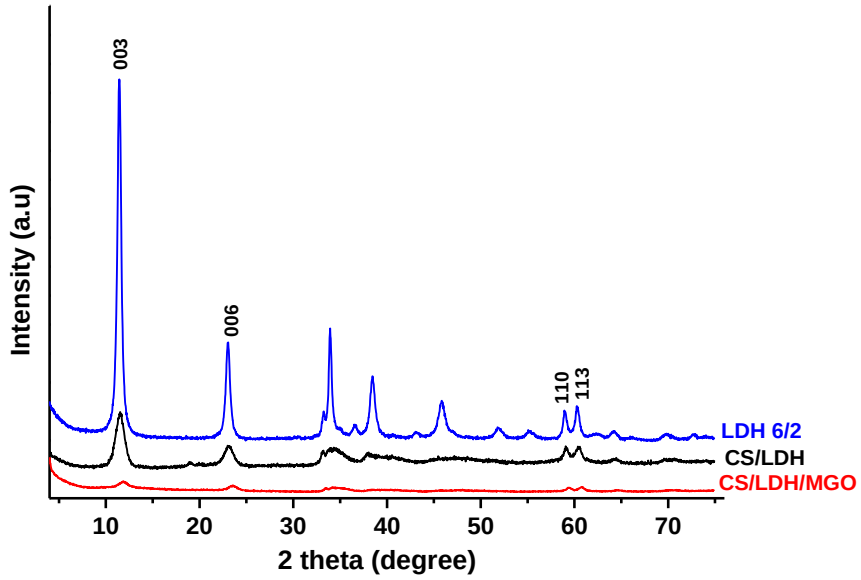

Figure 35. XRD diffractograms of CS (3%)/LDH/MGO (1.5%), CS (3%) /LDH and Co/Fe 6/2 LDH

Since chitosan contains different functional groups such as amino and hydroxyl groups that can be negatively charged at pH value of 14.0, this could lead to the intercalation of the biopolymer in the interlayer space of the formed LDHs. In order to verify this hypothesis, the d parameter, which is the interlayer spacing which value depends mainly on the intercalated anions, was determined. The value of d(003) for the CS/LDH composite is 7.62 Å which corresponds to the presence of carbonate anions in the interlayer region. This value is in good agreement with the d(003) of Co/Fe-CO_3 LDH with a cationic ratio of 6/2 (7.69 Å), the intercalation of chitosan chains in the interlayer region of LDHs did not occur. However, the CS/LDH/MGO beads have an interlayer spacing d(003) equal to 7.2 Å. This decrease in the d(003) value can be related to the possible intercalation of monolayer MGO which COOH groups are negatively charged, with lower hydration sphere, between the LDH sheets. The a parameter calculated using the (110) peak is respectively equal to 3.12 and 3.10 Å for the CS/LDH and CS/LDH/MGO composites, which is similar to the values found for the Co/Fe-CO_3 and Co/Fe-Cl LDHs with a cationic ratio of 6/2. This indicates the presence of Co-Fe bonds, which are metal-metal bonds, of the LDH structure, similar to those of Co/Fe 6/2 ratio LDH.

After identification of the LDH phases formed inside the different beads, AAS analysis was performed on the CS/LDH and CS/LDH/MGO composites. This technique quantified the amount of Co and Fe inside the chitosan beads. The global Co/Fe ratio determined was equal to 3.01, which is in good agreement with the theoretical ratio of 3.0 (Co/Fe 6/2).

The TGA analysis was performed on the different CS based samples to determine the amount of solid present in each type of beads.

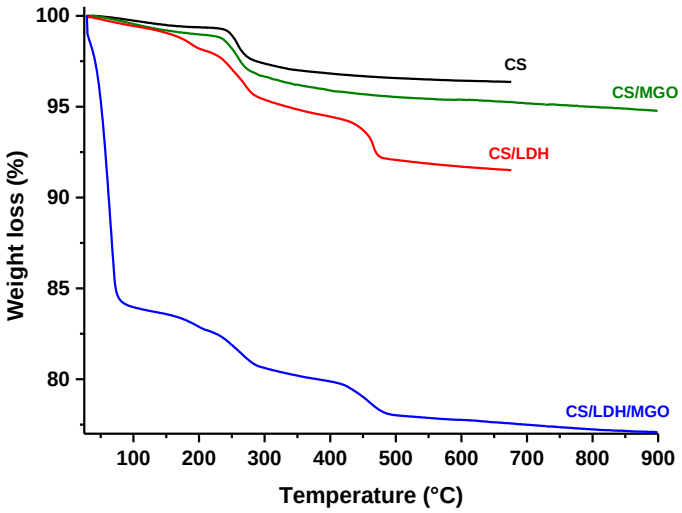

Figure 36. Weight loss (%) versus the temperature (°C) of CS, CS/MGO, CS/LDH and CS/LDH/MGO beads

The different weight losses were determined using the degradation curves (***Figure 36***). Since the temperature required for the MGO degradation was 900°C, which is higher than that of the CS and LDHs material degradation, the beads containing MGO were thermally treated up to 900°C. The degradation curve of the CS beads showed two degradation stages, the first one between 40-100°C was attributed to the loss of the physisorbed and trapped water molecules. The second stage between 242 – 383°C was caused by the deacetylation and decomposition of the CS chains (polysaccharide groups) [60], [61]. The CS/MGO beads, showed three degradation stages, correlated with a weight loss between 40-100°C corresponding to the removal of physisorbed and trapped water, followed by a second degradation stage between 150-300°C to the decomposition of CS chains and finally at temperature higher than 300°C, the slow and continuous weight loss was attributed to the degradation of the carboxylic groups (COOH) of MGO [62], [63]. This clearly demonstrates the presence of MGO particles inside the chitosan beads. The CS/LDH beads showed different behavior under thermal treatment. Since XRD analysis, discussed previously, proved the presence of Co/Fe LDHs inside the beads, the first weight loss between 40 – 200°C was attributed to the loss of physisorbed water, interlayer water, interlayer anions removal and dehydroxylation of the LDH structure. The weight loss occurring between 200°C and 350°C corresponds to the decomposition and the deacetylation of the chitosan chains as well as the de-hydroxylation of α-cobalt oxyhydroxide generated by thermal treatment. At higher temperature, between 400-500°C, the continuous loss of carbonate from the LDH structure may occur leading to the observed mass decrease

[36]. The CS/LDH/MGO grouped the degradation stages of CS, CS/LDH and CS/MGO curves resulting in four stages. A huge weight loss was observed at temperatures below 100°C due to the elimination of the physisorbed and trapped water molecules. The water molecules present mainly depends on the preparation of the beads prior to the analysis; this big quantity of water present for the CS/LDH/MHO beads may be due to the preparation of the sample. Then between 90 – 200°C, the loss of physisorbed, trapped and interlayer water, intercalated anions and dehydroxylation of LDH phases occurs. The weight loss between 200-290°C was caused by the decomposition and the deacetylation of CS chains [60], [61]. Finally, higher than 300°C, the weight loss was caused by the decarboxylation of the COOH groups of MGO [62], [63]. The degradation curves proved that the integration of MGO and LDH particles inside the chitosan matrix was successful. The quantity of each adsorbent present was also determined using these curves and were shown in the following table (**Table *18***). The weight loss to be considered for the calculation of the solid mass, present in the chitosan-based beads was the one higher than 100°C until the final temperature reached. This will allow the removal of the weight loss corresponding to water molecules. Indeed, as the quantity of water depends on the preparation of the sample before the analysis, it cannot be taken into consideration in the calculation of the solid mass.

Table 18. Solid mass determination (mg) depending on the weight loss (mg)

Beads	**Total weight loss (mg)**	**CS mass (mg)**	**MGO mass (mg)**	**LDH mass(mg)**
Pure CS	1.2	1.2	0.0	0.0
CS/MGO	1.4	1.0	0.4	0.0
CS/LDH	3.5	1.4	0.0	2.1
CS/LDH/MGO	2.8	1.2	0.5	1.1

The elaboration of CS bead was only obtained using CS flakes; water and chitosan molecules caused the total weight loss. Since approximately the same amount of chitosan was used for the elaboration of the different beads, it was used as a reference for the calculation of the adsorbent masses in the following hybrid beads. The CS/MGO beads showed a total solid mass of 1.4 mg divided into 1 mg of CS and 0.4 mg of MGO. On the other hand, the CS/LDH beads showed a total solid mass loss of 3.5mg divided into 1.4 mg from CS and 2.1 mg from LDHs. Finally, the solid mass loss of the CS/LDH/MGO beads was 2.8 mg divided into 1.2 mg from CS, 0.5 mg

from MGO and 1.1 mg from LDHs supposedly. This analysis allowed the determination of the solid mass present inside a given mass of different beads compositions.

Nearly the same mass of MGO was obtained between the CS/MGO (0.4 mg) and the CS/LDH/MGO (0.5 mg). However, a difference in the mass of LDHs was observed between the CS/LDH (2.1 mg) and CS/LDH/MGO beads (1.1 mg), even though the same amount of precursors was used. Visually, the coloration of the alkaline solution used for the beads formation was dark blue/grey, indicating the presence of precursors released from the elaborated gel in the alkaline solution instead of being incorporated in the beads. The nature of the alkaline solution was not adequate for AAS analysis, and thus, the determination of the metals concentration present was difficult.

The observation of the morphology of the synthesized beads was performed using cryo-SEM analysis in order to have a view of the pore network and the homogeneity of the dispersion of the adsorbents in the chitosan matrix. This study also confirmed the presence of Co, Fe and MGO inside the beads.

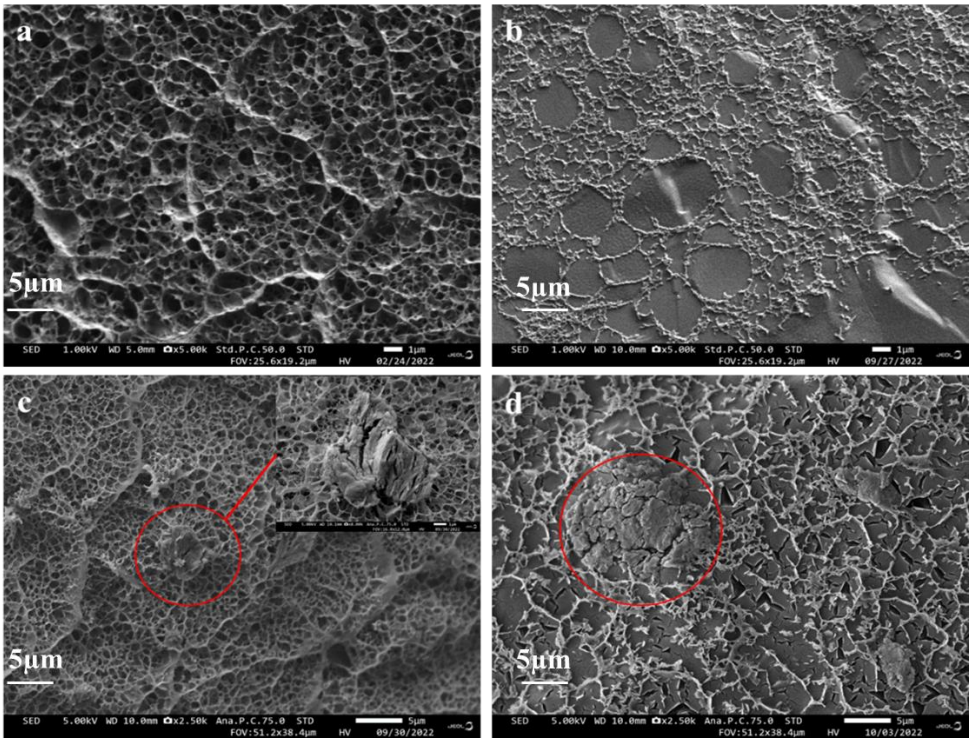

Figure 37. Cryo-SEM images of a) CS, b) CS/LDH, c) CS/MGO and d) CS/LDH/MGO beads

The porous network of chitosan was clearly seen in the different beads composition (***Figure 37***) The SEM image obtained for the CS beads (***Figure 37.a***) shows the porosity of the biopolymer, leading to accessible pore favoring transport properties of the pollutant from the

solution to the adsorbent sites for water treatment purposes. SEM shows that the beads are highly porous material as far as they were constituted of nearly 90% water and 10 % of CS creating a porous skeleton where the walls are made of CS chains.

The LDHs formed in the CS/LDH beads were nano-sized and cannot be observed at the SEM scale using the cryo-SEM analysis. ***Figure 37.c*** clearly demonstrates the presence of MGO particles attached to the chitosan matrix. These particles, highlighted using red circles, were dispersed in a homogeneous way in the porous chitosan network under different particle size differing between 5 to 10µm. This result is in good agreement with the experimental particle size synthesized, since a sieving step was performed using a stainless steel sieve having a sieving mesh of 50µm. MGO particles did not agglomerated into particles having sizes higher than 50µm. ***Figure 37*.d** shows the SEM image CS/LDH/MGO beads. In the final composite containing the two adsorbents clearly demonstrates the presence of the chitosan porous network with MGO material homogeneously dispersed within the polymer matrix were dispersed in the CS-HDL matrix. LDH containing beads (***Figure 37. b and d)***, showed slightly different morphology than pure CS or CS/MGO beads (***Figure 37 a and c)***. This difference is caused by the presence of LDH particles that could create a more divided polymer network, causing an impact on the overall morphology of the chitosan. This is correlated with the good dispersion of LDH particles into the polymer matrix and the deposition of LDHs on the chitosan walls during the preparation of the samples due to water sublimation.

In order to identify the presence of LDH phases dispersed in the chitosan network, EDX mapping analysis was performed on the CS/LDH/MGO composites (***Figure 38***).

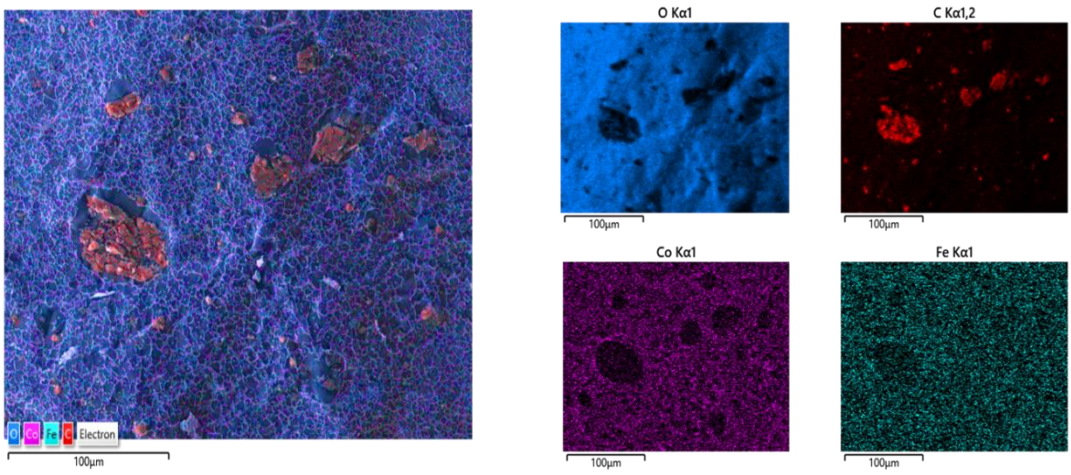

Figure 38. EDX mapping analysis of CS/LDH/MGO beads

Mapping analysis (***Figure 38***) clearly shows the presence of chitosan matrix by detecting the oxygen and in lesser extent the carbon signals emitted by the carbon skeleton and the hydroxyl groups of the chitosan chains. MGO was also identified by detecting more concentrated carbon in the region where MGO micrometric particles are dispersed.

The presence of Co and Fe on the surface of the chitosan matrix was determined using EDX mapping on CS/LDH/MGO beads.(***Figure 38)***. Both Fe and Co cartographies showed the complete dispersion of these metals in the chitosan porous network. During the gel formation, LDH precursors were added to the CS/MGO mixture while the pH value was 3.4. This pH value was lower than the pKa of the amino groups present on the CS chains (pKa=6.5) leading to positively charged groups. This will lead to electrostatic repulsions between the Co^{II} and Fe^{III} and the chitosan chains. After dropping the gel into alkaline solution, the amino groups were neutral (NH_2) leading to a bond between Co and Fe elements and chitosan chains which might be caused by the free electron pair of the amino groups (NH_2).

However, the presence of Fe and Co may simply come from LDH phases formed in the beads and then deposited on the chitosan due to the treatment applied to the samples before cryoSEM analysis. Indeed, freezing followed by sublimation, which leads to the elimination of the water constituting the beads, can result in the deposition of LDH phases on chitosan.

XII.1.3. Zinc adsorption using CS/MGO containing beads

In section X.1.1.Charaterization of MGO and adsorption sites determination, MGO showing a high amount of dissociated carboxylic groups is able to trap a significant amount of metallic cations. In order to understand the interaction between the different adsorbents, as well as to study the adsorption capacity of the obtained composite, the treatment of Zn^{2+} solutions was performed using CS, CS/MGO and CS/LDH/MGO beads. As previously observed using the cryo-SEM analysis, the chitosan-based beads were porous materials contradictory to the MGO material. The determination of the contact time required to reach Zn^{2+} adsorption equilibrium was important to allow the total diffusion of the Zn^{2+} cations inside the beads. The first absorption tests showed that the time required to reach the equilibrium was higher or equal to 200 minutes, after that the adsorption curves reach the plateau. Adsorption kinetics were performed over 420 min (7 hours). In order to confirm that 420 minutes was enough contact time to allow the diffusion of the Zn^{2+} cations inside the beads, EDX analysis was performed on CS/MGO beads after the 420 minutes of contact time (***Figure 39***).

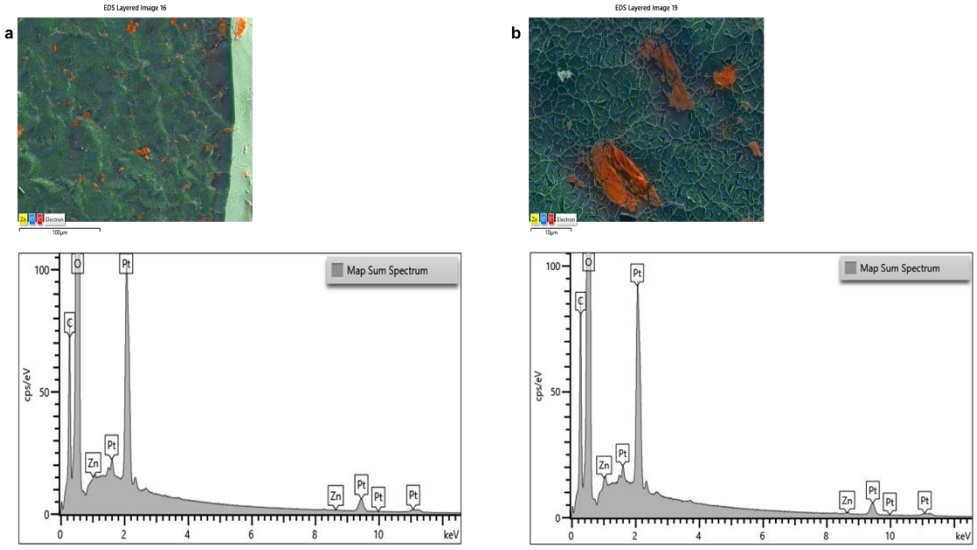

Figure 39. EDX analysis of CS/MGO beads after Zn^{2+} adsorption process (a) at the surface of the bead and (b) inside the bead

The EDX analysis was performed on two different regions of the CS/MGO bead. ***Figure 37*** shows the EDX analysis performed on the surface and in the core of the beads used for the adsorption of Zn^{2+}. By comparing the two spectra obtained, the intensity of EDX Zn peaks and consequently the amounts of Zn were in the same range for both analyzed regions, which means, during 420 min, Zn^{2+} was able to homogenously diffuse through the chitosan matrix from the surface to the core of the beads and to be adsorbed on MGO sites.

The first order reactions were described as chemical reactions of which the rate depends on the multiplication of the molar concentration power of the reactants involved in the reaction, which is equal to 1. However, the second order reaction rate depends on the multiplication of the molar concentration power of the reactants involved in the reaction which is equal to 2. The results of the experimental and modeled adsorption kinetics of Zn^{2+} by CS/MGO and CS/LDH/MGO beads are shown in ***Figure 40*** and **Table *19***. The adsorption of Zn^{2+} using the investigated materials was performed at pH 5 (see experimental conditions in ***VII.5.1. Cations trapping: application for Zinc***) for 420 min, in agreement with the time required for Zn diffusion/sorption equilibrium. Results were compared to those obtained using Cs beads (black squares). The pseudo first and second order were fitted using the different adsorption results of the chitosan-based beads, in order to determine the best fitting order.

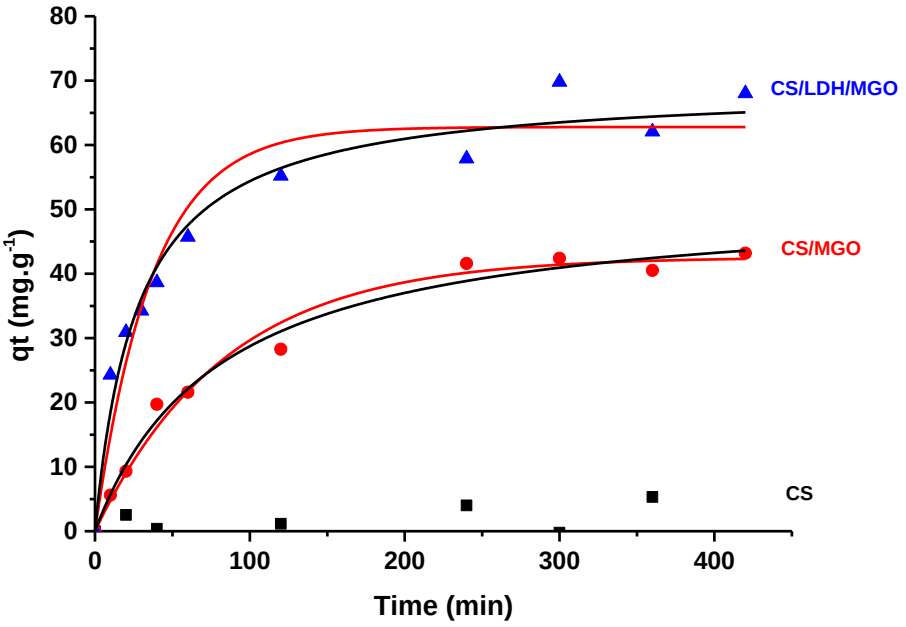

Figure 40. Adsorbed quantity of Zn (mg/g) using CS, CS/MGO and CS/LDH/MGO beads, where Vtot= 100 mL and pH =5. The red and black curves correspond respectively to the pseudo first and second order fittings.

The pure CS beads showed a low Zn^{2+} adsorption in the range of 5 $mg.g^{-1}$ (0.075 $mmol.g^{-1}$), because of the presence of amino groups partially positively charged (pKa =6.5) at the working pH value of 5.0. This will lead to an electrostatic repulsion between the positively charged amino groups and the Zn^{2+} cations present in the solution. On the other hand, the CS/MGO and CS/LDH/MGO beads showed an adsorption capacity q_t of 42 $mg.g^{-1}$ and 64 $mg.g^{-1}$ of Zn^{2+} respectively. The different parameters of the adsorption kinetic using the pseudo-first order and the pseudo-second order were calculated and presented in **Table *19***.

Table 19.Determined kinetic parameters of CS/MGO and CS/LDH/MGO beads

Adsorbents	Kinetic model	Kinetic parameters		
CS/MGO		R^2	$k_1.10^{-2}$ (min^{-1})	$k_2.10^{-4}$($g.mg^{-1}.min^{-1}$)
	1st	0.983	1.2 ± 0.1	-
	2nd	0.986	-	2.4 ± 0.4
CS/LDH/MGO	1st	0.934	3 ± 0.4	-
	2nd	0.970	-	5 ± 0.9

As shown ***Figure 40***, using CS/MGO beads, the Zn^{2+} adsorption curves can be fitted using a first and a second order model; with determination coefficients (R^2) of respectively 0.983 and 0.986. The quantity of adsorbed Zn^{2+} was determined by calculating the average of the last four points. Qt = 42 $mg.g^{-1}$ of MGO present in the beads which was lower than the adsorbed quantity of Zn^{2+} measured using pure MGO material (65 $mg.g^{-1}$)(view section ***XI.1.1. Characterization of MGO and adsorption sites*** **determination**). This may be caused by the interaction between the chitosan matrix and the MGO adsorbent, presumed from the DRX results. At a pH value of 5.0, the amino groups present on the chitosan chains were partially positively charged (pKa = 6.5). However, the carboxylic groups of the MGO adsorbent were negatively charged at this pH value (pKa =3.2). This opposite charges generated by the different functional groups of chitosan and MGO causes the neutralization of a part of COO^- groups responsible for the adsorption of Zn^{2+}.

For the CS/LDH/MGO, the fitting of the kinetic curves using a first and a second order are shown on ***Figure 40***. The second order was considered since the calculated R^2 for the second order (R^2 of 0.970), was higher than the R^2 of the first order (0.937). The adsorption capacity of the CS/LDH/MGO beads is of 64 $mg.g^{-1}$ is higher than that observed using CS/MGO beads (42 $mg.g^{-1}$). This higher adsorption capacity of the CS/LDH/MGO beads can be explained by the LDH buffering effect that kept the pH inside the beads at a value of approximately 8-9. At this pH value, two phenomena may occur:

- Negatively charged surface of the Co/Fe LDH sheets caused by pH value higher than pH of PZC (8.0) is responsible of a higher Zn^{2+}adsorption.

-It was noted that precipitation pH of zinc, between 6.0-6.5, was lower than the pH of 8-9 inside the beads. Therefore, some Zn^{2+} ion precipitates under the form of $Zn(OH)_2$ inside the beads, resulting in a higher adsorption capacity of the material, which was not attributed to an adsorption mechanism.

XII.1.4.Anionic exchange: properties of the composite beads

The target of the elaboration of composite beads including CS, MGO and LDH as sorbents was to capture both the anionic and cationic pollutants from industrial water containing sulfates, nitrates, nitrites and zinc cations. In order to achieve this, it is important to conserve

the anionic exchange properties of the Co/Fe LDHs precipitated inside the CS beads. XRD, AAS, TGA and EDX analyses clearly demonstrate that the developed composite beads allows maintaining the LDH structure. The anionic exchange capacity of encapsulated LDHs was studied using CS/LDHs and CS/LDH/MGO beads in which LDHs Co/Fe ratio was 6/2. It consisted in mixing 100 ml of anionic solution with 10 ml of Co/Fe-Cl LDH suspension for 24 hours in an abiotic glove box. The results are summarized in **Table *20***.

Table 20. Comparison between the amount of anions exchanged and the excess positive charges provided by Fe

Exchanged anions	CS/LDHs Anion exchanged quantity (eq/mol of Fe)	CS/LDH/MGO Anion exchanged quantity (eq/ mol of Fe)	CS/LDHs Excess charges provided by Fe (mol)	CS/LDH/MGO Excess charges provided by Fe (mol)
SO_4^{2-}	0.17	1.78	1.00	1.00
NO_3^-	0.12	0		
NO_2^-	0	0.04		
Total amount	0.29	1.81		

For the CS/LDHs 6/2 beads, the sulfates anions have shown the highest anionic exchange/adsorption (0.17 eq/mol of Fe) amount compared to the one for the nitrates (0.12 eq/mol of Fe). Nitrites showed no exchange process using the CS/LDHs beads. The total amount of exchanged anions was lower than the excess positive charge provided by the Fe^{3+} in the LDH sheets. This might be explained by the contamination of the CS/LDHs beads by carbonate anions during the beads formation. Since LDHs have high affinity towards carbonates, it is difficult to exchange them with sulfates, nitrates and nitrites. For the CS/LDH 6/2/MGO, high affinity towards sulfate was observed. For nitrates and nitrites, both anions are mono-charged with oxygenated groups, which led to an exchange competition between them. This was also observed using the Co/Fe-Cl LDHs with different cationic ratios described in the section IX.1.1.

The CS/LDH/MGO composites demonstrated higher anionic exchange process (1.78 eq/mol of Fe) than the CS/LDH beads (0.17 eq/mol of Fe). This difference may be caused by the presence

of MGO inside the beads, which will cause the interactions between hydrogen atoms of phenolic groups and oxygen groups of the exchange anions or the presence of partially positive charged amino groups of the chitosan matrix since the pH value of the anionic solution is 7.

These results show that the LDH containing beads can be used for the anionic exchange process, with an exchange capacity higher than the one expected for the incorporated LDH and MGO adsorbents. This may be attributed to the partially positive charged amino groups of the chitosan matrix or to the presence of hydrogen bonds between phenolic groups of MGO and the exchanged anions.

XIII. References

[1] C. Morcos, A. Seron, N. Maubec, I. Ignatiadis, and S. Betelu, "Comprehension of the Route for the Synthesis of Co/Fe LDHs via the Method of Coprecipitation with Varying pH," *Nanomaterials*, vol. 12, no. 9, Art. no. 9, Jan. 2022, doi: 10.3390/nano12091570.

[2] A. Seron and F. Delorme, "Synthesis of layered double hydroxides (LDHs) with varying pH: A valuable contribution to the study of Mg/Al LDH formation mechanism," *Journal of Physics and Chemistry of Solids*, vol. 69, no. 5, pp. 1088–1090, May 2008, doi: 10.1016/j.jpcs.2007.10.054.

[3] A. A. Sertsova, E. N. Subcheva, and E. V. Yurtov, "Synthesis and study of structure formation of layered double hydroxides based on Mg, Zn, Cu, and Al," *Russ. J. Inorg. Chem.*, vol. 60, no. 1, pp. 23–32, Jan. 2015, doi: 10.1134/S0036023615010167.

[4] K. Abderrazek, N. Frini Srasra, and E. Srasra, "Synthesis and Characterization of [Zn-Al] Layered Double Hydroxides: Effect of the Operating Parameters: Synthesis and Characterization of [Zn-Al] LDH," *Journal of the Chinese Chemical Society*, vol. 64, no. 3, pp. 346–353, Mar. 2017, doi: 10.1002/jccs.201600258.

[5] N. Louvain, J. Peyroux, M. Dubois, W. Simond, and F. Leroux, "Efficient Fluorinating Agent through Topochemical Fluorination of Co−Fe Layered Double Hydroxides.," *Inorganic Chemistry*, vol. 53, pp. 852–860, 2014, doi: 10.1021/ic402193x.

[6] H. Wu, Q. Jiao, Y. Zhao, S. Huang, X. Li, H. Liu and M. Zhou, "Synthesis of Zn/Co/Fe-layered double hydroxide nanowires with controllable morphology in a water-in-oil microemulsion," *Materials Characterization*, vol. 61, no. 2, pp. 227–232, Feb. 2010, doi: 10.1016/j.matchar.2009.12.003.

[7] Y. Zhao, J. Liang, F. Li, and X. Duan, "Selectivity of crystal growth direction in layered double hydroxides," *Tsinghua Science and Technology*, vol. 9, no. 6, pp. 667–671, Dec. 2004.

[8] S. Radha, S. V. Prasanna, and P. V. Kamath, "Polytype Selection by Intercalated Anions: Design and Synthesis of the 3R 2 Polytype of the Layered Double Hydroxide of Zn and Al," *Crystal Growth & Design*, vol. 6, no. 11, pp. 2287–2293, 2011, doi: 10.1021/cg101707n.

[9] B. GREGOIRE, C. RUBY, and C. CARTERET, "Structural Cohesion of MII-MIII Layered Double Hydroxides Crystals: Electrostatic Forces and Cationic Polarizing Power," *Cryst. growth des*, vol. 12, no. 9, pp. 4324–4333, 2012.

[10] A. I. Khan and D. O'Hare, "Intercalation chemistry of layered double hydroxides: recent developments and applications," *J. Mater. Chem.*, vol. 12, no. 11, pp. 3191–3198, Oct. 2002, doi: 10.1039/B204076J.

[11] R. D. Shannon, "Revised effective ionic radii and systematic studies of interatomic distances in halides and chalcogenides," *Acta Cryst A*, vol. 32, no. 5, Art. no. 5, Sep. 1976, doi: 10.1107/S0567739476001551.

[12] S. Miyata, "Anion-exchange properties of hydrotalcite-like compounds," *Clays and Clay Minerals*, 1983.

[13] M. del Arco, P. Malet, R. Trujillano, and V. Rives, "Synthesis and Characterization of Hydrotalcites Containing Ni(II) and Fe(III) and Their Calcination Products," *Chem. Mater.*, vol. 11, no. 3, pp. 624–633, Mar. 1999, doi: 10.1021/cm9804923.

[14] A. Vaccari, "Clays and catalysis: a promising future," *Applied Clay Science*, vol. 14, no. 4, pp. 161–198, Apr. 1999, doi: 10.1016/S0169-1317(98)00058-1.

[15] "Capacity, selectivity, and reversibility for nitrate exchange of a layered double-hydroxide (LDH) mineral in simulated soil solutions and in soil - Torres-Dorante - 2008 - Journal of Plant Nutrition and Soil Science - Wiley Online Library." https://onlinelibrary.wiley.com/doi/abs/10.1002/jpln.200700330 (accessed Jun. 10, 2021).

[16] S. Miyata, "Physico-Chemical Properties of Synthetic Hydrotalcites in Relation to Composition," *Clays Clay Miner.*, vol. 28, no. 1, pp. 50–56, Feb. 1980, doi: 10.1346/CCMN.1980.0280107.

[17] L. Perrin, J. Bourgois, and V. Laforest, "Piégeage du CrVI par les boues d'hydroxydes polymétalliques," p. 8, 2010.

[18] J. Wang, Y Song, Z Li, Q Liu, J Zhou and X Jing, "*In Situ* Ni/Al Layered Double Hydroxide and Its Electrochemical Capacitance Performance," *Energy Fuels*, vol. 24, no. 12, pp. 6463–6467, Dec. 2010, doi: 10.1021/ef101150b.

[19] F. Zhang, J. Jiang, C. Yuan, L. Hao, L. Shen, L. Zhang and X. Zhang, "Glycine-assisted hydrothermal synthesis of nanostructured CoxNi1−x–Al layered triple hydroxides as electrode materials for high-performance supercapacitors," *J Solid State Electrochem*, vol. 16, no. 5, pp. 1933–1940, May 2012, doi: 10.1007/s10008-011-1596-0.

[20] F. Cavani, F. Trifirò, and A. Vaccari, "Hydrotalcite-type anionic clays: Preparation, properties and applications.," *Catalysis Today*, vol. 11, no. 2, pp. 173–301, Dec. 1991, doi: 10.1016/0920-5861(91)80068-K.

[21] F. Basile, G. Fornasari, M. Gazzano, and A. Vaccari, "Synthesis and thermal evolution of hydrotalcite-type compounds containing noble metals," *Applied Clay Science*, vol. 16, no. 3, pp. 185–200, Mar. 2000, doi: 10.1016/S0169-1317(99)00053-8.

[22] F. M. Labajos, M. D. Sastre, R. Trujillano, and V. Rives, "New layered double hydroxides with the hydrotalcite structure containing Ni(II) and V(III)," *Journal of Materials Chemistry*, vol. 9, no. 4, pp. 1033–1039, 1999, doi: 10.1039/A808544G.

[23] J. Pérez-Ramírez, G. Mul, and J. A. Moulijn, "In situ Fourier transform infrared and laser Raman spectroscopic study of the thermal decomposition of Co–Al and Ni–Al hydrotalcites," *Vibrational Spectroscopy*, vol. 27, no. 1, pp. 75–88, Nov. 2001, doi: 10.1016/S0924-2031(01)00119-9.

[24] F. A. Miller and C. H. Wilkins, "Infrared Spectra and Characteristic Frequencies of Inorganic Ions," *Anal. Chem.*, vol. 24, no. 8, pp. 1253–1294, Aug. 1952, doi: 10.1021/ac60068a007.

[25] Z. Hz, Z. Lq, D. Jh, H. Y, and L. Xf, "Fabrication of porous Co3O4 with different nanostructures by solid-state thermolysis of metal-organic framework for supercapacitors," *J. Mater. Sci.*, vol. 53, no. 11, pp. 8474–8482, 2018.

[26] F. Papa, I. Balint, C. Negrila, E.-A. Olaru, I. Zgura, and C. Bradu, "Supported Pd–Cu Nanoparticles for Water Phase Reduction of Nitrates. Influence of the Support and of the pH Conditions," *Ind. Eng. Chem. Res.*, vol. 53, no. 49, pp. 19094–19103, Dec. 2014, doi: 10.1021/ie503070f.

[27] S.-L. Wang and P.-C. Wang, "In situ XRD and ATR-FTIR study on the molecular orientation of interlayer nitrate in Mg/Al-layered double hydroxides in water," *Colloids and Surfaces A: Physicochemical and Engineering Aspects*, vol. 292, no. 2, pp. 131–138, Jan. 2007, doi: 10.1016/j.colsurfa.2006.06.014.

[28] K. Nakamoto, "Infrared and Raman Spectra of Inorganic and Coordination Compounds," in *Handbook of Vibrational Spectroscopy*, American Cancer Society, 2006. doi: 10.1002/0470027320.s4104.

[29] J. Pérez-Ramírez, G. Mul, F. Kapteijn, and J. A. Moulijn, "In situ investigation of thethermal decomposition of Co–Al hydrotalcite in different atmospheres," *J. Mater. Chem.*, vol. 11, no. 3, pp. 821–830, Jan. 2001, doi: 10.1039/B009320N.

[30] J. Purmova, K. F. D. Pauwels, W. van Zoelen, E. J. Vorenkamp, A. J. Schouten, and M. L. Coote, "New Insight into the Formation of Structural Defects in Poly(Vinyl Chloride)," *Macromolecules*, vol. 15, no. 38, pp. 6352–6366, 2005, doi: 10.1021/ma050035p.

[31] E. UZUNOVA, D. KLISSURSKI, I. MITOV, and P. STEFANOV, "Cobalt-iron hydroxide carbonate as a precursor for the synthesis of high-dispersity spinel mixed oxides," *Chem. mater*, vol. 5, no. 4, pp. 576–582, 1993.

[32] Q. Wang, *C Yuan, L Hao, L Shen, L Zhang, X Zhang*, "Morphology and composition controllable synthesis of Mg–Al–CO3 hydrotalcites by tuning the synthesis pH and the CO2 capture capacity," *Applied Clay Science*, vol. 55, pp. 18–26, Jan. 2012, doi: 10.1016/j.clay.2011.07.024.

[33] L. Legrand, S. Savoye, A. Chausse, and R. Messina, "Study of oxidation products formed on iron in solutions containing bicarbonate/carbonate," *Electrochimica Acta*, vol. 46, no. 1, pp. 111–117, Oct. 2000, doi: 10.1016/S0013-4686(00)00563-6.

[34] X. Xie, P. Shang, Z. Liu, Y. Lv, Y. Li, and W. Shen, "Synthesis of Nanorod-Shaped Cobalt Hydroxycarbonate and Oxide with the Mediation of Ethylene Glycol," *The Journal of Physical Chemistry C*, vol. 5, no. 114, pp. 2116–2123, Feb. 2010, doi: 10.1021/jp911011g.

[35] A. D. Jagadale, V. S. Kumbhar, R. N. Bulakhe, and C. D. Lokhande, "Influence of electrodeposition modes on the supercapacitive performance of Co 3 O 4 electrodes," *Energy*, vol. 64, pp. 234–241, Jan. 2014, doi: 10.1016/j.energy.2013.10.016.

[36] C. Morcos, "PROCEDE DE CAPTAGE ET LIBERATION DU CO2 ASSISTE PAR L'ELECTROLYSE UTILISANT DES MATERIAUX DE TYPE BRUCITIQUES," *http://www.theses.fr*, Dec. 13, 2021. http://www.theses.fr/s294216 (accessed Jun. 14, 2022).

[37] M. Shao, J. Han, M. Wei, D. G. Evans, and X. Duan, "The synthesis of hierarchical Zn–Ti layered double hydroxide for efficient visible-light photocatalysis," *Chemical Engineering Journal*, vol. 168, no. 2, pp. 519–524, Apr. 2011, doi: 10.1016/j.cej.2011.01.016.

[38] Q. Wang *Dr., H.Huang Tay, D. Jia Wei Ng, L. Chen Dr., Y. Liu Dr., J. Chang Dr., Z. Zhong Dr., J. Luo Dr., A. Borgna Dr.*, "The effect of trivalent cations on the performance of Mg-M-CO(3) layered double hydroxides for high-temperature CO(2) capture," *ChemSusChem*, vol. 3, no. 8, pp. 965–973, Aug. 2010, doi: 10.1002/cssc.201000099.

[39] X. He, P. Zhong, and X. Qiu, "Remediation of hexavalent chromium in contaminated soil by Fe(II)-Al layered double hydroxide," *Chemosphere*, vol. 210, pp. 1157–1166, Nov. 2018, doi: 10.1016/j.chemosphere.2018.07.048.

[40] P. Benito, I. Guinea, F. M. Labajos, J. Rocha, and V. Rives, "Microwave-hydrothermally aged Zn,Al hydrotalcite-like compounds: Influence of the composition and the

irradiation conditions," *Microporous and Mesoporous Materials*, vol. 110, no. 2, pp. 292–302, Apr. 2008, doi: 10.1016/j.micromeso.2007.06.013.

[41] J. Zhang, F. Zhang, L. Ren, D. G. Evans, and X. Duan, "Synthesis of layered double hydroxide anionic clays intercalated by carboxylate anions," *Materials Chemistry and Physics*, vol. 85, no. 1, pp. 207–214, May 2004, doi: 10.1016/j.matchemphys.2004.01.020.

[42] S. Miyata, "Anion-exchange properties of hydrotalcite-like compounds," *Clays and Clay Minerals*, 1983.

[43] Q. Yin, *D. Rao, G. Zhang, Y. Zhao, J. Han, K. Lin, L. Zheng, J. Zhang, J. Zhou, M. Wei,* "CoFe–Cl Layered Double Hydroxide: A New Cathode Material for High-Performance Chloride Ion Batteries," *Advanced Functional Materials*, vol. 29, no. 36, p. 1900983, 2019, doi: 10.1002/adfm.201900983.

[44] M. Badreddine, A. Legrouri, A. Barroug, A. De Roy, and J. P. Besse, "Ion exchange of different phosphate ions into the zinc–aluminium–chloride layered double hydroxide," *Materials Letters*, vol. 38, no. 6, pp. 391–395, Mar. 1999, doi: 10.1016/S0167-577X(98)00195-5.

[45] Z. Liu, R. Ma, M. Osada, K. Takada, and T. Sasaki, "Selective and Controlled Synthesis of α- and β-Cobalt Hydroxides in Highly Developed Hexagonal Platelets," *J. Am. Chem. Soc.*, vol. 127, no. 40, pp. 13869–13874, Oct. 2005, doi: 10.1021/ja0523338.

[46] L. Lv, *P Sun, Z Gu, H Du, X Pang, X Tao, R Xu and L. Xu.*, "Removal of chloride ion from aqueous solution by ZnAl-NO3 layered double hydroxides as anion-exchanger," *Journal of Hazardous Materials*, vol. 161, no. 2, pp. 1444–1449, Jan. 2009, doi: 10.1016/j.jhazmat.2008.04.114.

[47] ZA Hu, YL Xie, YX Wang, LJ Xie, GR Fu, XQ. Jin, ZY.Zhang, YY. Yang, and HY. Wu, "Synthesis of α-Cobalt Hydroxides with Different Intercalated Anions and Effects of Intercalated Anions on Their Morphology, Basal Plane Spacing, and Capacitive Property," *J. Phys. Chem. C*, vol. 113, no. 28, pp. 12502–12508, Jul. 2009, doi: 10.1021/jp8106809.

[48] L. Tian, J. L. Zhu, L. Chen, B. An, Q. Q. Liu, and K. L. Huang, "Synthesis and characterization of α-cobalt hydroxide nanobelts," *J Nanopart Res*, vol. 13, no. 8, pp. 3483–3488, Aug. 2011, doi: 10.1007/s11051-011-0269-3.

[49] F. Bouyahmed, F. Muller, A.Richard, TA. Mostefaoui, I.Belabbas, F.Warmont, M. Roulet, L. Reinert, L.Duclaux, S. Delpeux-Ouldriane, "Chitosan-multilayered graphene

oxide hybrid beads for [Zn^{2+}]and metoprolol adsorption," *Comptes Rendus. Chimie*, vol. 25, no. G1, pp. 205–223, 2022, doi: 10.5802/crchim.183.

[50] C. Kiang Chua and M. Pumera, "Chemical reduction of graphene oxide: a synthetic chemistry viewpoint," *Chemical Society Reviews*, vol. 43, no. 1, pp. 291–312, 2014, doi: 10.1039/C3CS60303B.

[51] "Manganese | Periodic Table - FR." https://www.thermofisher.com/fr/fr/home/materials-science/learning-center/periodic-table/transition-metal/manganese.html (accessed Nov. 08, 2022).

[52] "Potassium | Periodic Table - FR." https://www.thermofisher.com/fr/fr/home/materials-science/learning-center/periodic-table/alkali-metal/potassium.html (accessed Nov. 08, 2022).

[53] A. T. Al-Hinai, M. H. Al-Hinai, and J. Dutta, "Application of Eh-pH diagram for room temperature precipitation of zinc stannate microcubes in an aqueous media," *Materials Research Bulletin*, vol. Complete, no. 49, pp. 645–650, 2014, doi: 10.1016/j.materresbull.2013.10.011.

[54] G. Z. Kyzas, E. A. Deliyanni, and K. A. Matis, "Graphene oxide and its application as an adsorbent for wastewater treatment," *Journal of Chemical Technology & Biotechnology*, vol. 2, no. 89, pp. 196–205, Jan. 2014, doi: 10.1002/jctb.4220.

[55] G. Pavoski, T. Maraschin, F. de Carvalho Fim, NM. Balzaretti, G. Barrera Galland CS. Moura, NR. de Souza Basso, "Few Layer Reduced Graphene Oxide: Evaluation of the Best Experimental Conditions for Easy Production," *Mat. Res.*, vol. 20, pp. 53–61, Nov. 2016, doi: 10.1590/1980-5373-MR-2015-0528.

[56] S. Ruiz, JA. Tamayo, JD. Ospina, D. Porras, M. Zapata, J. Hernandez, C.Valancia, F.Zuluaga and C.Tovar, "Antimicrobial Films Based on Nanocomposites of Chitosan/Poly(vinyl alcohol)/Graphene Oxide for Biomedical Applications," *Biomolecules*, vol. 9, no. 3, Art. no. 3, Mar. 2019, doi: 10.3390/biom9030109.

[57] M. Gineys, "Régénération électrochimique de carbones nanoporeux utilisés pour le piégeage de micropolluants," These de doctorat, Orléans, 2015. Accessed: Nov. 08, 2022. [Online]. Available: https://www.theses.fr/2015ORLE2020

[58] A. Aloui and A. Zertal, "ÉTUDE DE L'ELIMINATION DU PARACETAMOL PAR LE CHARBON ACTIF EN MILIEU AQUEUX," p. 6, 2016.

[59] M. Li, A. Dopilka, A. N. Kraetz, H. Jing, and C. Chan, "Layered Double Hydroxide/Chitosan Nanocomposite Beads as Sorbents for Selenium Oxoanions,"

Industrial & Engineering Chemistry Research, vol. 57, no. 14, pp. 4978–4987, Apr. 2018, doi: 10.1021/acs.iecr.8b00466.

[60] Z. A. Sutirman, M. M. Sanagi, K. J. Abd Karim, A. Abu Naim, and W. A. Wan Ibrahim, "Enhanced removal of Orange G from aqueous solutions by modified chitosan beads: Performance and mechanism," *International Journal of Biological Macromolecules*, vol. 133, pp. 1260–1267, Jul. 2019, doi: 10.1016/j.ijbiomac.2019.04.188.

[61] C. Sandolo, T. Coviello, P. Matricardi, and F. Alhaique, "Characterization of polysaccharide hydrogels for modified drug delivery," *Eur Biophys J*, vol. 36, no. 7, pp. 693–700, Sep. 2007, doi: 10.1007/s00249-007-0158-y.

[62] Z. Feng, A. Simeone, K. Odelius, and M. Hakkarainen, "Biobased Nanographene Oxide Creates Stronger Chitosan Hydrogels with Improved Adsorption Capacity for Trace Pharmaceuticals," *ACS Sustainable Chem. Eng.*, vol. 5, no. 12, pp. 11525–11535, Dec. 2017, doi: 10.1021/acssuschemeng.7b02809.

[63] S. C. Lau, H. N. Lim , M. Basri , H.R.F. Masoumi, A. A. Tajudin, N. M. Huang, A. Pandikumar, C. H. Chia, Y. Andou, "Enhanced Biocatalytic Esterification with Lipase-Immobilized Chitosan/Graphene Oxide Beads," *PLOS ONE*, vol. 9, no. 8, p. e104695, Aug. 2014, doi: 10.1371/journal.pone.0104695.

[64] B. H. Hameed and M. I. El-Khaiary, "Malachite green adsorption by rattan sawdust: Isotherm, kinetic and mechanism modeling," *Journal of Hazardous Materials*, vol. 159, no. 2, pp. 574–579, Nov. 2008, doi: 10.1016/j.jhazmat.2008.02.054.

[65] B. An, "Cu(II) and As(V) Adsorption Kinetic Characteristic of the Multifunctional Amino Groups in Chitosan," *Processes*, vol. 8, no. 9, Art. no. 9, Sep. 2020, doi: 10.3390/pr8091194.

General conclusion and perspectives

The main objective of this thesis was to elaborate a hybrid material containing two different types of adsorbents for the capture of ionic pollutants present in wastewater. The first adsorbent was layered double hydroxides (LDHs), which presents a positive charge sheets obtained by isomorph replacement of divalent cations by trivalent ones. This positive charge was counterbalanced by anionic species intercalated in the interlayer space. The expected role of LDH was to exchange anionic pollutants such as sulfates, nitrates and nitrites. To this, multilayered graphene oxide (MGO), was added. At pH values lower than the pH_{PZC} of the MGO (3.2), this adsorbent containing functional oxygenated group, especially COOH which is negatively charged leading to the adsorption of cationic pollutants such as Zn^{2+}. Both adsorbents were grouped in a chitosan matrix, which is a biopolymer obtained from crustacean shells. The chitosan/layered double hydroxide/multilayered graphene oxide composite was elaborated under the form of homogeneous beads for industrial applications.

The synthesis and the characterization of each adsorbent, as well as the study of the capture process was performed using components, such as LDHs and MGO, and elaborated composite like pure chitosan (CS), CS/LDH, CS/MGO and CS/LDH/MGO beads.

In order to study the effect of the cationic ratio and the pH value on the crystallinity and purity of LDH phases, the synthesis of carbonated LDHs, having Co/Fe ratios between 2/2 and 10/2, using the co-precipitation at variable pH value method to reach a pH of 8.0 and 11.5 was performed. The XRD characterization technique performed on the synthesized carbonated LDHs at pH value of 8.0, showed, between 2/2 and 8/2 cationic ratios, well crystallized LDH structure was obtained. However, the 10/2 ratio showed a slight amount of Co_3O_4 impurity. Further characterization including AAS and FTIR analysis proved the obtainment of Co/Fe LDHs with the global desired ratios with mainly carbonate anions in the interlayer region. However, EDX analysis showed a variation of the local Co/Fe cationic ratios depending on the analyzed particles. Increasing the pH value until 11.5 resulted in the obtainment of LDHs along with impurity phases.

On the other hand, an evaluation of the anionic exchange capacity of LDHs was conducted by studying the capacity of the chloride LDHs to capture sulfates, nitrates and nitrites. It was confirmed that the affinity of these materials for sulfates was higher than that for nitrates and nitrites. However, the 8/2 and 10/2 ratios presented higher anionic exchange capacity compared

to the excess of positive charges present on the LDH sheets may be caused by the α-$Co(OH)_2$ impurity.

Multilayered graphene oxide (MGO), which will be used for Zn^{2+} adsorption, was obtained using the modified Hummer's method. This allows the creation of oxygenated groups such as carboxylic, epoxy, hydroxyl etc… on the surface of the graphene. The determination of the amount of oxygenated groups used for the adsorption process was performed using different techniques such as XPS and pKa titration. The obtained functional groups are pH depended and at pH values lower than 5, 1 $mmol.g^{-1}$ of MGO were used for the adsorption of Zn^{2+}. Zinc was chosen as test metal since it is frequently present in industrial effluents mainly metal surface treatment industries.

The determination of the adsorption capacity of the synthesized MGO was carried out at a pH value of 5 using Zn^{2+} solution. The pH value of 5 was chosen for the following reasons: - Above the pH value of 3.0 the dissociation of a part of the carboxylic groups present on the surface of the MGO leading to a negatively charged the surface of this material;

- The risk of precipitation of zinc occurs when the pH value is 6-6.5.

It is found that 70% of initial quantity of Zn^{2+} was adsorbed onto MGO.

After the study of the behavior of each component (LDHs and MGO) regarding anionic and cationic capture, the elaboration of the chitosan-based beads was performed for capture purposes: chitosan (CS), chitosan and LDHs (CS/LDHs), chitosan and MGO (CS/MGO) and finally, chitosan, LDHs and MGO (CS/LDH/MGO) were elaborated using different gels obtained from different procedures.

The capacity of the elaborated materials to capture Zn^{2+}, sulfates, nitrates and nitrites was studied. In order to understand the interaction between the different components constituting the hybrid beads and to study the adsorption capacity of each material, the capture of Zn^{2+}, sulfates, nitrates and nitrites was performed using chitosan beads, CS/MGO and CS/LDHs/MGO beads.

The adsorption of Zn^{2+} on pure CS beads showed that the capture capacity of chitosan towards this cation was close to zero (5 $mg.g^{-1}$). While CS/OG beads showed a Zn^{2+} adsorption capacity of 42.0 mg of Zn^{2+} per g of MGO present in the beads. The later value was lower than the sorption capacity of Zn^{2+} on MGO powder, which amounts to 65.1 $mg.g^{-1}$. This decrease in the adsorption capacity was most likely due to the interaction between the positively charged amino

groups present on the CS chains and the negatively charged MGO. This interaction leads to the neutralization of part of the adsorption sites of the MGO and thus to the reduction of the zinc capture capacity. For zinc adsorption using CS/LDH/MGO beads, the observed adsorption capacity was about 64 mg of zinc per g of MGO present in the bead. The difference (22 mg /g) between the amount of zinc adsorbed by the CS/MGO beads and by the CS/LDHs/MGO beads can be related to the buffering effect of LDHs present in the beads. This increase of the pH value was likely to lead to the precipitation of some of the Zn^{2+}. Furthermore, the point of zero charge of LDHs was close to a value of 8.0. Therefore, at pH values above 8.0, the surface of LDHs was negatively charged, which may result in Zn adsorption.

The study of the exchange on CS/LDH and CS/LDH/MGO beads showed the highest capture rate for sulfates followed by a competition between nitrates and nitrites. The exchange capacity obtained was higher than the one of LDHs present in the beads. This can be explained by the presence of chitosan which at pH=7 (pKa=6.5) always presents positively charged groups likely to participate in the capture of anions.

Following the work performed during this PhD thesis, perspectives could be considered. Since Co/Fe LDHs are brittle materials that can be affected by elevated temperature and vacuum process, the need to find the optimal parameters for the analysis of Co/Fe LDHs using different techniques like XPS, TEM… should be performed. To get an overview about the local ratios on precise LDH particles, further studies using EDX analysis should be performed.

For the understanding of the interaction of the adsorbents inside the beads, further characterization such as TEM analysis to observe the LDH structure, should be performed on the hybrid beads in order to understand the mechanism of formation of the materials. The adsorption study of a mixture of cationic metals such as Cu^{2+},Pb^{2+} and Zn^{2+} to evaluate the competition between them will be performed using chitosan-based beads. Additionally, the depollution of real industrial effluents should be considered in order to see the efficiency of the hybrid beads facing real polluted wastewater. Finally, the regeneration of the material is highly necessary in order to reuse the elaborated beads and to recover the adsorbed pollutants. This step should include the study of the capture/regeneration cycle of the beads using electrochemistry. The choice of electrochemistry was based on the oxidation/reduction of the electroactive metal present on the LDH sheets (cobalt), leading to the creation of excess positive charge causing the intercalation of anionic pollutants. The reduction process of the oxidized cobalt metals will decrease the positive charge already created during the oxidation process, leading to the release of the intercalated anions. The presence of multilayered graphene oxide

will increase the conductivity of the material allowing faster oxidation of cobalt metals. Electrochemistry will also be used to alter the pH of the solution which may allow the desorption of the adsorbed metals on the surface of the MGO.

Almaza ABI KHALIL

Etude et développement d'un matériau composite innovant et éco-compatible pour le piégeage universel et réversible de polluants métalliques : application à la remédiation d'effluents industriels et au recyclage de métaux

Les industries spécialisées dans le domaine du traitement de surfaces métalliques génèrent des effluents contaminés par des métaux tels que le Cr, Zn, Ni, Cu … et des polluants inorganiques tels que les nitrates, nitrites et sulfates. Les travaux de recherche effectués durant cette thèse concernent le développement de matériaux composites innovants constitués d'hydroxydes doubles lamellaires (HDLs) et d'oxyde graphitique (OG). Les HDLs, possédant une charge structurelle de part des substitutions isomorphiques, sont utilisés pour la capture par intercalation interfoliaire des anions majeurs. Quant à l'oxyde graphitique, chargé négativement pour des valeurs de pH supérieures au pH_{PZC}, il est utilisé pour la capture par adsorption de surface des différents métaux cités précédemment. Le matériau composite est réalisé sous forme de billes hybrides par dispersion des adsorbants dans une matrice de chitosane (CS), un bio polymère naturel. Les HDLs carbonatés et chlorurés avec des rapports cationiques Co/Fe compris entre 2/2 et 10/2, ont été synthétisés en utilisant la méthode de co-précipitation à pH variable. L'OG a été synthétisé par voie chimique suivant la méthode de Hummers modifiée. Des billes de différentes compositions : chitosane pure (CS), chitosane et HDL (CS/ HDL), chitosane et OG (CS/OG), ainsi que CS/HDL/OG ont été élaborées en formulant un gel adapté. Pour l'élaboration des billes CS/HDL/OG, la poudre de chitosane est dissoute dans de l'acide acétique dilué puis l'OG dispersé par traitement ultra-sonique est ajouté et finalement les précurseurs de HDL (sel de métaux) sont ajoutés. Le gel est ensuite transféré dans une solution de soude pour la formation des billes. Une fois formées, une étape de lavage est nécessaire afin d'abaisser le pH dans les billes, favorisant ainsi la formation des HDLs. La caractérisation physico-chimique réalisée sur les HDLs carbonatés a montré l'obtention de phases bien cristallisées avec les rapports cationiques compris entre 2/2 et 8/2. Pour le rapport 10/2, une faible quantité d'impureté de type Co_3O_4 a été détectée. La spectroscopie FTIR et la spectroscopie d'absorption atomique ont permis de préciser la composition chimique des produits de synthèse en termes à la fois d'anions interfoliaires et de rapport Co/Fe. Cependant, les analyses EDX réalisées sur des particules individualisées ont montré que le rapport Co/Fe pouvait varier localement, spécifiquement pour les compositions 2/2 et 10/2. La capacité des matériaux à piéger des cations a été testée en ciblant le zinc. Les essais d'adsorption du Zn vis à vis des billes de CS/OG ont montré une capacité d'adsorption de Zn de 42,0 mg par g de OG. Cette dernière valeur est inférieure à la capacité de sorption du zinc sur l'oxyde graphitique seul qui s'élève à 65,1 mg/g. Cet abaissement de la capacité de capture est très probablement dû à l'interaction entre le CS chargé positivement et l'OG chargé négativement. Concernant la capture du zinc par les billes de CS/HDL/OG, la capacité de capture est de l'ordre de 64.4 mg de zinc par g d'OG présent dans la bille. La différence entre la quantité de zinc adsorbée par les billes de CS/OG et celle par les billes de CS/HDL/OG peut être reliée à l'effet tampon du HDL à un pH ≥ 8.0. Une évaluation de la capacité d'échange anionique des HDLs a été menée en étudiant la capacité de capture des sulfates, nitrates et nitrites par les HDLs chlorurés. Il apparait que l'affinité de ces matériaux pour les sulfates est supérieure à celle pour les nitrates et nitrites. L'étude de l'échange sur les billes de CS/HDLs et CS/HDLs/GO a montré un taux de capture des sulfates, des nitrates et nitrite supérieur à la capacité d'échange des HDLs présents dans les billes. Cela peut être expliqué par la présence du chitosane qui à pH=7 présente toujours des groupements chargés positivement susceptibles de participer à la capture des anions.

Mots clés : dépollution de l'eau, Hydroxyde double lamellaire, Oxide graphitique, chitosane, polluants metalliques., anions majeurs.

Development of an innovative and eco-compatible composite material for the reversible trapping of pollutants: application to the depollution of industrial effluents

Industries specialized in the field of metal surface treatment generate effluents contaminated by metals such as Cr, Zn, Ni, Cu ... and inorganic pollutants such as nitrates, nitrites and sulfates. The research work carried out during this thesis concerns the development of innovative composites made of layered double hydroxides (LDHs) and graphene oxide (GO). The first are used for the capture by intercalation of major anions because of the structural charge carried by such materials due to isomorphic substitutions. As for the graphene oxide, negatively charged for pH values higher than pHPZC, it was used for the capture by surface adsorption of the various metals mentioned above. The composite material was made in the form of hybrid beads by dispersion of the adsorbents in a matrix of chitosan (CS), a natural bio-polymer. Carbonated and chlorided LDHs with Co/Fe cationic ratios between 2/2 and 10/2, were synthesized using the co-precipitation at variable pH value method. While GO was synthesized chemically following the modified Hummers method. Beads of different compositions: pure chitosan (CS), chitosan and LDHs (CS/ LDHs), chitosan and GO (CS/GO), as well as CS/LDH/GO were elaborated by formulating a suitable gel. For the elaboration of CS/LDH/GO beads, chitosan powder was dissolved in dilute acetic acid, then GO dispersed by ultrasonic treatment followed by LDH precursors (metal salt) were added. The gel was then transferred to an alkaline solution to form the beads. A washing step was necessary to lower the pH in the beads promoting LDH formation. The physico-chemical characterization was carried out using the CO32- LDHs showed the obtainement of well-crystallized phases with Co/Fe ratios between 2/2 and 8/2. For the 10/2 ratio, a small amount of Co3O4 impurity was detected. FTIR spectroscopy and atomic absorption spectroscopy allowed to specify the chemical composition of the synthesis products in terms of both interlayer anions and Co/Fe ratio. However, EDX analysis performed on single particles showed that the Co/Fe ratio could differ locally, precisely for the 2/2 and 10/2 compositions. The ability of the materials to trap cations was tested by targeting zinc. Zn adsorption tests towards CS/GO beads showed an adsorption capacity of 42.0 mg per g of GO. This value was lower than the sorption capacity of zinc on pure graphene oxide (65.1 mg/g). This decrease in capture capacity was most likely due to the interaction between the positively charged CS and the negatively charged GO. Concerning zinc capture by CS/LDH/GO beads, the capacity was about 64.4 mg of zinc per g of GO present in the bead. The difference between the amount of zinc adsorbed by CS/GO beads and CS/LDH/GO beads can be related to the buffering effect of LDH (pH of 8.0). An evaluation of the anion exchange capacity of chlorinated LDHs for sulfates, nitrates and nitrites was conducted. It appears that the affinity of these materials for sulfates was higher than for nitrates and nitrites. The study of the exchange capacity on CS/LDHs and CS/LDHs/GO beads showed a capture rate of sulfates, nitrates and nitrites higher than the exchange capacity of the LDHs present in the beads. This can be explained by the presence of chitosan which at pH=7 always shows positively charged groups able to participate in the capture of anions.

Keywords : Water depollution, layered double hydroxide, multi-layered graphene oxide, chitosan, metals, major anions.

ICMN Interfaces Confinement Matériaux et Nanostructures

ICMN, 2b rue de la Ferollerie
45071 Orléans cedex 2
BRGM, 3 av. Claude Guillemin
45100- Orléans

Géosciences pour une Terre durable brgm